# POLYMORPHISM IN BEA-TYPE STRUCTURE:

# SYNTHESIS, CHARACTERIZATION AND

# CATALYTIC APPLICATIONS

**A THESIS**

**SUBMITTED TO THE**

**UNIVERSITY OF PUNE**

**FOR THE DEGREE OF**

**DOCTOR OF PHILOSOPHY**

**IN**

**CHEMISTRY**

**BY**


**MAHESH D. KADGAONKAR**

**Dr. RAJIV KUMAR**
**(RESEARCH GUIDE)**

**CATALYSIS DIVISION**
**NATIONAL CHEMICAL LABORATORY**
**PUNE 411 008**
**INDIA**


**DECEMBER 2007**

# CERTIFICATE

Certified that the work incorporated in the thesis entitled: "**POLYMORPHISM IN BEA-TYPE STRUCTURE: SYNTHESIS, CHARACTERIZATION AND CATALYTIC APPLICATIONS**", submitted by Mr. Mahesh D. Kadgaonkar, for the Degree of ***Doctor of Philosophy***, was carried out by the candidate under my supervision at Catalysis Division, National Chemical Laboratory, Pune-411008, India. Such materials as has been obtained from other sources have been duly acknowledged in the thesis.

**Dr. Rajiv Kumar** Date: 31-12-2007

(Research Guide) Place: Pune

# DECLARATION BY RESEARCH SCHOLAR

I hereby declare that the thesis entitled "**POLYMORPHISM IN BEA-TYPE STRUCTURE: SYNTHESIS, CHARACTERIZATION AND CATALYTIC APPLICATIONS**", submitted for the Degree of ***Doctor of Philosophy*** to the University of Pune, has been carried out by me at Catalysis Division, National Chemical Laboratory, Pune-411 008, India, under the supervision of Dr. Rajiv Kumar. The work is original and has not been submitted in part or full by me for any other degree or diploma to this or any other University.

**Mahesh D. Kadgaonkar** Date: 31-12-2007

(Research Scholar) Place: Pune

*…….dedicated to my beloved parents*

# *ACKNOWLEDGEMENTS*

*I find it difficult to write something in short to acknowledge my research supervisor, Dr. Rajiv Kumar. His constant inspiration, invaluable guidance and constructive criticism helped me a lot to focus my views in the proper perspective. I grasp this opportunity to express my intense reverence towards him for the extensive scientific discussions and giving me the liberty to carry out my research work independently. Although, this eulogy is insufficient, I preserve an everlasting gratitude for him.*

*I am deeply indebted to Dr. N. M. Gupta who was my mentor in understanding the essence of FTIR spectroscopy. His tireless attitude has been an impetus for me throughout the course of study. My deepest personal regards are due for him forever for his timely helps and being a strong support, both scientific and personal, on all stages of my research period. I am thankful to Dr. P. N. Joshi and Dr. M. W. Kasture for the stimulating discussions, valuable suggestions and constant encouragement and support. I convey my sincere gratitude to Dr. A. P. Singh and Dr. A. K. Kinage for helping me in every possible way. I duly acknowledge the constant help provided by Dr. (Mrs.) Veda Ramaswamy and Shubhangi Umbarkar for XRD and FTIR study.*

*I wish to convey my sincere gratitude to Dr. S. Sivasankar, former Head Catalysis division for not only providing divisional facilities but also for helpful stimulating discussions and personal help whenever required.*

*My heartfull thanks are due to Dr. D. Srinivas, Dr. M. K. Dongare, Dr. (Mrs.) Chandwadkar, Dr. G. M. Chaphekar, Dr. S. B. Halligudi, Dr. P. Manikandan, Dr. S. P. Mirajkar, Dr. (Mrs) S. Deshpande, Dr. (Mrs) Pardhy, Dr. N. Devi, Dr. P. Dhepe, Dr. Selvaraj, Dr. Raja, Dr. Bokade, Ms. Samuel Violet, Dr. Nalini Jacob, Dr. S. Ganpathy, Mr. R. K. Jha, Mrs. R. Parischa, Mr. Gholap, Mr. Gaikward, Mr. Jagtap, Mr. Akhbar, Mr. Purushottamm, Mr. Madhu and all other scientific and non-scientific staff of the division and NCL for their valuable help and cooperation.*

*It gives me great pleasure to thank my labmates, Dr. Laha, Dr. Patra, Dr. Mandal, Dr. Ghosh, Dr. Senapati, Dr. Deshmukh, Raina, Pranjal, Rajesh, Sonu, Atul, Ramakanta, Puja, Binu, Pravin, Dr. Bhagawat, Aparna, Tushar and Jutika for listening my woes and making me feel comfortable all the time when I was depressed with the outcomes and lively atmosphere in the lab. Without their supports it wouldnot have been possible to complete this task. I would like to express my gratefulness to colleagues in the division- Dr. Venkatesh, Dr. Shylesh, Dr. Chidam, Dr. Amit Dubey, Dr. (Mrs). Vandana, Surendran, Shrikant, Selvakumar, Prinson, Bala, Rajesh, Jino, Shital, Mehe Jabeen, Trupti, Ankush, Sanyo, Neelam, Dr. Dhanashri, Dr. Trisa, Shanbhag, Suman, Ankur,*

*Dr. Surekha, Dr. Sankar, Rohit, Dr. Kalaraj, Dr. Vijay Raj, Dr. Thiru, Maitri, Devu, Pallavi, Dr. Pai, Dr. Reddy, Sachin, Ganesh, Rao, Sivram, Upendra, Lakshi, Dr. Prashant, Tejas, Umesh and Niphadkar.*

*I would like to convey my appreciation towards my collegues from NCL Singare, Santosh, Yeshwant, Sandeep, Naresh, Mahesh Bhure, Panjab, Ravindra, Pushpesh, Pratap Patil, Dr. Anish, Dr. Sachin, Dr. Manish Chandra, Dr. Nandkumar, and all other research scholars for such a friendly and cheerful working atmosphere, for their constant support, love and care throughout my stay in NCL.*

*I should not forget my beloved friends- Dr. Mangesh, Aniruddha, Niturkar, Balaji, Amar and Santosh. Special thanks to Prashant for kind support and calm listening to me. It has been a great pleasure to share cup of tea and spend the lively time with Prasad, Amit, Rohit and Ankush..*

*I take this opportunity to express my profound respect to my teachers throughout my carrier, who are the key inspiration and help to build up my research career in science.*

*It gives me an immense pleasure to thank my parents and family members for their love, unfailing support, patience, trust and encouragement during many years of studies that they have shown in their own special way. They have been a constant source of strength and determination, and have brought a great deal of happiness to my life.*

*I would like to confess that even though I try my best, it is not possible for me to acknowledge and thank all the known and unknown faces individually for their direct and indirect help for the completion of this work. I am grateful to all of them for their kind cooperation throughout the course of study.*

*Finally, my thanks are due to Council of Scientific and Industrial Research, Government of India, for awarding research fellowships and Dr. S. Sivaram, Director, and Dr. B. D. Kulkarni, Deputy Director, National Chemical Laboratory for allowing me to carry out my research works, extending all infrastructural facilities and to submit this work in the form of a thesis for the award of Ph. D. degree.*

*December 2007* *Mahesh D. Kadgaonkar*

# Table of Contents

# 3. CHARACTERIZATION TECHNIQUES

## List of Figure

## List of Table

## List of Scheme

## Abbreviations

| | |
|---|---|
| AAS | Atomic Absorption Spectroscopy |
| Al $PO_4$-5 | Aluminum Phosphate |
| *BEA | Zeolite Beta with proportion of polymorph B : polymorph A = 55 : 45 |
| BET | Brunauer-Emmett-Teller |
| Conv. | Conversion |
| CTABr | Cetyltrimethylammonium Bromide |
| DABCO | 1, 4-diazabicyclo[2.2.2]octane |
| DIFFaX | Diffracted Intensities From Faulted Xtals |
| FID | Flame Ionization Detector |
| FTIR | Fourier Transform Infrared |
| GC | Gas Chromatography |
| GC-MS | Gas chromatography-Mass spectroscopy |
| GC-IR | Gas chromatography-Infrared |
| HF | Hydrogen Fluoride |
| IPA | Isopropanol (2-Propanol) |
| K | Kelvin |
| MAS NMR | Magic Angle Spinning Nuclear Magnetic Resonance |
| MCM | Mobil Composite Material |
| MEL | Mobile Eleven |
| MFI | Mobil Five |
| MOR | Mordenite |
| MTG | Methanol To Gasoline |
| NCL-5 | Polymorph B-enriched analog of zeolite Beta with proportion of polymorph B : Polymorph A = 90 : 10 synthesized at National Chemical Laboratory. |
| NCL-6 | Polymorph B-enriched analog of zeolite Beta with proportion of polymorph B : Polymorph A = 75 : 25 synthesized at National Chemical Laboratory. |
| NCL-7 | Polymorph B-enriched analog of zeolite Beta with proportion of |

| | |
|---|---|
| | polymorph B : Polymorph A = 65 : 35 synthesized at National Chemical Laboratory. |
| QENS | Quasi Electron Neutron Scattering |
| SBU | Secondary Building Unit |
| SDA | Structure Directing Agent |
| SEM | Scanning Electron Microscopy |
| TBAOH | Tetrabutylammonium Hydroxide |
| TBU | Tertiary Building Unit |
| TEOS | Tetraethylorthosilicate |
| TOF | Turn Over Frequency |
| TPAOH | Tetrapropylammonium Hydroxide |
| UV-Vis | Ultraviolet-Visible |
| USY | Ultra Stable Y |
| PXRD | Powder X-ray Diffraction |
| ZSM | Zeolite Synthesized Mobil |

## 1.1. GENERAL BACKGROUND AND INTRODUCTION

Zeolites are crystalline microporous silica based materials, which are extensively used as heterogeneous catalysts in industry particularly in oil refining, petrochemical sector and production of fine and speciality chemicals.[1-3] Zeolites play an important role particularly dealing with the molecules having kinetic diameters below 1 nm. Therefore, the study on the synthesis, characterization and catalytic applications of different types of zeolites and related materials form a useful subject in heterogeneous catalysis.

Traditionally, zeolites (aluminosilicates) are defined as crystalline materials in which Si and Al are tetrahedrally coordinated by oxygen atoms in a three-dimensional network. The crystallographic unit cell of the zeolites may be represented as:

$$M_{x/n}\,[(AlO_2)_x\,(SiO_2)_y]\,zH_2O$$

Where M is a charge compensating cation with valency '*n*'. The ratio '*x/y*' may have value ranging from zero to one. The number of water molecules, which can be reversibly adsorbed and desorbed in the zeolite pores, are represented by '*z*'. The presence of trivalent Al atoms in the lattice develops a unit negative charge per Al atom in the framework, compensated either by cation such as proton ($H^+$) thus producing acidity in zeolites.

Following main characteristics of the zeolites are responsible for the utility of these materials as workhorses in chemical industry:

- High surface area and adsorption capacity.
- Tunable adsorption properties from hydrophobic to hydrophilic.
- Active sites, for example acid sites, can be generated in the framework and their strength and concentration can be tailored for a particular application.

- The sizes of their channels and cavities match with the dimensions of most of the molecules involved in various chemical processes (i.e. 0.55-1.2 nm), and the strong electronic fields existing in those micropores together with an electronic confinement of the guest molecules.
- The complex channel structure in the zeolites allows different kinds of shape selectivities, i.e. product, reactant, and transition state.

In view of the growing industrial importance and inherent scientific interest in structural complexity and diverse chemistry of these materials, considerable efforts have been directed into synthesis of zeolites. There has been subsequent rise in the number of known synthetic zeolites and also the discovery of zeolite-like or zeolite related materials referred as "zeotypes".[3-4]

## 1.2. NOMENCLATURE

Although, there is no systematic nomenclature for molecular sieve materials, the structure commission of International Zeolite Association (IZA) and IUPAC have assigned a three capital alphabets as structural codes to synthetic and natural zeolites.[5-8] These three capital letters have been used to identify structure types (Table 1.1). The codes for zeolite identification have generally been derived from the names of the type of species, and do not include numbers and characters other than roman letters. Structure type codes are independent of chemical composition, distribution of various possible T atoms, (e.g. $Si^{4+}$, $Al^{3+}$, $Ti^{4+}$, etc.), cell dimensions or crystal symmetry.

**Table 1.1**

Some Common Structural Codes of Zeolites

| Structural Codes | Zeolites |
|---|---|
| FAU | Faujasite: X and Y |
| MFI | Mobil Five: ZSM-5 |
| MEL | Mobil Eleven: ZSM-11 |
| MOR | Mordenite |
| FER | Ferrierite |
| BEA | Beta |

## 1.3. CLASSIFICATION

Several attempts have been made to classify the families of zeolites on the basis of their crystal structure,[1,2,9] chemical composition,[1,2,10] effective pore diameter[1,2,11] and natural occurrence.[1,2] The detail account is summarized below.

### 1.3.1. Nature of Secondary Building Units

Smith,[12] Fischer[13] and Breck[14] classified zeolites on the basis of differences in the secondary building units (SBU) (Fig.1.1). SBU are the aluminosilicate oligomers having chain, ring and cage like structures, which are basic building units of zeolite framework structure. The different SBU are pictorially presented in Fig.1.1. These secondary building units combine together in different combination to form zeolite structures. All known zeolitic structures can be synthesized using the secondary building units mentioned above.

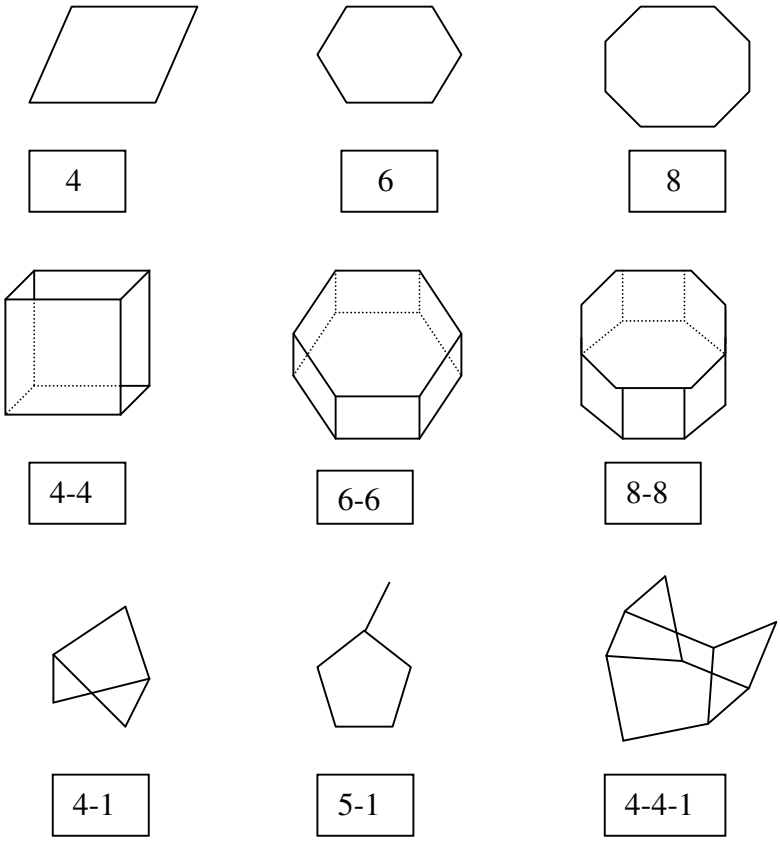


**Figure 1.1.** Secondary Building Units (SBU) in zeolite synthesis **[Source: Ref. 3]**

### 1.3.2. Chemical Composition

Flanigen classified zeolites using their chemical composition.[10] Depending on silica to alumina ratio zeolites are classified as low silica zeolites, intermediate silica zeolites, high silica zeolites and pure silica zeolites (silicalites) (Table 1.2).

**Table 1.2**

Classification of Zeolites on the Basis of Chemical Composition

| Type | Si/Al ratio | Examples |
|---|---|---|
| Low silica | 1.0 to 1.5 | Sodalite, A, X |
| Intermediate silica | 2 to 5 | L, Mordenite, Omega, FAU |
| High silica | 5 to several thousands | ZSM-5, EU-1 |
| Silicate (all silica) | ∝ | Silicate-1, Silicate-2, Si-NCL-1 |

### 1.3.3. Pore Opening Size

Zeolites have also been classified according to their effective pore diameter. The effective pore diameter of the zeolite depends upon the number of tetrahedra present in the ring aperture. On the basis of pore openings, zeolites are commonly classified into small pore (6 or 8-member ring), medium pore (10-member ring), large pore (12-member ring) and ultra large pore (14-or more member ring). Table 1.3 illustrates the examples on the basis of pore size classification.

**Table 1.3**

Classification of Zeolites on the Basis of Effective Pore Diameter

| Pore size | Ring size | Pore Diameter (nm) | Example | Ref |
|---|---|---|---|---|
| Small | 8 | 0.42 | Ca A | 15 |
| | 8 | 0.45 | ZSM-39 | 7 |
| Medium | 10 | $0.53 \times 0.56$ | ZSM-48 | 7 |
| | 10 | $0.53 \times 0.56$ | ZSM-5 | 16 |
| Large | 12 | 0.74 | Faujasite | 17 |
| | 12 | 0.74 | USY | 18 |
| | 12 | $0.55 \times 0.59$ | ZSM-12 | 19 |
| | 12 | $0.57 \times 0.71$ | Mordenite | 7, 20 |
| | 12 | $0.68 \times 0.72$ | Beta | 21, 22 |
| Extra Large | 14 | $0.75 \times 1.0$ | Si-UTD-1 | 23 |

## 1.4. ZEOLITE SYNTHESIS

Molecular sieves, particularly, zeolites are finding widespread application in diverse areas. The close connection between the microscopic structure and the macroscopic properties of these materials allows one to use molecular sieves to recognize, discriminate, and organize molecules with precisions. The utility of these materials leads to the increase in curiosity towards synthesis of new zeolites and zeolite-

like structures. Till recently, more than 175 synthetic zeolites have been reported and the urge for newer structures still exists in the researchers working in material science.

Zeolites are usually crystallized under hydrothermal conditions, at basic pH and temperatures in the range of 333-473 K, from gels containing the silica and alumina sources, basic reagents and alkali metal cations. In many cases, the zeolite synthesis requires the presence of organic compounds (quaternary ammonium salts, amines, alcohols, etc.), that may play the role of pore filling agents or act as templates that direct the crystallization towards the formation of a specific structure. Developments in zeolite synthesis include the use of (i) $F^-$ ion, (ii) non-aqueous solvents and (iii) heating by microwave radiation.[24-27]

Zeolites are metastable phases that are produced via kinetic path. A thermodynamic analysis of zeolite synthesis shows that both enthalpic and entropic driving forces are responsible. In the presence of aqueous medium, the structure directing agents (SDA) become hydrophobically hydrated, which provides these two forces that drive zeolite crystallization. The enthalpic force arises due to clathering of SDA in the hydrophobic silicate and the entropic force is due to release of hydration sphere. As the zeolites crystallization is a kinetically controlled process, it is usually the structure that nucleates first that is ultimately produced.[28-30] In more aluminum rich synthesis, zeolites with large cavities (connected by small pore networks) are the likely products if the guest organo-cation (template) is incorporated into the crystallizing host lattice. In the high silica synthesis, large pore zeolites can be obtained but they tend to be one dimensional, parallel pore systems. The cavity-type materials are more likely to be formed with the smaller organo-cations. Zeolite crystallization proceeds through two primary steps:

nucleation of discrete particles of new phase, and subsequent growth of those entities. Fig.1.2 illustrates the proposed structure for the inorganic-organic entities, and their role in synthesis process.[31]

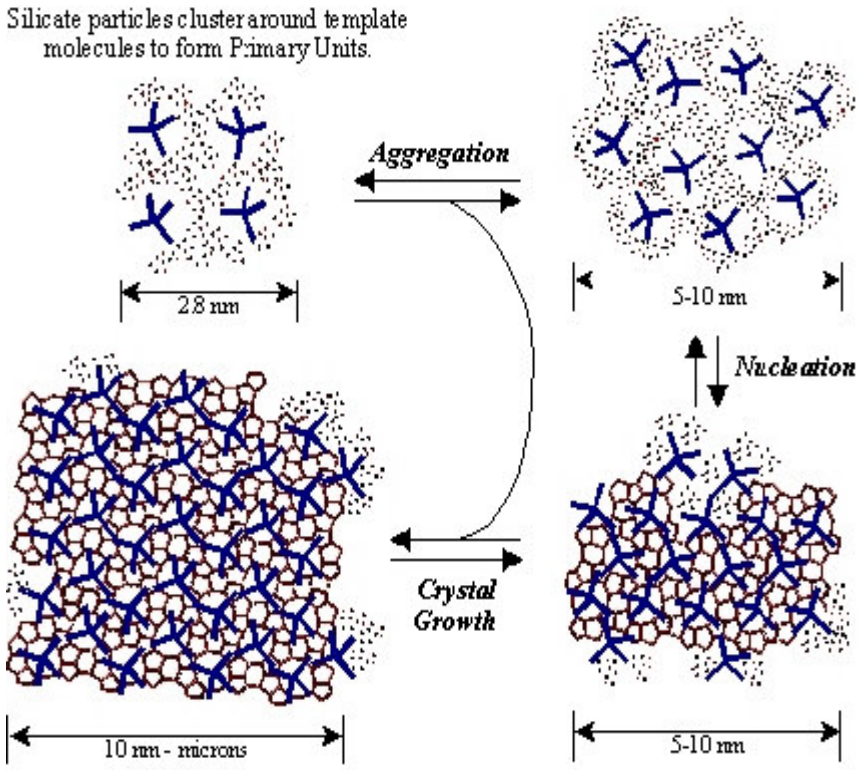


**Figure 1.2.** Schematic illustration of the proposed conceptual model for the template facilitated nucleation and crystal growth of all silica ZSM-5. **[Source: Ref. 29]**

### 1.4.1. Factors Affecting Zeolite Synthesis

There are several factors that influence the synthesis of zeolites. Each variable contributes to the specific aspect of the crystallization. However, there is substantial interplay between these elements during the course of crystallization. Various important parameters that affect the synthesis of molecular sieves may be categorized as follows.

- Historical Parameters:
    - Aging
    - Seeding
- Physical Parameters:
    - Temperature
    - Time
- Chemical Parameters:
    - Silica/Alumina Ratio
    - Hydroxide Concentration
    - Role of Inorganic Cation
    - pH of Synthesis Gel
    - Structure Directing Agent or Template
    - Water Content

Influence of these parameters is discussed below in detail.

#### *1.4.1.1. Historical Parameters*

Along with physical and chemical parameters, historical parameters have an effect on the zeolite synthesis. The commonly observed historical parameters are aging, stirring and seeding.

##### *1.4.1.1.1. Aging*

The process, where the initial reaction mixture or gel is cured/aged at certain temperature (most preferably at room temperature) is referred as aging. Aging of

synthesis gel helps in distribution of particular precursor unit required for desired zeolite. The synthesis of zeolite Y using colloidal silica requires an aging step prior to hydrothermal crystallization in order to avoid the formation of impurities of zeolite P and S.[1,32]

#### *1.4.1.1.2. Seeding*

Seeding means the addition of the pre-synthesized material in small quantity (roughly 2-5 wt %). The use of seed results in reduction of synthesis time and synthesis of desired phase with consequent reduction/elimination of potential impurities. It is also possible to exercise control over crystal size distribution.[33-36] The enhanced rate of synthesis can be attributed not only to the increase in rate at which the solute is integrated into solid phase from solution due to increase in the available surface area, but also might be the result of enhanced nucleation of new crystals. When the synthesis of EUO-type zeolite (EU-1, ZSM-50) was carried out using 5 wt % seed with respect to silica, the desired phase is obtained in 72 h at crystallization temperature of 423 K.[37] In the absence of seed, the reaction mixture gives low yield and higher content of impurity phases such as EU-2 and cristobalite, and takes 154 h.

Apart from above factors the stirring condition and stirring speed also affect the synthesis of zeolite.

#### *1.4.1.2. Physical Parameters*

Temperature and crystallization time are the two important physical parameters that influence the synthesis of zeolites.

#### *1.4.1.2.1. Temperature*

Temperature influences several factors involved in zeolite synthesis. It can alter the zeolite phase as well as the induction period. The decrease in the induction period is observed with increase in temperature. As a thumb rule, the rate of crystallization increases with temperature. However, it is important to note that variation in the temperature may also lead to the formation of other phase. The synthesis of ZSM-11 represents a typical example of effect of the temperature on the crystallization of phase from a molar gel composition.[38]

$$33\ Na_2O : 0.1\ Al_2O_3 : 110\ SiO_2 : 40\ TBPCl : 7150\ H_2O : 22\ H_2SO_4$$

Where TBPCl represents tetrabutylphosphonium chloride

At lower temperature (below 403 K) pure phase of ZSM-11 was obtained. The rate of crystallization of ZSM-11 phase is found to increase with temperature. But when the synthesis gel was heated at the temperatures above 423 K, ZSM-5 phase was formed.

#### *1.4.1.2.2. Time*

Synthesis time plays an important role in the formation of particular zeolitic phase. It follows Ostwald's law of successive transformation. At constant temperature and initial molar gel composition, the transformation proceeds from amorphous to metastable to more stable phase. The thermodynamically least stable phase will crystallize fast, and successively replaced by more stable phases with time.[39] During synthesis of zeolite Y, the amorphous phase initially yields faujasite phase and further gets converted into zeolite P with time.

### *1.4.1.3. Chemical Parameters*

Chemical parameters such as silica alumina ratio, $OH^-$ concentration, template, presence of inorganic cation and water concentration influence the zeolite synthesis. All these parameters control the synthesis of zeolitic phases.

#### *1.4.1.3.1. Silica/Alumina ratio*

The presence of hetero metal ion like $Al^{3+}$ in the gel places a constraint on the framework composition of the zeolite. All the aluminum present in the reaction mixture normally occupies framework positions in the zeolite leaving varying amounts of silicate in solution, depending upon other factors such as hydroxide ion concentration and the presence of various organic and inorganic cations in the synthesis gel. Changing $SiO_2/Al_2O_3$ ratio in the input gel in order to obtain the desired amount of aluminum in the obtained product sometimes changes the zeolitic phase. For example, analcime can be obtained with silica/alumina ratio in the range of 4 to 5. When the silica/alumina ratio is increased to 8, the obtained phase was mordenite. Further increase in Si/Al the ratio to 12 yields non-zeolitic quartz.[2]

Generally an increase in the silica/alumina ratio in zeolite leads to

- Increased acid resistance
- Increased thermal stability
- Increased hydrophobicity
- Decreased affinity for polar absorbates
- Decreased cation content

***1.4.1.3.2. Hydroxide concentration***

The hydroxide content in the reaction mixture influence molecular or polymeric species present in the reaction mixture as well as the rate of hydrolysis. It modifies the nucleation time by influencing the transport of silicates from solid phase to solution and further enhancing the crystal growth by influencing the transport between the solution phases and growing crystals.[40] In short, it controls phase purity by influencing the rate of transport of silicate species from one crystalline phase to another. Therefore, it is worth of mentioning that $OH^-$ may also serve as a structure director.

An increase in hydroxide concentration to an optimum value in the reaction mixture accelerates the crystal growth and shortens the induction period, which in turn leads to the decrease in the crystallization period. The decrease in the nucleation time can be attributed to high concentration of the reactant dissolved in alkali by increasing hydroxide concentration in initial gel. The nuclei will grow more quickly due to numerous encounters between the more concentrated precursor species in solution phase. Due to higher solubility of silicon species in hydroxide ion in comparison with aluminum species, higher $OH^-$ in the reaction gel prefers the formation of lower silica/alumina ratio. Also, the higher hydroxide concentration leads to the lower yield. Crystallization time and yield decreases with increase in hydroxide ion concentration.[41]

***1.4.1.3.3. pH of synthesis gel***

The pH of the reaction mixture does not relate directly to the total hydroxide content in the system, however it appears as an important parameter in the synthesis of zeolite in terms of the presence of free $OH^-$ ions in the system. Although, the reaction

mixtures in zeolite synthesis are generally alkaline before crystallization begins, one can easily note the increase in the pH with the crystal formation particularly in the case of high silica zeolite synthesis. The rise in pH with crystallization is due to the incorporation of $SiO_2$ unit in the framework. Crystallization is accompanied with the rise in free OH/Silica molar ratio. However, incorporation of aluminum species does not affect the pH. In short, monitoring pH of the gel during crystallization provides first hand information about the formation of zeolitic structure, especially for more silica-rich samples.[42,43]

#### *1.4.1.3.4. Role of inorganic cation*

Apart from working as counter ion to balance the zeolite framework charge, the inorganic cation often plays dominant role in determining the structure to be obtained. These cations also play an important role in crystal morphology, crystallinity and the yield of the product.[1] Role of various inorganic cations such as Li, Na, K and Cs has been studied in the hydrothermal synthesis of the silica polymorph of zeolite NCL-1 (Si-NCL-1). The crystallization time decreases in the order (Cs + Na) > K > Na > (Li + Na) under identical gel composition and crystallization condition. The samples prepared using different inorganic cation shows typical needle shaped crystals with a crystal size ranging from 3-5 pm.[44 a] In some cases, the morphology of the zeolites synthesized in presence of different cations varies with the change in cation. During the synthesis of high silica ZSM-5 contribution of alkali ions play vital role in the morphology as reported earlier.[44 b] In this system these inorganic cations are found to have a pronounced effect on the time of nucleation and the size of the resulting crystals. Crystal size of the resultant sample

changes from few micron to 20 micron and finally to 26 micron with change in inorganic cations from $NH_4^+ \rightarrow Na^+ \rightarrow K^+$. When the synthesis trials were conducted using lithium cation, the formation of large lath shaped ZSM-5 crystals over 100 micron in length was observed. Besides the change in size of ZSM-5 crystals obtained, the alkali metal cation also affects the crystallization time. In the absence of alkali metal cation the crystallization time was found to be significantly longer.

#### *1.4.1.3.5. Structure directing agent or template*

Certain organic quaternary ammonium cations and amines act as structure directing agents (SDA), void filler and/or gel modifier or mineralizer. These amines/organic cations are trapped inside the pores of molecular sieves during nucleation and crystal growth. Although, the exact mechanism for the templating effect is not fully understood, it is visualized that zeolites grow around the template and stabilize certain pore structures and subunits. Interestingly, a particular organic molecule can lead to the different molecular sieves framework and different organic molecules utilized in the gel lead to the formation of a particular structure. For instance, tetramethylammonium cation can form as many as 17 structures. Clearly, the presence of other cation(s) and substantially different gel chemistry also influence the formation of different structure from same SDA.[2] Similarly the structure of $AlPO_4$-5 can be formed in the presence of 23 SDAs. The cross-sectional size of these organic species varies from ~ 6 Å for choline and DABCO to 8 Å for TPA. This is due to the fact that some organic species must fit better than others in the straight channel (~7.4 Å) of $AlPO_4$-5 indicating that template-fit is not

the only factor in structure determination. Table 1.4 depicts different organic templates and the zeolite structure formed.

**Table 1.4**

Organic Template and Correspondingly Formed Zeolite Structure

| Organic additive | Zeolite structure |
|---|---|
| Tetramethylammonium (TMA) | Gismondine, sodalite, gmelinite, faujasite, zeolite E, A, ZSM-4, Nu-1, Fu-1, P, O, Offertite, ZSM-47, ZSM-6, ZSM-39 |
| Tetraethylammonium (TEA) | ZSM-8, ZSM-12, ZSM-20, ZSM-5, Mordenite, Beta |
| Tetrapropylammonium (TPA) | ZSM-5 |
| Tetrabutylammonium (TBA) | ZSM-11, ZSM-12 |
| 1, 2-diaminoethane | ZSM-5 |
| 1, 3-diaminoproane | ZSM-5, ZSM-35, ZSM-21 |
| 1, 4-diaminobutane | ZSM-35, ZSM-5 |
| 1, 5-diaminopentane | ZSM-5 |
| 1, 6-diaminohexane | ZSM-5, ZSM-22 |
| 1, 7-diaminoheptane | ZSM-11 |

***1.4.1.3.6. Water content***

Water content in initial reaction gel plays crucial role in zeolite synthesis. Water is supposed to interact strongly with cations present in the solution, thus itself becoming the part of "template" for structure direction. In presence of water, the organic cation as well as the silicate species get hydrated leading to the formation of specific structure.

Transport properties within the gel and viscosity of the reacting gel change with water concentration. Amount of water in the reacting gel sometimes determine the structure that will be formed under similar synthesis conditions. In mordenite synthesis, for example, the production of large pore mordenite depends strongly on water content.[46] The $H_2O/Na_2O$ ratio in the starting mixture is inversely proportional to the alkalinity. With increase in $H_2O/SiO_2$ ratio and at constant temperature, time and silica/alumina ratio, the trends in the product formation were: analcime/phillipsite $\rightarrow$ mordenite $\rightarrow$ amorphous phase. At higher $H_2O/SiO_2$ in the initial mixture corresponds to lower concentration of various components (aluminum and silicon) in the liquid phase. This in turn results in the formation of the less metastable phase. Conversely, lower ratios of $H_2O/SiO_2$ in the starting mixture correspond to higher concentration of various components in the liquid phase, resulting in the formation of more stable phases.[47,48] Generally, increase in the water content in the gel ($H_2O/SiO_2$) leads to increase in overall synthesis time and larger crystallites.[49] In the present study, an increase was observed in the concentration of polymorph of B in BEA type structure from 65 % to 95 % by the varying the water content in the gel ($H_2O/SiO_2$) from 9.5 to 7.5 in presence of perchloric acid as promoter using hydrogen fluoride as mineralizer.[50,51]

The important role played by water in the crystallization of zeolite structure is further reinforced by the results obtained from crystallizing systems containing nonaqueous system.[52,53] In contrast to wide diversity of structures formed with aqueous systems, only few zeolites were found to crystallize in the presence of nonaqueous solvents. The commonly used nonaqueous solvents are hexanol, propanol, glycol, glycerol, sulfolane and pyridine.

## 1.5. USE OF FLUORIDE AS MINERALIZER

Flanigen and Patton demonstrated for the first time use of fluoride ion as mineralizer in the synthesis of Silicalite-1.[54] Most common and preferred fluoride sources are $NH_4F$, $NH_4HF_2$ and HF. Fluoride may also be combined with the source of framework material elements such as $(NH_4)_2SiF_6$ or $AlF_3.H_2O$ and can released on hydrolysis. The utility of fluoride as mineralizer spread its application from high to low pH systems and further to non-aluminosilicate syntheses.[55-58] It is paramount to mention that the structures, which could not be achieved using the hydroxide route, can be realized using this system.[59-60] This may be through access to new regions of synthetic chemistry. The important issue is the incorporation of fluoride ion into the product. The unambiguous location of fluoride by diffraction or MAS NMR methods have shown that the $F^-$ ion appears always to be occluded in small cages within the zeolite framework, usually close to a 4-T-ring window.[61,62] Fluoride ions could therefore be considered as a structure-director[63] and has been shown from NMR studies to interact strongly with framework silicon atoms.[64,65] Influence of fluoride ions on the crystallization kinetics of zeolite Y was studied by Lindner and Lechert.[66] On comparing $Al(OH)_4^-$ and $AlF(OH)_3^-$ as potential growth species, their incorporation into the growing crystals was identified as the rate-determining step of zeolite Na-Y crystallization in this system. Materials prepared by fluoride medium show low density of Si-OH groups (connectivity defects) probably due to the combination of various factors such as charge balance between $F^-$ and $SDA^+$, low synthesis pH, absence of $Si\text{-}O^-\ldots HO\text{-}Si$ hydrogen bonds. The low density of connectivity defects in materials prepared through fluoride route has important implications on the synthesis of high silica porous materials.

## 1.6. USE OF OXYANIONS AS PROMOTER

Most of the zeolites made by hydrothermal synthesis suffer from the impediment of long crystallization time. Ever since the discovery of the synthetic zeolites, consistent efforts have been made to decrease their synthesis time.[67] Kumar *et al*. reported that the addition of catalytic amount of certain oxyanions such as $ClO_4^-$, $PO_4^{3-}$, $NO_3^-$, $SO_4^{2-}$, $CO_3^{2-}$, $AsO_4^{3-}$, $ClO_3^-$, $BrO_3^-$ and $IO_3^-$ was found to enhance the crystallization process significantly in variety of zeolitic structures.[68] These oxyanions can be used either as acids or as sodium or potassium salt depending upon the need to keep the molar gel composition constant. Along with enhancing the nucleation and crystallization, they stabilize the less metastable phases. The crystallite size of the samples prepared using promoter was found to be smaller and more uniform. This can be attributed to the enhanced nucleation and crystallization rate. The polarizing ability and charge to radius ratio of these oxyanions are the key factors for increasing crystallization rate and stabilizing the phases. The presence of promoter oxyanions greatly polarizes the hydrophobic hydration spheres formed around silicate units and alkyl group of structure directing agents (SDA), thereby facilitating the overlap of SDA-enclathrated silicate polyanions. Such overlapping, in turn, gives rise to the formation of the composite species at the onset of crystallization. In support of this view, a good correlation was observed between the charge to radius ratio of central cation of promoter oxyanions and the corresponding crystallization time as shown in Fig. 1.3. Rate of crystallization was found to increase with charge to radius ratio of promoter. The polarizing ability of promoter follows the order $NO_3^-$> $ClO_4^-$> $ClO_3^-$> $PO_4^{3-}$> $SO_4^{2-}$> $CO_3^{2-}$> $AsO_4^{3-}$> $IO_3^-$> $BrO_3^-$.[68-70] Similarly, mesoporous MCM-41 and MCM-48 materials were synthesized

using heteropolyacids as novel promoters, and a probable mechanism for the rapid nucleation was proposed on basis of HSAB theory. Authors from our laboratory reported 3 to 4 times decrease in the syntheses times of the mesoporous materials by catalytic addition of Keggin type heteropolyacids, compared to the conventional approaches.[71]

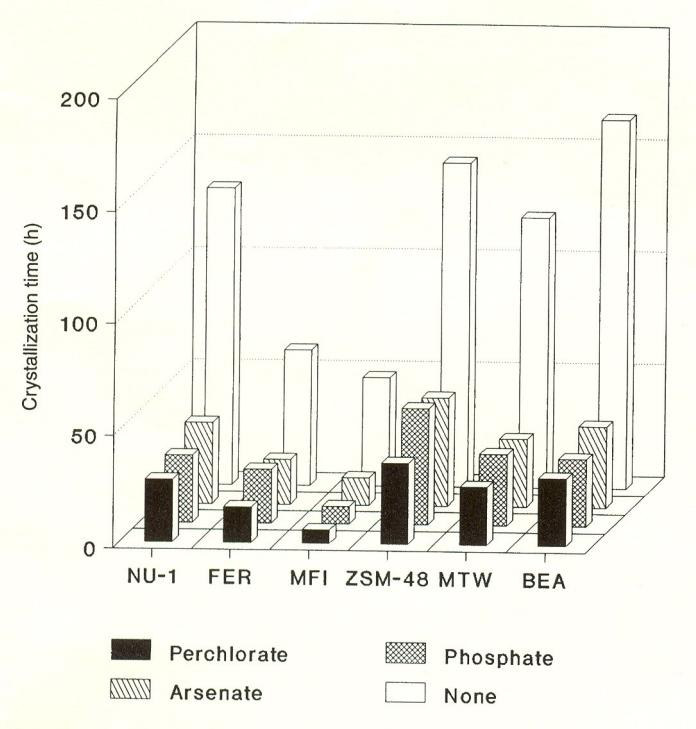


**Figure 1.3**. Effect of different promoters on crystallization time (hours) of various zeolites. **[Source: Ref. 69]**

## 1.7. FAULTING IN ZEOLITIC STRUCTURE

Faulting within the zeolite framework is one of the major difficulties encountered in the structural analysis. When faulting occurs repeatedly but in an irregular manner the resulting structure is disordered. When the repeat distances between the faults become small enough, the diffuse strips perpendicular to the fault planes are observed in the powder X-ray diffraction (XRD) pattern. When the fault planes repeat in every unit cell a

new framework topology emerges. Faulting on a very small and/or irregular frequency will seriously hamper a precise structure determination. Broad and sharp peaks in the powder pattern indicate the faulting in the structure. It is noteworthy that powder pattern can also have broader and sharper lines when one dimension of the crystal is very thin. However, this can be easily noticed using electron microscopy photographs.

Attempts have been made to explain the faulting in the structure and to postulate the resulting powder pattern. Examples on the studies of zeolite types such as BEA, FAU-EMT, MFI, MEL, OFF-ERI, RUB-n and SSZ-n/CIT-n series are well documented in the literature. Different intermediate phases and unfaulted examples of the end members can be obtained for other intergrown materials. Thus the end members of FAU and EMT,[72] MFI and MEL, OFF and ERI, some end members in RUB-n series (zincosilicates RUB-17)[73] and VPI-7 (VSV),[74,75] beryllosilicate lovdarite (LOV),[76] decasil RUB-3 (RTE),[77] borosilicate RUB-13 (RTH),[78] and one end member in the SSZ/CIT series (borosilicate CIT-1) (CON)[79,80] are hypothetically proposed. The synthesis of these materials can be realized using proper choice of synthesis conditions and templates. Partial blocking of the pores can occur in some of the faulted intergrowths, thereby drastically changing the properties of the materials.

Among all the molecular sieves, zeolite Beta represents a classical example of faulting within the structure. Zeolite Beta, synthesized by Wadlinger *et al*., is one of the most useful high silica zeolite.[45] Its interconnected large pore network and strong acidity give zeolite Beta special catalytic properties. It is highly disordered, made up of random intergrowth of polymorph A and polymorph B in the ratio *ca.* 45 : 55, respectively.[1-3,81,82] Polymorph A, forms an enatiomorphic pair, space group symmetries $P4_122$ and $P4_322$,

with a = 1.25 nm, c = 2.66 nm. Polymorph B is a achiral structure with space group C2/c and a = 1.76 nm, b = 1.78 nm, c = 1.44 nm, β = 114.5° were theoretically proposed by Newsam *et al*.[83] Both the polymorphs A and B are constructed from the same centrosymmetric, tertiary building unit (TBU) arranged in layers successively which interconnect either in left handed (L) or right handed (R) manner. Polymorph A represents uninterrupted sequence either left handed or right handed (LLLLLLL …or RRRRRR …), whereas the polymorph B has alternative stacking sequence (RLRLRL… or LRLRLRLR…). TBU has no preference for either mode of connection leading both to occur with almost equal possibility in the structure of Beta, which enhances the growth of faulty structure. The faulting in zeolite Beta does not affect the accessible pore volume but influences the tortuosity along *c* direction. The high stacking fault gives rise to complex powder X-ray diffraction (PXRD) pattern comprising both sharp and broad features. By exploiting recursive relation between possible stacking sequences, calculated PXRD pattern as a function of faulting probability shows *ca.* 60 % chiral stacking sequence showing slightly higher preference for polymorph B in comparison with polymorph A. Another analog of BEA family, polymorph C (not present in zeolite Beta) was also proposed along with polymorph A and polymorph B. In contrast to these two polymorphs, polymorph C consists of double 4-ring (D4R) cages as secondary building units and a 3D intersecting channel formed by straight 12-ring pores. The synthesis of polymorph C was recently reported.[84] However, it is pertinent to mention that the synthesis of pure polymorph A or B or even altering the polymorphic proportion in zeolite Beta eluded the scientific society till very recent reports from our laboratory.[50,51]

Following are representative structural modules for polymorph A (Fig. 1.4), polymorph B (Fig. 1.5) and polymorph C (Fig. 1.6).[85] Figure 1.7 shows proposed powder X-ray diffraction pattern of zeolite Beta with different intergrowth of polymorphs ranging from 0 % polymorph B to pure 100 % polymorph B with an increment of 10 %, calculated computationally using diffracted intensity from faulted complex materials exploiting the recursive properties of faulting sequence in crystals.[83] Figure 1.8 illustrates detail account of possible structure distortions and their influence over subsequent stacking of layers using eight distinct layer types in zeolite Beta. The notation ABCD and A'B'C'D' represents these eight layers. These notations represent four mutually rotated layers and their enantiomorphs. The end member polymorph A formed by right handed stacking, the four layers stack in such a fashion that layer A is followed by B, C and D. Previous layer is rotated by right handed rotation by +90 ° to obtain the next layer. For a perfect right handed crystal of polymorph A, the stacking repeats in ABCDABCD….. sequence. Similarly, for left-handed enantiomorph follows the stacking sequence A'B'C'D'A'B'C'D'… etc. On the other hand, polymorph B with C2/c space group can stack as AB'AB'AB'…, or BA'BA'BA'……, etc. For proper connectivity, layers can not attach to other layers which are related by 0° or 180° rotations. Therefore, A can not attach to the layers of type A and A'. Similar restrains apply to all other layer.

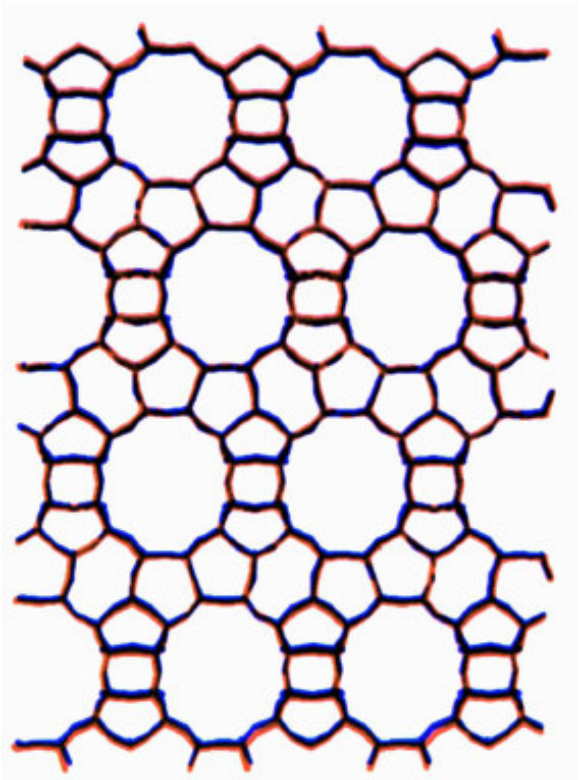

**Figure 1.4.** Energy minimized (orange) and proposed (blue) structures of polymorph A. **[Source: Ref. 85]**

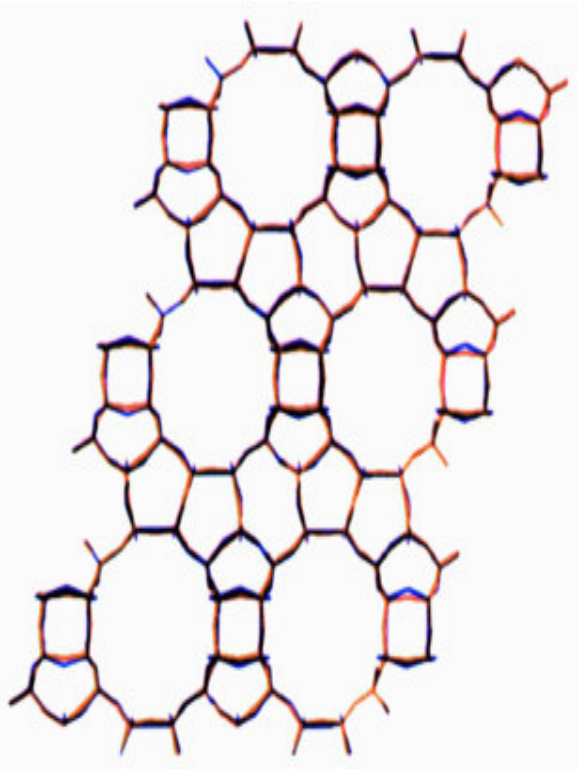

**Figure 1.5.** Energy minimized (orange) and proposed (blue) structures of polymorph B. **[Source: Ref. 85]**

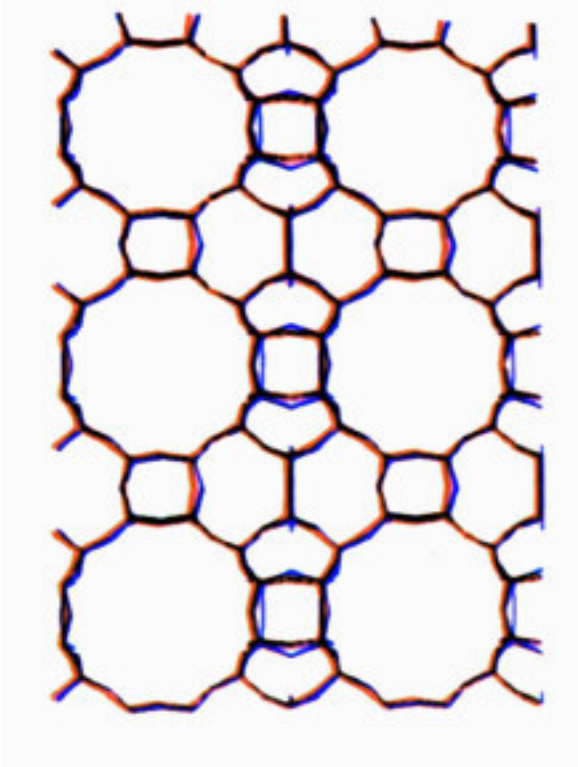

**Figure 1.6.** Energy minimized (orange) and proposed (blue) structures of polymorph C. **[Source: Ref. 85]**

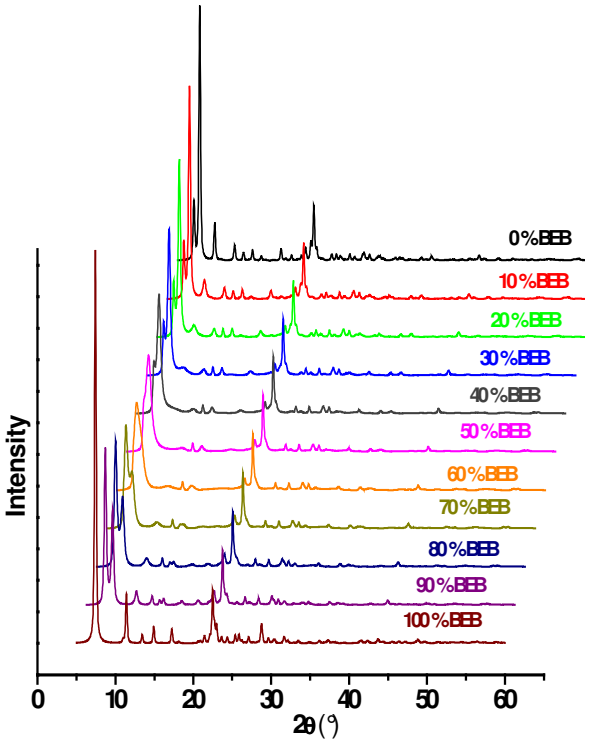


**Figure 1.7.** Simulated powder XRD pattern of the BEA "Polymorph B" series in steps of 10 % intergrowth. The 0 % BEB pattern corresponds to the 100 % "Polymorph A" pattern. **[Source: Ref. 83]**

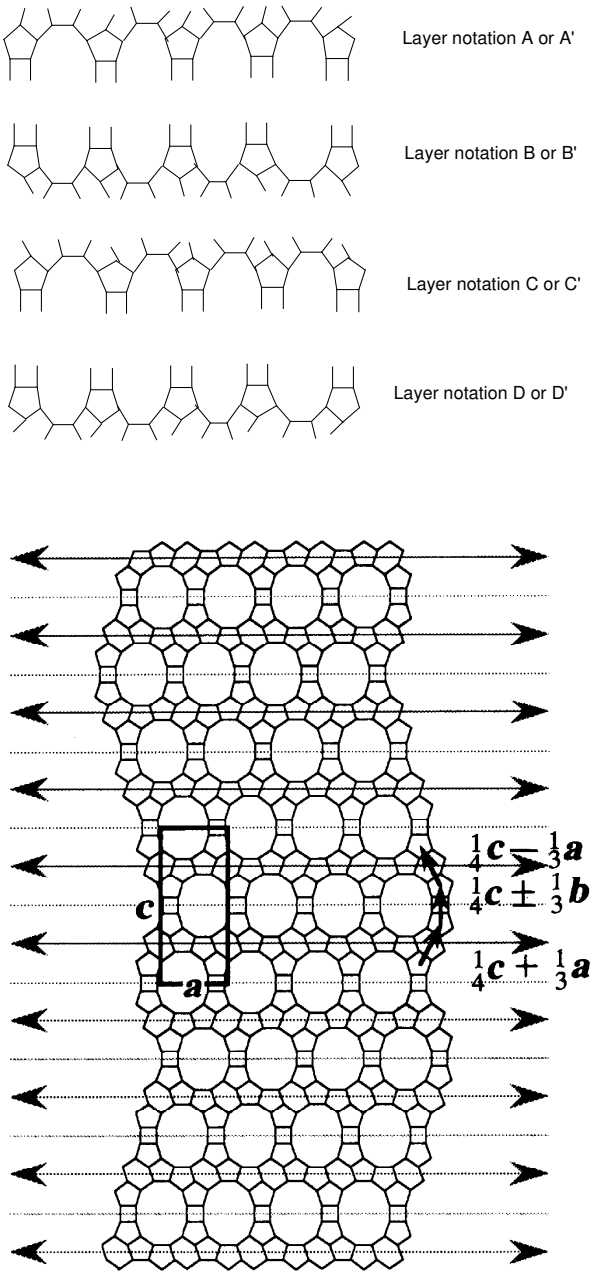


**Figure 1.8.** The framework of typical zeolite Beta crystallite along [100] view. **[Source: Ref. 86]**

## 1.8. PHYSICO-CHEMICAL CHARACTERIZATION

A number of techniques have been used to characterize different types of microporous and mesoporous molecular sieve materials. Each technique is unique by itself and provides important information for the understanding of different structural features of a particular material. Following instrumental methods are commonly used to characterize the zeolites.

1. Powder X-ray diffraction
2. Diffuse reflectance UV-Vis spectroscopy
3. Fourier transform infrared (FTIR) spectroscopy
4. Nuclear magnetic resonance (NMR) spectroscopy
5. Atomic absorption spectroscopy (AAS)
6. Scanning electron microscopy (SEM)
7. Surface area and porosity measurement by nitrogen adsorption

### 1.8.1. X-Ray Diffraction

Powder X-ray diffraction is the most important and commonly used tool to monitor structure, phase purity, degree of crystallinity and unit cell parameters of crystallite materials. Microporous solids generally show characteristic peaks in the $2\theta$ range of 5-50º. Isomorphous substitution of a heteroatom in the framework of the molecular sieves can be easily predicted by calculating the changes in the unit cell parameters and unit cell volume. This is one of the indirect ways to confirm isomorphous

substitution.[87,88] X-ray diffraction is one of the nondestructive techniques and does not require elaborative work for the sample preparation.

X-ray diffraction broadening analysis has been widely used to determine the crystal size of the materials. The crystallite size L in Å can be estimated using corrected line broadening β in the sample using the Scherrer equation: $L = k\lambda / \beta\cos\theta$, where L = thickness of the crystal, *k* is a constant approximately 0.9-1.0, λ = wavelength of X-rays, β = corrected line broadening measured in radian.[89] Above all, powder X-ray diffraction pattern is preferentially used for the structure determination of unknown materials.

### 1.8.2. Diffuse Reflectance UV-Vis Spectroscopy

The diffuse reflectance UV-Vis spectroscopy is known to be a very sensitive and useful technique for the identification and characterization of the metal ion coordination and its existence in the framework or extra-framework position in metallosilicate molecular sieves. The position of "ligand-to-metal charge transfer" (L→M) band depends on the ligand field symmetry surrounding the metal center and the electronic transitions from ligand-to-metal require higher energy for a tetra-coordinated metal ion than for a hexa-coordinated one. For most of the isomorphously substituted microporous and mesoporous metallo-silicate (particularly Ti- and V-containing) molecular sieves,[90-92,70] transitions in the UV region (200-400 nm) are of prime interest. Ti-containing samples exhibit a strong charge transfer band at *ca*. 220, 260, 330 nm. Band at *ca*. 220 nm reflects tetra-coordinated titanium in the walls of zeolitic materials. Charge transfer bands at *ca*. 260 and 330 nm are assigned to site-isolated Ti atoms in pentahedral and octahedral coordination of titanium.

### 1.8.3. Fourier Transform Infrared (FTIR) Spectroscopy

The FTIR spectroscopy in the framework region (400-1300 $cm^{-1}$) provides additional information about the structural details including isomorphous substitution in molecular sieves, whereas the hydroxyl region vibrations (3000-4000 $cm^{-1}$) help in the determination of different acid sites (Brönsted and Lewis)[93] and silanol groups.[94] The band at 960 $cm^{-1}$ in the framework region is very important and generally attributed to incorporation of metal ions in the framework of silica matrix particularly for Ti-containing molecular sieves.[95] Acidic and basic properties as well as its strength in molecular sieves can also be determined by FTIR spectroscopy using $CO_2$, ammonia, pyridine, triphenylphosphine, etc. as probe molecules.[96] IR spectroscopy along with powder XRD can be used as a supplementary tool for structure elucidation. It also can be employed for the detection of transient surface species formed on catalyst surface in a reaction.[97]

### 1.8.4. Nuclear Magnetic Resonance (NMR) Spectroscopy

Nuclear magnetic resonance spectroscopy, both in the liquid and the solid state, is a very important tool for understanding the structure of zeolites, for determining the active species formed at the molecular level during synthesis (*in situ*), and also to characterize the local environment of framework metal ions in solids. Lippama *et al.* showed that $^{29}Si$ MAS NMR spectra are very sensitive to the nature and chemical environment of the atoms.[98] MAS NMR of $^{27}Al$, $^{51}V$, etc. has also been extensively studied to characterize the incorporation of heteroatom in the framework by determining the local environment of Al, Ga, V, etc.[99,100-102] in corresponding metallosilicates

molecular sieves.[103,104] $^{29}$Si MAS NMR can be used to calculate Si/Al ratio on the basis of relative intensities of Si(nAl) peaks ($I_{Si\text{-}nAl}$).

### 1.8.5. Atomic Absorption Spectroscopy (AAS)

The principle of atomic absorption spectroscopy is based on the energy absorbed during the transitions between electronic energy levels of an atom. When some sort of energy is provided to an atom in ground state by a source such as a flame (temperature ranging from 2373-3073 K), outer shell electrons are promoted to a higher energy excited state. The radiation absorbed as a result of this transition between electronic levels can be used for quantitative analysis of metals and metalloids present in solid matrices, which have to be dissolved by appropriate solvents before analysis. The basis of quantitative measurement of radiation intensity and the assumption that radiation absorbed is proportional to atomic concentration. Analogy of relative intensity values for reference standards is used to determine elemental concentration.[105]

### 1.8.6. Scanning Electron Microscopy (SEM)

This is important tool for morphological characterization of microporous and mesoporous molecular sieve materials. Different types of morphologies of the synthesized materials as well as the presence of any amorphous phase in the samples can be characterized using this technique. The major advantage of SEM is that the bulk samples can also be studied directly by this technique.

### 1.8.7. Adsorption Measurements

The ability of molecular sieves to adsorb selective molecules of comparable sizes through the pores into the channels makes them interesting and useful heterogeneous catalysts. The sorption properties of molecular sieves provide information about the hydrophobic/hydrophilic character, pore size distribution and pore volume as well as surface area. The adsorption of nitrogen measured by Brunauer-Emmett-Teller (BET) equation at low pressure ($10^{-4}$ Torr) and liquification temperature of $N_2$ (77 K) is the standard method for the determination of surface area, pore volume and pore size distribution of molecular sieves.[106]

## 1.9. HOST-GUEST INTERACTION IN THE ZEOLITE

Sorption, binding and transport characteristics of guest molecules in the confined geometry of zeolite pore system are vital for fundamental understanding of the behavior of these molecules in intracrystalline spaces which governs the molecular shape selectivity in zeolite-catalyzed reactions. Various small molecules, such as CO, $CO_2$, $CH_4$, $C_2H_4$ and $C_6H_6$, are widely employed as probe molecules.[107] IR adsorption bands undergo remarkable changes such as frequency shift, band splitting and change in line width on adsorption of probe molecules entrapped in the zeolite cavity. The factors responsible for these changes are channel structure of host matrix, polarity of the guest molecules and the presence of charge balancing cations.

CO being a polar molecule has been extensively employed as a probe molecule to demonstrate the role of active sites on binding state of CO on materials such as ZSM-5, X, Y, Alumina, Silica, etc.[108-110]

Adsorption and diffusion of hydrocarbons, especially benzene, inside the zeolites has also received a lot of attention due to their utility in the synthesis of fine chemicals and product intermediates catalyzed by zeolites. Various techniques such as Fourier transform infrared spectroscopy (FTIR), Fourier transform Raman spectroscopy (FT Raman), Microcalorimetry, Nuclear magnetic resonance (NMR), Quasielastic neutron scattering (QENS) etc., have been employed to study these interactions. The adsorption of benzene was investigated over silica, and zeolites such as X, Y, ZSM-5, H-EMT, Na-EMT and BEA type using IR technique due to the sensitivity of these IR bands to the geometrical and chemical nature of the adsorbent zeolite.[111-115] The transport properties and the binding states of benzene molecule are studied by monitoring of in-plane C-H/C-C stretches (3100-3000 $cm^{-1}$), out-of-plane C-H vibrations (2000-1800 $cm^{-1}$) and fundamental $\nu_{19}$ C-C stretch (1479 $cm^{-1}$). Among these, in-plane C-H/C-C stretches and fundamental $\nu_{19}$ vibrations show the similar spectrum to liquid phase benzene. However, out-of-plane C-H bending vibrations, combination band at 1960 $cm^{-1}$ ($v_5 + v_{17}$ vibrations) and 1815 $cm^{-1}$ ($v_{10} + v_{17}$) for liquid benzene splits into overlapping bands. Similar splitting of the out-of-plane vibrations has been reported earlier for adsorption of benzene in microporous aluminosilicates including zeolite Beta, and these observations have been generally attributed to the interaction of benzene molecules with framework cations through the π-electron cloud.[116-120] Dzwigaj *et al*. reported the splitting of C-H out-of-plane bands of benzene into two pairs on adsorption over Beta zeolite.[121] Out of these two pairs, the low frequency pair of bands was attributed to the interaction of benzene with cations through π electron cloud while the high frequency pair of bands originated due to the interaction of C-H groups with the framework oxygen. Armaroli *et al.* noticed the

development of broad and weak $\nu_{(OH)}$ bands at 3250 and 3505 $cm^{-1}$ during adsorption of benzene on H-ZSM-5 and attributed them to the perturbation of bridging OH groups and terminal silanols, respectively.[122]

Comparison of benzene and cyclohexane on zeolites has also been studied using IR and it was reported that the lack of π electrons in case of cyclohexane results in its lower adsorption as compared to that of benzene.[123-124] In IR study of adsorption of benzene in ZSM-5, Angell and Howell, reported that the spectral changes occurring in out-of-plane bands of benzene may not be because of the interaction of π bonds of aromatic system with hydroxyl group or cations but might be due to the orientation of molecules and molecule-molecule interactions giving rise to spectral features similar to that of crystalline benzene.[125] Schematic representation of benzene interacting with different zeolite sites is shown below (Scheme 1.1).

Gupta *et al*. reported an alternative explanation to the splitting in out-of-plane region on the basis of pore size/volume rather than electronic bonding of benzene molecules with the framework.[126-127] According to the authors, formation of dimers or higher clusters of benzene in zeolitic pores will lead to an increased number of bands in infrared and Raman spectra. Any 'g' (or 'u') modes from two molecules can be combined to give 'g' and 'u' mode in a bimolecular cluster. Hence, the mutual exclusion rule for the single molecules will be altered, and 'u' mode of a dimer, generated from the original 'g' mode for the monomer, can become infrared active, and similarly for Raman bands. The shift of out-of-plane bands to the frequencies higher than those of liquid phase benzene and their splitting by 10-15 $cm^{-1}$, can be attributed to the transition of benzene from liquid to solid state also. The IR bands at 1815 and 1959 $cm^{-1}$ for liquid benzene are observed in

the form of doublets with new frequencies around 1825, 1836 $cm^{-1}$ and 1972, 1980 $cm^{-1}$, respectively in the case of solid benzene. The exact frequency of the bands depended on temperature. However, during the phase transformation of benzene from liquid-solid phase, no measurable frequency changes or splitting were observed for in-plane fundamental vibrations of benzene during such liquid-solid transformations. The benzene adsorbed in zeolite exists in a compressed (or clustered) state. The change in the intensity ratio of the fundamental vibration (1479 $cm^{-1}$) and the other in-plane vibrations at 3092, 3071 and 3039 $cm^{-1}$ further supports the transition of liquid to solid-like state of benzene. Benzene molecules are likely to observe immense wall pressure inside the cavity of the zeolitic materials resulting into strong benzene-benzene interaction, leading to highly clustered state.

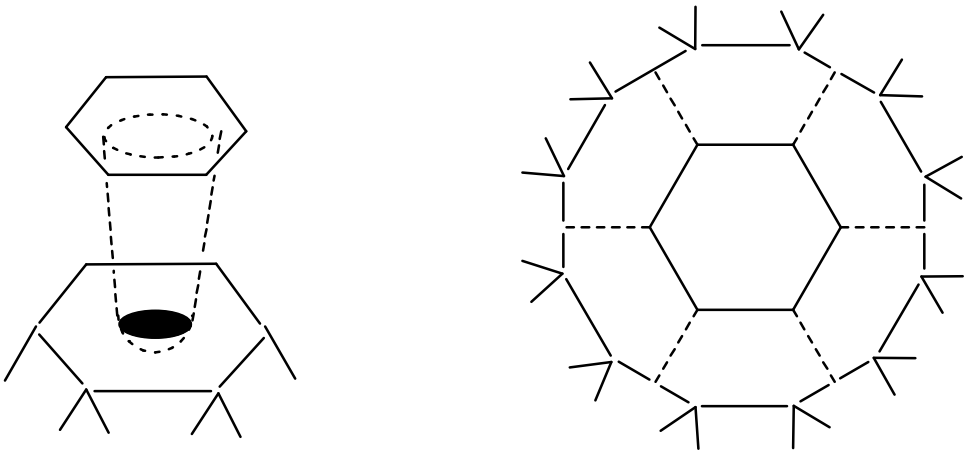

**Scheme 1.1:** Schematic representation of benzene interacting with zeolite sites. (a) Cation in hexagonal face interacting with π-electrons of benzene; (b) CH of benzene in interaction with the oxygen atoms of 12 R window. The T atoms (Si or Al) are at the apex. **[Source: Ref. 110]**

## 1.10. CATALYTIC APPLICATIONS AND PROSPECT

Zeolites offer advantages over conventional catalysts in acid, acid-base, oxidation and reduction reactions. The major properties such as well defined structure, high thermal stability, high surface area, easy regeneration, and uniform pore opening make zeolites unique heterogeneous catalysts. In the context of growing environmental demand for eco-friendly and selective processes, opportunities for catalysis and particularly for zeolitic catalysis are growing rapidly. Zeolites are successfully used in the industries. Some of the examples are mentioned below.

- Faujasite is used in the hydrocracking process to produce kerosene, toluene, xylenes and jet-fuels and it is the second largest process.
- ZSM-5 is used in numerous applications such as:

    A. Dewaxing to produce low pour point lubes.

B. Benzene alkylation to produce styrene and in xylene isomerization for the production of paraxylene, and in toluene disproportionation to produce xylenes and benzene from toluene.

C. The New Zealand Synfuels plant uses ZSM-5 for methanol to gasoline (MTG) technology.

D. ZSM-5 catalysts are also used for controlling $NO_x$ emissions. Due to more stringent controls in $NO_x$ emissions worldwide, this should prove to be one of the fastest growing applications of zeolite catalysts.

- Zeolite Beta is commercially used in the production of commune through alkylation of benzene with propylene.
- Ca A catalysts is used for the separation branched paraffin from n-paraffin utilized for air enrichment and removal of $H_2S$ from sour gases.
- Linde A zeolite has also found applications in the diverse areas such as removal of $CO_2$ from submarines and spacecraft and the concentration of alcohols. It is also used to remove moisture and organic vapor from sealed double pane (double-glazed) windows. Zeolite A is also used as an ion exchanger to replace phosphates in detergents. A recent application is the protection of automobile exhaust systems with Linde A, which adsorbs moisture and gases when the motor is shut off. The active form of the zeolite is regenerated when the motor is switched on.
- Chnoptilolite, a natural zeolite, has been used to remove radioactive cesium and strontium from waste streams of nuclear installations and also ammonia from sewage and agricultural effluents.

On the basis of scientific and patent literature, two rapidly growing areas of research are acid-catalyzed and redox reactions, possibly for their relevance in organic synthesis and the variety of acid and redox zeolites.

### 1.10.1. Acid Catalyzed Reactions

Acid-catalyzed reactions are by far the most numerous and best studied reaction type,[128-132] in which organic functional groups undergo an array of different transformations with nucleophilic reagents in the presence of acids as catalysts. The acidic zeolites are used as one of the important materials in synthesis of intermediates and fine chemicals. They are widely practiced in the different acid catalyzed reactions such as alkylation, acylation, reaction of carbonyl compounds and isomerization reactions.

In 1986, Chiche *et al*. reported the acylation of toluene with linear $C_2$-$C_{22}$ carboxylic acids, catalyzed by CeNaY in the liquid phase showing higher *p*-selectivity (94 %) in comparison with 79 % using conventional $AlCl_3$.[133] Van Bekkum *et al*. showed an alternative and cleaner route for the acylation of resorcinol with benzoic acid on strong solid acids, e.g. sulfonic resins and zeolites, in the liquid phase.[134,135]

The synthetic potential of carbonyl compounds has been explored over acidic zeolites under extremely different experimental conditions. In high temperature (673-773 K) and gas phase conditions, pyridine and various methyl-substituted pyridines were produced by the condensation of lower aldehydes and ketones with ammonia.[136] Selectivity could be advantageously varied by loading H-ZSM-5 with heavy metals or by adjusting the composition of feed. The condensation of formaldehyde with benzene, on H-Y zeolites with different Si/Al ratios at below 353 K, produced diphenylmethane and

higher oligomers.[137] H-Y catalysts (lower Si/Al ratio) showed higher yield. The catalyst was reported to be less prone to the deactivation due to the hydrophobicity of catalyst. More drastic conditions were necessary on medium pore H-ZSM-5.[138]

The isomerization of both α-pinene and α-pinene oxide was reported under acidic conditions, on USY zeolite with higher conversions and selectivities.[139] Operating at 273 K with an acid-washed catalyst, the yields were not far from 85 %, a value afforded by zinc halides. The performance of USY was attributed to the presence of highly dispersed Lewis acidic Al sites. The same reaction was catalyzed by Ti-Beta, both in liquid and gas phase conditions. Initial yields up to 93 % were achieved at 363 K, co-feeding a gaseous stream of *α*-pinene oxide and an inert organic compound (e.g. *n*-heptane, methylcyclohexane) into a continuous flow fixed-bed reactor.[140]

Aromatic alkylation on zeolites has been the subject of several studies leading to industrially relevant results, such as the ethylbenzene and cumene processes. A more recent example is the synthesis of 2, 6-dimethylnaphthalene, in which the combined use of methanol and polymethylated aromatics play a major role, through shape selective transalkylation reactions. ZSM-12, with its unidimensional pore system, proved to be significantly more active and selective than tridimensional Beta and Y zeolites.[141]

Acidic zeolites and α-methylbenzyl alcohol were studied, as possible substitutes of sulphuric acid and styrene, in the alkylation of toluene and *m*-xylene.[142-144] Mordenite proved to be a more selective and stable catalyst than Beta and Y zeolites. The yields to1-phenyl-1-xylyl ethane did not exceed *ca.* 70 %, owing to side-reactions and catalyst deactivation. Benzyl and alkyl chlorides, also proposed as alkylating agents, are liable to same remarks as the previous ones concerning the use of acyl chlorides.[145,146] A range of

coumarin derivatives was reported by the reaction of 3-substituted phenols, resorcinol and 6-ethylresorcinol with various α, β-unsaturated carboxylic acids/esters or with keto esters, on Beta zeolite.

### 1.10.2. Redox Reactions

In the area of catalytic oxidation, the role of hydrogen peroxide has progressively increased due to the growing interest for clean technologies and the discovery of new and effective catalysts, particularly redox molecular sieves. Catalytic properties are greatly dependent on the individual nature of the metal site, the structure and the sorption properties of the molecular sieve. In Ti- and V-zeolites, having similar compositions and structural features, different catalytic properties correspond to the different redox sites, under analogous reaction conditions. Besides dimensions, the hydrophilic/hydrophobic properties of pores have also a major effect on the course of the reaction.[147] In case of TS-1, one can carry out oxidation reactions with hydrogen peroxide in polar and protic solvents due to hydrophobic nature of silicate, which itself is hydrophobic enough to minimize the sorption of water on Ti-sites.[148] Redox molecular sieves have been applied to the epoxidation of double bonds, the hydroxylation of aliphatic and aromatic C-H bonds and the oxidation of O, N and S functionalities. Since, the synthesis of these catalysts are at relatively new, much attention has been paid towards the synthetic and characterization aspect of these materials and studies on fine chemicals synthesis is the area of growing interest.

TS-1, Ti-Al-Beta and Ti-Beta zeolites have been explored for the epoxidation of olefins, in dilute solutions of hydrogen peroxide, at below 353 K. Consistently with a

heterolytic mechanism, the reaction occurs with the full retention of double bond configuration.[149] These features satisfy the basic requirements of mildness and selectivity, turning hydrogen peroxide and Ti-zeolites into promising alternatives, or into complementary synthetic tools, to conventional epoxidation reagents. Urea hydrogen peroxide adduct was also explored as oxidizing agent in the epoxidation of olefinic compounds. Although, TS-1 is most commonly used redox catalyst, the pore size of the zeolitic materials plays a crucial role in the reaction. The bulkier molecules norbornene and cyclohexane are bulkier to undergo epoxidation over TS-1. To investigate the effect of pore size various titanium catalysts, Ti-Beta, TS-1, Ti-Al-Beta and Ti-MCM-41 were tested for the epoxidation of norbornene with hydrogen peroxide and methanol as the solvent.[150] The catalytic performance of the these catalyst follows the order Ti-Beta > Ti, Al-Beta > Ti-MCM-41 > TS-1. The lower activity of Ti, Al-Beta is attributed to the protic aluminum site, which reduces the hydrophobicity in the protic solvent like methanol. The lower activity and selectivity in Ti-MCM-41 is presumably due to less accessibility of titanium sites due to incorporation inside the silica walls.[151] TS-1 was found to be inactive due to pore constraint caused for bulkier molecules like norbornene. (Pore opening for TS-1 = $0.56 \times 0.53$ nm, Ti-Beta = $0.64 \times 0.76$ nm).

## 1.11. SCOPE AND OBJECTIVE OF THE THESIS

Zeolite Beta is one of the most useful high silica large pore zeolite. It is highly disordered and made of the random intergrowth of polymorph A and polymorph B in the ratio *ca.* 45 : 55, respectively. Both the polymorphs A and B are constructed from the same centrosymmetric, tertiary building unit (TBU) arranged in layers successively which interconnect either left handed (L) or right handed (R) manner. Polymorph A represents uninterrupted sequence either left handed or right handed, whereas the polymorph B has alternative stacking sequence. TBU has no preference for either mode of connection leading both to occur with almost equal possibility in the structure of Beta, which enhances the growth of faulty structure. Polymorph A (with space group symmetry $P4_122$ and $P4_322$) and polymorph B (with space group C2/c), were theoretically proposed by Newsam *et al.*[83] Realizing the synthesis of polymorph A and B is one of the daunting tasks for the researchers working in the area. Even significant alteration of the concentration of polymorphs has eluded the scientific community over 20 years. The main reason for not realizing the synthesis of either of these two polymorphs seems to be linked with their lower metastability as compared to their nearly equal intergrowth in *BEA structure. It may be recalled that a chemical method has been developed at our laboratory to enhance the rate of nucleation/crystallization of zeolite by using oxyanions as promoters.[50,51] It has been demonstrated that polarizing ability of these oxyanions, such as perchlorate, helps not only to enhance the rate of nucleation but also stabilizes the less metastable phases. Synthesis of polymorph A will meet the need of stable chiral catalyst, which can be utilized as enantio-selective catalyst. Polymorph B is a more stable structure. Synthesis of any of these individual polymorphs or enrichment of one

polymorph in zeolite Beta will give an opportunity to compare the new material with existing zeolite Beta.

Taking into consideration the importance of above work following work has been undertaken for the present study

- To synthesize certain novel analogs of zeolite Beta with different intergrowth of polymorph A and polymorph B.
- Determination of the structures of new materials using XRD and quantification of polymorphic proportions.
- Study the effect of various synthesis variables such as template concentration, water content, seeding, promoter and its concentration and temperature.
- Incorporation of hetero metal atoms, particularly Al and Ti in framework and their utilization
- To study the adsorption and diffusivity of benzene and hexadeutorated benzene in the channel system as a function of on subtle structural changes arising due to changes in polymorphic proportions.

## 1.12. OUTLINE OF THE THESIS

The **THESIS** is presented in **six (6)** chapters and a brief summary is given below.

**Chapter 1** presents a general introduction of various physicochemical aspects of zeolitic materials. The different characteristic properties of these materials, their synthesis, different approaches, characterization techniques, and application as supports, separation and catalyst in the synthesis of fine chemicals and drug intermediates are

discussed in brief. Zeolite Beta, a classical example of faulting within the structure is also outlined. Sorption, binding and transport properties of guest molecules in the confined geometry of zeolitic pore system, which is important for the fundamental understanding of the behavior of these molecules in intercrystalline spaces governing the molecular shape selectivity in zeolite catalyzed reactions is discussed. Based on these informations, the scope and objective of the present work has been outlined.

**Chapter 2** presents experimental results on synthesis of new polymorph B-enriched of zeolite Beta family (BEB) namely NCL-5, NCL-6 and NCL-7 having the polymorph B and A in the proportions of 65 : 35, 75 : 25 and 90 : 10, respectively. The synthesis procedure for the reference materials used for comparison purpose such as Al-ZSM-5, Silicalite-1, Si-Beta, Al-MCM-41 and Si-MCM-41 is also discussed. Synthesis parameters such as effect of water concentration, concentration of structure directing agent (SDA), use of different promoters and its concentration and crystallization temperature were studied thoroughly. The incorporation of hetero metals such as Al- and Ti- in NCL-7 samples with the variation in Al and Ti content has been described in detail.

**Chapter 3** deals with the characterization of novel BEA type materials NCL-5, NCL-6 and NCL-7 in comparison with Si-Beta. The phase purity of the samples was established using XRD. The composition and enrichment of polymorph B is derived using DIFFaX. UV-visible and FTIR are used to ascertain the incorporation and presence of transition metal in different environment. The results obtained on characterizing the material with different techniques are discussed with intrinsic details.

**Chapter 4** focuses on monitoring of the binding state of $C_6H_6$ and $C_6D_6$ molecules in the zeolites of BEA family, differing from each other in Si/Al ratio and consisting of the intergrowth of polymorphs B and A in different proportions. The *in-situ* FTIR spectroscopy has been employed in the present study with a view to investigate how subtle chemical and structural changes in BEA family, caused by a change in Si/Al ratio or proportions of polymorphs A and B, would influence the binding and the transport properties of an adsorbate. Benzene, a non-polar molecule of dimensions matching that of the channels and pore openings of zeolite samples under study, has been chosen as a probe molecule for this purpose. In order to further discern the nature of the guest-host interaction, hexadeuterated benzene ($C_6D_6$) was also employed as adsorbate. The results were compared with different topologies such as MFI (Silicalite-1 and Al-ZSM-5), M41S (Si-MCM-41 and Al-MCM-41).

**Chapter 5** outlines the comparison of Ti- and Al-containing NCL-7 (polymorph B : polymorph A = 65 : 35) samples with different Si/M ratio (where M = Ti or Al) with normal Beta in catalytic reactions. The catalytic activity is further compared using M/Beta and M/NCL-7 synthesized using post synthesis modification methods.

**Chapter 6** summarizes the results obtained and the basic findings of the present work.

## 1.13. REFERENCES


1. Breck, D. W. *Zeolite Molecular Sieves*; Wiley: New York, 1974.
2. Barrer, R. M. *Hydrothermal Chemistry of Zeolites*; Academic Press: London, 1982.
3. Szostak, R. *Molecular Sieves-Principles of Synthesis and Identification*; Blackie: London, 1998.
4. Flanigen, E. M.; Patton, R. L.; Wilson, S. T. *Stud. Surf. Sci. Catal*. **1988**, *37*, 13.
5. Chatterjee, A.; Iwasaki, T.; Ebina, T.; Miyamoto, A. *Microporous Mesoporous Mater*. **1998,** *21*, 421.
6. Sierka, M.; Sauer, *J. Faraday Discuss.* **1997**, *106*, 41.
7. Meier, W. M.; Olson, D. H. *Atlas of Zeolite Structure Types,* 2 nd ed.; Butterworth: London, 1987.
8. Bragg, W. L. *The Atomic Structure of Minerals;* Cornell University Press: Ithaca, New York, 1937.
9. Meier, W. M. In *Molecular Sieves*; Soc. Chem. Ind.: London, 1968; p 10.
10. Flanigen, E. M. *Proc. 5th Int. Conf. Zeolites;* Ress, L. V. C. Ed.; Heyden and Sons: London, 1980, p 760.
11. Sand, L. B. *Econ. Geol.* **1967**, 191.
12. Grabowska, H.; Mista, W.; Trawczynsky, J.; Wrzyszcz, J.; Zawadzki, M. *Appl. Catal. A*. **2001**, *220***,** 207.
13. Yamanaka, T. *Bull. Chem. Soc. Japan* **1976**, *49***,** 2669.
14. Pierantozzi, R. Eur. Patent 245797 A2, 1987.
15. Hayhurst, D. T. *Chem. Eng. Comm.* **1980**, *4*, 729.
16. Schlenker, J. L.; Rohrbaugh, W. J.; Chu, P.; Valyocsik, E. W.; Kokotailo, G. T. *Zeolites* **1985**, *5***,** 355.
17. Van Koningsveid, H.; Jansen, J. C.; Van Bakkum, H. *Zeolites* **1990,** *10***,** 235.
18. Olson, D. H. *J. Phys. Chem.* **1970**, *74***,** 2758.
19. Fyte, C. A.; Gies, H.; Kokotailo, G. T.; Marler, B.; Cox, D. E. *J. Phys. Chem.* **1990**, *94***,** 3718.

20. Tsybulevskii, A. M. *React. Kinet. Catal. Lett.* **1979**, *12***,** 537.
21. Szostak, R. *Handbook of Molecular Sieves;* Van Nostrand Reinhold: New York, 1992.
22. Higgins, J. B.; LaPierre, R. B.; Schlenker, J. L.; Rohrman, A. C.; Wood, J. D.; Keer, G. T.; Rohrbaugh, W. J. *Zeolites* **1988**, *8*, 446.
23. Freyhardt, C. C.; Tsapatsis, M.; Lobo, R. F.; Balkus, K. J. Jr.; Davis, M. E. *Nature* **1995**, *381***,** 369.
24. Guth, J. L.; Kessler, H.; Higel, J. M.; Lamblin, J. M.; Patarin, J.; Seive, A.; Chezeau, J. M.; Wey, R. *ACS Symp. Ser.* **1989**, *398*, 176.
25. Kessler, H. *Stud. Surf. Sci. Catal.* **1989**, *52*, 17.
26. Guth, J. L.; Caullet, P.; Seive, A.; Patarin, J.; Delprato, F. In *Guidelines for Mastering the Properties of Molecular Sieves*; In Barthomeuf, D.; Derouane, E. G.; Hölderich, W.; Eds.; NATO ASI Series, No. B221; Plenum: New York, 1990 p 69.
27. Gilson, J. -P. In *Zeolite Microporous Solids: Synthesis, Structure and Reactivity;* Derouane, E. G.; Lemos, F.; Naccache, C.; Ribeiro, F. R., Eds. NATO ASI Series, No. C352; Kluwer: Dordrecht, 1992 p 19.
28. Helmkamp, M. M.; Davis, M. E. *Annu. Rev. Mater. Sci.* **1995**, *25*, 161**.**
29. Davis, M. E. *Nature* **1996**, *382***,** 583.
30. Davis, M. E. *Stud. Surf. Sci. Catal*. **1995,** *97*, 35.
31. Burkett, S. L.; Davis, M. E. *J. Phys. Chem.* **1994**, *98*, 4647.
32. Breck, D. W. U. S. Patent 3,130,007, 1964.
33. Kacirek, H.; Lechert, H. *J. Phys. Chem*. **1975**, *79*, 1589.
34. Cundy, C. S.; Henty, M. S.; Plaisted, R. J. *Zeolites* **1995**, *15*, 353.
35. Verduijn, J. P. World Patent 9308124, 1993.
36. Cundy, C. S.; Forrest, J. O.; Plaisted, R. J. *Microporous Mesoporous Mater*. **2003**, *66*, 143.
37. Baerlocher, C.; Meier, W. M.; Olson, D. H. *Atlas of Zeolite Structure Types*, 5th ed.; Elsevier: Amsterdam, 2001.
38. Hou, L. Y.; Sand, L. B. *Proc. 6th Int. Confer. Zeolites*, Olsan, Bissio Eds. Buttersworth: London, 1984, p 887.

39. Lok, B. M.; Cannan, T. R.; Massina, C. A. *Zeolites* **1983**, *3*, 282.
40. Iler, R. K. In *The Chemistry of Silica: Solubility, Polymerization, Colloid and Surface Properties and Biochemistry*; Wiley: New York, 1979.
41. Hogan, P. J.; Whittam, T. V.; Birtill, J. J.; Stewart, A. *Zeolites* **1984**, *4*, 275.
42. Casci, J. L.; Lowe, B. M. *Zeolites* **1983**, *3*, 186.
43. Lowe, B. M. *Zeolites* **1983**, *3*, 300.
44. (a) Sasidharan, M.; Kumar, R. *Microporous Mater.* **1997**, *8*, 43. (b) Nastro, L.; Sand, L. B. *Zeolites* **1983**, *3*, 57.
45. Wadlinger, R.; Keer, G. T.; Rosinski, E. J. U. S. Patent 3 30 8069, 1967.
46. Sand, L. B. In *Molecular Sieves*; Society of Chemical Industry: London, 1968, p 71.
47. Sand, M. L.; Coblenz, W. S.; Sand, L. B. *ACS Adv. Chem. Series* **1971**, *101*, 127.
48. Bajpai, P. K. *Zeolites* **1986**, *6*, 2.
49. Martens, J. A.; Jacobs, P. A. *Stud. Surf. Sci. Catal.* **1988**, *33*, 1.
50 Kadgaonkar, M. D.; Kasture, M. W.; Bhange, D. S.; Joshi, P. N.; Ramaswamy V.; Kumar, R. *Microporous Mesoporous Mater.* **2007**, *101*, 108.
51. Kadgaonkar, M. D.; Kasture, M. W.; Bhange, D. S.; Joshi, P. N.; Ramaswamy, V.; Gupta, N. M.; Kumar, R. *Microporous Mesoporous Mater.* **2007**, *105*, 82.
52. Bibby, D. M.; Dale, M. P. *Nature* **1985**, *317*, 157.
53. Van Erp W. A.; Kouwenhoven J. M. *Zeolites* **1987**, *7*, 286.
54. Flanigen, E. M.; Patton, R. L. U. S. Patent 4,073,865, 1978.
55. Guth, J. L.; Kessler, H.; Higel, J. M.; Lamblin, J. M.; Patarin, J.; Seive, A.; Chezeau, J. M.; Wey, R. *ACS Symp. Ser.* **1989**, *398*, 176.
56. Kessler, H. *Stud. Surf. Sci. Catal.* **1989**, *52*, 17.
57. Guth, J. L.; Caullet, P.; Seive, A.; Patarin, J.; Delprato, F. In *Guidelines for Mastering the Properties of Molecular Sieves* In Barthomeuf, D.; Derouane, E. G.; Ho¨lderich, W. Eds.; NATO ASI Series, No. B221; Plenum: New York, 1990, p 69.
58. Gilson, J. -P. In *Zeolite Microporous Solids: Synthesis, Structure and Reactivity* Derouane, E. G.; Lemos, F.; Naccache, C.; Ribeiro, F. R. Ed. NATO

ASI Series, No. C352; Kluwer: Dordrecht, 1992, p. 19.

59. Kessler, H.; Patarin, J.; Schott-Darie, C. *Stud. Surf. Sci. Catal.* **1994**, *85*, 75.
60. Guth, J. L.; Kessler, H.; Higel, J. M.; Lamblin, J. M.; Patarin, J.; Seive, A.; Chezeau, J. M.; Wey, R. *ACS Symp. Ser.* **1989**, *398*, 176.
61. Estermann, M.; McCusker, L. B.; Baerlocher, C.; Merrouche, A.; Kessler, H. *Nature* **1991**, *352*, 320.
62. Camblor, M. A.; Villaescusa, L. A.; Diaz-Cabanas, M. J. *Top. Catal.* **1999**, *9*, 59.
63. Guth, J. -L.; Kessler, H.; Caullet, P.; Hazm, J.; Merrouche, A.; Patarin, J. In *Proc. 9th Int. Zeolite Conf.* Von Ballmoos Ed.; Butterworth-Heinemann: Boston, 1993, p 73.
64. Koller, H.; Wölker, A.; Eckert, H.; Panz, C.; Behrens, P. *Angew. Chem., Int. Ed. Engl.* **1997**, *36*, 2823.
65. Koller, H.; Wolker, A.; Villaescusa, L. A.; Dıaz-Cabanas, M. J.; Valencia, S.; Camblor, M. A. *J. Am. Chem. Soc.* **1999**, *121*, 3368.
66. Lindner, T.; Lechert, H. *Zeolites* **1994**, *14*, 582.
67. Nui, T. In Occelli, M. L.; Robson, H. E. Ed, *Zeolite Synthesis, ASC Symp. Ser. 398, American Chemical Society*: Washington, DC, 405, **1989**.
68. Kumar, R.; Mukherjee, P.; Pandey, R. K.; Rajmohanan, P.; Bhaumik, A. *Microporous Mesoporous Mater.* **1998**, *22*, 23.
69. Kumar, R.; Bhaumik, A.; Ahedi, R. K.; Ganapathy, S. *Nature* **1996**, *298,* 381.
70. Laha, S. C.; Kumar, R. *Microporous Mesoporous Mater.* **2002**, *53*, 163.
71. Mukhopadhyay, K.; Ghosh, A.; Kumar, R. *Chem. Commun.* **2002**, *2404*.
72. Delprato, F.; Delmotte, L; Guth, J. L.; Huve, L. *Zeolites* **1990**, *10*, 546.
73. Rohrig, C.; Gies, H. *Angew Chem. Int. Ed.* **1995**, *34*, 63.
74. Annen, M. J.; Davis, M.E.; Higgins, J. B.; Schlenker, J. L. *J. Chem. Soc. Chem. Commun.* **1991**, 1175.
75. Rohrig, C.; Gies, H.; Marler, B. *Zeolites* **1994**, *14*, 498.
76. Merlino, S. *Eur. Journal of Mineral* **1990**, *2*, 809.
77. Marler, B.; Grunewald luke A.; Gies, H. *Zeolites* **1995**, *15*, 338**.**
78. Vortmann, S.; Marler, B.; Gies, H.; Daniels, P. *Microporous Mater.* **1995**, *4*,

111.

79. Lobo, R. F.; Pan, M.; Chan, I.; Li, H. X.; Medrud, R. C.; Zones, S. I.; Crozier, P.A.; Davis, M. E. *Science* **1993**, *262*, 1543.
80. Lobo, R. F.; Davis, M. E. *J. Am. Chem. Soc.* **1995**, *117*, 3766.
81. Corma, A. *Chem. Rev.* **1997**, *97*, 2273.
82. *Introduction to zeolite science and practice;* Bekkum, H. V.; Flanigen, E. M.; Jacobs, P. A. Eds.; Elsevier: Amsterdam, 2001.
83. Newsam, J. M.; Treacy, M. M. J.; Koetsier, W. T.; De Gruyter, C. B. *Proc. R. Soc. London* **1988**, *A420*, 375.
84. (a) Corma, A.; Novarro, M. T.; Rey, F.; Rius, J.; Valencia, S. *Angew. Chem. Int. Ed.* **2001**, *40*, 2277. (b) Corma, A.; Novarro, M. T.; Rey, F.; Rius, J.; Valencia, S. *Chem. Commun.* **2001**, 1486. (c) Cantin, A.; Corma, A.; Diaz-Carbanas, M. J.; Jorda J. L.; Moliner, M. Novarro, M. T.; Rey, F.; *Angew. Chem. Int. Ed.* **2006,** *45*, 8013.
85. Tomlinson, S. M.; Jackson, R. A.; Catlow, C. R. A. *J. Chem. Soc. Chem. Commun.* **1990**, 813.
86. Treacy, M. M. J.; Deem, M. W.; Newsam, J. M. *Computer Code DIFFaX, Version 1.807* NEC Research Institute, Inc.: Princeton, New Jersey, **2000**.
87. Ratnasamy, P.; Kotasthane, A. N.; Shiralkar, V. P.; Thangaraj, A.; Ganapathy, S. In *Zeolite Synthesis*; *ACS Symp. Ser.* **1989**, *398***,** 405.
88. Simmons, D. K.; Szostak, R.; Agarwal, P. K. *J. Catal.* **1987**, *106***,** 287.
89. Rau, R. C. In *Advances in X-ray Analysis*, Mueller, W. M. Ed: Sir Isaac Pitman and Sons Ltd.: London, 1962*, Vol. 5*, p 104. (b) Birks, L. S.; Friedman, H. *J. Appl. Phys.* **1946**, *17*, 687.
90. Carvalho, W. A.; Varaldo, P. B.; Wallau, M.; Schuchardt, U. *Zeolites* **1997**, *18*, *408*.
91. Sen, T.; Rajmohanan, P. R.; Ganapathy, S.; Sivasanker, S. *J. Catal.* **1996**, *163*, 354.
92. Zecchina, A.; Spoto, G.; Bordiga, S.; Ferrero, A.; Petrini, G.; Leofanti, G.; Padovan, M. *Stud. Surf. Sci. Catal.* **1991,** *69,* 251.
93. Freyhardt, C. C.; Tsapatsis, M.; Lobo, R. F.; Balkus Jr.; Davis, M. E. *Nature*

**1996**, *381*, 295.

94. Jacobs, P. A.; Martier, W. Y. *Zeolites* **1982**, *2*, 226.
95. Notari, B. *Stud. Surf. Sci. Catal*. **1987**, *37*, 413.
96. Ryczkowski, J. *Catal. Today* **2001**, *68*, 263.
97. Gupta, N. M. In *Catalysis, Principles and Applications*; Viswanathan, B.; Sivasankar, S.; Ramaswamy, A. V. Eds. Narosa: India, 2001, p 127.
98. Lippama, E.; Magi, M.; Samoson, A.; Tarmak, M.; Engelhardt, G. *J. Am. Chem. Soc*. **1981**, *103*, 4992.
99. Klinowski, J.; Thomas, J. M.; Fyfe, C. A.; Hartman, J. S. *J. Phys. Chem.* **1981**, *85*, 2590.
100. Dewaele, N.; Bodart, P.; Gabelica, Z.; Nagy, J. B. *Acta Chem. Acad. Sci. Hung*. **1985**, *119*, 233.
101. Bodart, P.; Dewaele, N.; Gabelica, Z.; Nagy, J. B.; Derouane, E. G. *J. Chim. Phys. Phys. Chim. Biol.* **1986**, *83*, 777.
102. Hayashi, S.; Suzuki, K.; Shin, S.; Hayamizu, K.; Yamamoto, O. *Chem. Phys. Lett.* **1984**, *110*, 54.
103. Fyfe, C. A.; Gobbi, G. C.; Klinowski, J.; Thomas, J. M.; Ramdas, S. *Nature* **1982**, *296*, 530.
104. Reddy, K. M.; Moudrakovski, I.; Sayari, A. *J. Chem. Soc., Chem. Commun*. **1994**, *1059*.
105. Robinson, J. W. *Atomic Absorption Spectroscopy;* Marcel Dekker: New York, 1972.
106. Brunauer, S.; Emmett, P. H.; Teller, E. *J. Am. Chem. Soc*. **1938**, *60*, 309.
107. Corma, A. *Cat. Rev. Sci. Engg*. **1985**, *27*, 29.
108. (a) Angell, C. L.; Schaffer, P. C. *J. Phys. Chem*. **1966**, *70*, 1413; (b) Mirsojew, I.; Ernst, S.; Weitkamp, J.; Knozinger, H. *Cat. Lett*. **1994**, *24*, 235.
109. (a) Kamble, V. S.; Gupta, N. M.; Kartha, V. B.; Iyer, R. M. *J. Chem. Soc. Faraday Trans. I* **1993**, *89*, 1143; (b) Shete, B. S.; Kamble, V. S.; Gupta, N. M.; Kartha, V. B. *J. Phys. Chem. B* **1998**, *102*, 5581; (c) Shete, B. S.; Kamble, V. S.; Gupta, N. M.; Kartha, V. B. *Phys. Chem. Chem. Phys.* **1999**, *1*, 191.
110. Zecchina, A.; Bordiga, S.; Spoto, G.; Scarano, D.; Petrini, G.; Leofanti, G.;

Padovan, M.; Otero, C. *J. Chem. Soc. Faraday Trans I* **1992**, *88*, 2959.

111. Barthomeuf, D. *Catal Review Sci. Eng*. **1996**, *38*, 521.
112. Shen, J. P.; Ma, J.; Sun, T.; Jiang, D. Z.; Min, E. Z. *J. Chem. Soc. Faraday Trans.* **1994**, *90*, 1351.
113. Coughlan, B.; Carroll, W.; Malley, P. O.; Nunam, J. *J. Chem. Soc. Faraday Trans. I* **1981**, *77*, 3037.
114. Ward, J. W. *J. Catal*. **1968,** *10*, 34.
115. Su, B. L.; Manoli, J. M.; Potvin, C.; Barthomeuf, D. *J. Chem. Soc. Faraday Trans.* **1993**, *89*, 857.
116. Primet, M.; Garbowski, E.; Mathieu, M. V.; Imelik, B. *J. Chem. Soc. Faraday Trans.* **1980**, *76,* 1942.
117. Abramov, V. N.; Kiselev, A. V.; Lygin, V. I. *Russ. J. Phys. Chem.* **1963**, *37*, 613.
118. Coughlan, B.; Keane, M. A. *J. Chem. Soc. Faraday Trans.* **1990**, *86,* 3961.
119. Dzwigaj, S.; De Mallmann, A.; Barthomeuf, D. *J. Chem. Soc. Faraday Trans.* **1990**, *86,* 431.
120. Shen, J. -P.; Ma, J.; Sun, J.; Jaing, D. –Z. *J. Chem. Faraday Trans.* **1994**, *90,* 1351.
121. Dzwigaj, S.; De Mallmann, A.; Barthomeuf, D. *J. Chem. Soc. Faraday Trans*. **1990,** *86*, *431*.
122. Armaroli, T.; Trombetta, M.; Alejandre, A. G.; Solis, J. R.; Busca, G. *Phys. Chem. Chem. Phys.* **2000**, *2*, 3341.
123. Barthomeuf, D.; Ha, B. H. *J. Chem. Soc. Faraday Trans. I* **1973**, *69*, 2147.
124. Barthomeuf, D.; Ha, B. H. *J. Chem. Soc. Faraday Trans. I* **1973**, *69*, 2158.
125. Angell, C. L.; Howell, M. V. *J. Collid. Interface Sci*. **1968**, *28*, 279.
126. Sahasrabudhe, A.; Kamble, V. S.; Tripathi, A. K.; Gupta, N. M. *J. Phys. Chem. B* **2001**, *105,* 4374.
127. Sahasrabudhe, A.; Mitra, S.; Tripathi, A. K.; Mukhopadhyay, R.; Gupta, N. M. *Phys. Chem. Chem. Phys.* **2003**, *5,* 3066.
128. *Selectivities in Lewis Acid Promoted Reactions*; Kluwer Academic Publishers: Dordrecht, 1989.

129. Pons, J. M.; Santelli, M.; Eds.; *Lewis acids and selectivity in organic synthesis*; CRC Press: Boca Raton, FL, 1996.

130. Leach, M. R. Ed.; *Lewis Acid/Base Reaction Chemistry Meta- Synthesis*; Brighton: 1999.

131. Yamamoto, H. Ed.; *Lewis Acids in Organic Synthesis*, *Vol. 1*; Wiley VCH: Weinheim, 2000.

132. Yamamoto, H. Ed.; *Lewis Acids in Organic Synthesis*, *Vol. 2*; Wiley VCH: Weinheim, 2000.

133. Chiche, B.; Finiels A.; Gauthier C.; Geneste P.; Graille J.; Pioch D. *J. Org. Chem.* **1986**, *51*, 2128.

134. Hoefnagel, A. J.; Van Bekkum H. *Appl. Catal. A* **1993**, *97*, 87.

135. Van Bekkum, H.; Hoefnagel, A. J.; Vankoten, M. A.; Gunnewegh, E. A.; Vogt, A. H. G.; Kouwenohoven, H. W. *Stud. Surf. Sci. Catal.* **1994,** *83*, 379.

136. Hölderich, W.; Hesse, M.; Näumann, F. *Angew. Chem. Int. Ed. Engl*. **1988**, *27*, 226.

137. Climent, M. J.; Corma, A.; Garcia, H.; Primo, J. *Appl. Catal. A* **1989,** *51*, 113.

138. Wu, X.; Anthony, R. G. *J. Catal.* **1999**, *184*, 294.

139. Hölderich, W. F.; Heitmann, G. *Catal. Today* **1997**, *38*, 227.

140. Kunkeler, P. J.; Van der Waal, J.; Bremmer, J.; Zuurdeeg, B. J.; Dowing, R. S.; Van Bekkum, H. *Catal. Lett.* **1998**, *53*, 135.

141. Pazzuconi, G.; Perego, C.; Millini, R.; Frigerio, F.; Mansani, R.; Rancati, D. Eur. Patent 950650, 1999, to **Enichem**.

142. Coq, B.; Gourves V.; Figuéras, F. *Appl. Catal. A* **1993**, *100*, 69.

143. Kwak, B. S.; Kim, T. J. *Appl. Catal. A* **1999**, *188*, 99.

144. Kwak, B. S.; Kim, T. J. *Catal. Lett.* **1999**, *59*, 55.

145. Singh, A. P.; Jacob, B.; Sugunan, S. *Appl. Catal. A* **1998**, *174*, 51.

146. Singh, A. P.; Pandey, A. K. *Catal. Lett.* **1999**, *60*, 157.

147. Langhendries, G.; De Vos, D. E.; Baron, G. V.; Jacobs, P. A. *J. Catal.* **1999**, *187*, 453.

148. (a) Kumar, R.; Mukherjee, P.; Bhaumik, A. *Catal. Today* **1999**, *49*, 185. (b) Bhaumik, A.; Mukherjee P.; Kumar R. *J. Catal.* **1998**, *178*, 101.

149. Clerici, M.G.; Ingallina, P. *J. Catal.* **1993**, *140*, 71.

150. Van derWaal, J. C.; Rigutto, M. S.; Van Bekkum, H. *Appl. Catal. A*, **1998**, *67*, 331.

151. Tatsumi, T.; Nakamura, M.; Nigishi, N.; Tominaga, H. In Yoshida, S., Takezama, N., Ono, T. Eds. *Catalysis Science and Technology;* **1990**, *1*, 213.

## 2.1. INTRODUCTION

In chapter 1 the general aspects of zeolite synthesis and influence of different parameters on the synthesis of the microporous materials have been reviewed. Among different zeolites, zeolite Beta represents the first few examples of high silica large pore zeolite.[1] It is commonly used in adsorption of hydrocarbons from exhaust gas emission, $NO_x$ reduction, different organic rearrangement reactions, isomerization of waxes and Friedel Crafts reactions.[2-8] As described in chapter 1, zeolite Beta represents the classical example of faulting within the structure. It is an intergrowth of two polymorphs, polymorph A and polymorph B, as proposed on the basis of simulated studies by Newsman *et al.*[9-10] Realization of synthesis of these polymorphs individually or an enrichment of one of the polymorphs in zeolite Beta has eluded the scientific community for more than two decades. Lower metastability of these polymorphs seems to be one of the reasons for the synthesis of faulty structure in zeolite Beta (almost equal proportions of polymorphs A and B). Utilization of oxyanions from VA, VIA and VIIA group are shown to overcome the hurdle of longer crystallization period and also known to stabilize less metastable phases.[11] The use of these promoters in the synthesis of different microporous and mesoporous materials had been widely studied in hydroxide medium.[12,13] However, their utilization in fluoride medium remained to be overlooked till date and will definitely be useful in the synthesis of novel and less stable structures. In the present dissertation, oxyanions have been used to preferentially obtain enrichment of the polymorph B in zeolite Beta in fluoride medium.

The present chapter gives a detailed description of the synthesis of polymorph B enriched intergrowth of zeolite Beta denoted as NCL-5, NCL-6 and NCL-7. Effect of

different physical parameters such as time, temperature; chemical variables including effect of $H_2O/SiO_2$, $TEAOH/SiO_2$ and $HClO_4/SiO_2$ molar ratio has been discussed. The synthesis of Ti- and Al-NCL-7 is also discussed. The chapter also includes a brief description for the synthesis of microporous materials, Si-Beta, Silicalite-1, Al-ZSM-5, Al-Beta along with mesoporous structures, Si-MCM-41 and Al-MCM-41 incorporated in the present thesis mainly for comparison purpose.

## 2.2. MATERIALS

Materials used for the synthesis of polymorph B enriched intergrowth of zeolite Beta, NCL-5, NCL-6 and NCL-7 and other microporous as well as mesoporous materials are tabulated in Appendix A (Table A.1). The chemicals were used in the received form without any further purification if not mentioned specifically.

## 2.3. SYNTHESIS OF POLYMORPH B-ENRICHED INTERGROWTH OF ZEOLITE BETA (NCL-5, NCL-6, NCL-7) and *BEA

Generally, the synthesis of all silica Beta, *BEA (zeolite Beta with the proportion of polymorph B : polymorph A in the ratio 55 : 45, respectively), is carried out hydrothermally in an autoclave under autogeneous pressure using tetraethylammonium halide/hydroxide as template and hydrofluoric acid as a mineralizer. In the present work, all silica analogs of zeolite Beta with the enrichment of polymorph B in NCL-7, NCL-6 and NCL-5 structures as *ca.* 65 %, 75 % and 90 %, respectively, were synthesized in fluoride medium in presence of $HClO_4$ as promoter at concentrated synthesis conditions (low $H_2O/SiO_2$). The polymorphic composition of polymorph A and polymorph B in

NCL-5, NCL-6 and NCL-7 sample was established using DIFFaX code (XRD) and discussed in detail in chapter 3.[10,14-15] To understand the role of individual synthesis parameters, on phase formation, the synthesis of NCL-7 and NCL-5 was studied in detail. Effect of different synthesis parameters such as template concentration, crystallization temperature, time, use of different promoters, promoter concentration and water concentration in the reaction gel were investigated thoroughly.

### 2.3.1. Experimental

#### *2.3.1.1. Synthesis of NCL-5, NCL-6, NCL-7 and *BEA*

The synthesis of B-enriched samples NCL-5, NCL-6 and NCL-7 was carried out using Tetraethylorthosilicate (TEOS) as silica source and tetraethylammonium hydroxide (TEAOH) as template. Hydrofluoric acid (HF) and perchloric acid ($HClO_4$) were employed as mineralizer and promoter, respectively. In a typical synthesis procedure of NCL-5, 62.4 g of TEOS was slowly added to 85.7 g aqueous TEAOH solution under vigorous stirring. The stirring was further continued till desired weight loss (~ 47 wt %) was achieved due to liberation of ethanol. To this mixture, 8.53 g of 40 % aqueous hydrofluoric acid was added with constant stirring and stirring was further continued for another 30 min. Finally, 3.88 g of 70 % aqueous perchloric acid, employed as promoter, was added to the above mixture with vigorous stirring, which was continued till homogeneous gel was formed. A representative molar composition of the resultant gel was estimated to be $SiO_2$ : 0.68 TEAOH : 0.57 HF : 0.09 $HClO_4$ : 7.5 $H_2O$. Further, the gel was hydrothermally treated in a 300 mL Parr autoclave at 408 K for 96 h to obtain the fully crystalline desired phase. The solid product was separated from the mother liquor by

filtration and washed thoroughly with copious amount of distilled water and dried at 383 K under vacuum for 2 h. The solid obtained was further calcined at 833 K for 12 h in presence of air to ensure the removal of template. The synthesis of two other polymorph B enriched structures, NCL-6 and NCL-7, was also achieved using similar methodology varying the water content in the gel ($H_2O/SiO_2$) to 8.5 and 9.5, respectively. All-Silica Beta (*BEA) sample was obtained from the same molar gel composition without $HClO_4$ after crystallization period of 142 h at 408 K. The corresponding molar gel composition of NCL-5, NCL-6, NCL-7 and *BEA is given in Table 2.1.

**Table 2.1**

Effect of Molar Gel Composition on Enrichment of Polymorph B and Phase Obtained. Molar gel composition $SiO_2$ : 0.68 TEAOH : 0.57 HF : x $HClO_4$ : y $H_2O$, Temperature: 408 K

| Entry No. | Sample Name | x | y | Synthesis Time (h) | % Polymorph B (BEB)/phase |
|---|---|---|---|---|---|
| 1 | NCL-5 | 0.09 | 7.5 | 96 | 90-95 |
| 2 | NCL-6 | 0.09 | 8.5 | 110 | 70-75 |
| 3 | NCL-7 | 0.09 | 9.5 | 120 | 60-65 |
| 4 | *BEA | 0 | 9.5 | 142 | *BEA |

### 2.3.2. Results and Discussion

#### *2.3.2.1. Effect of Synthesis Parameters on NCL-7 (Polymorph B : Polymorph A = 65 : 35)*

Influence of different synthesis parameters such as temperature, structure directing agent, promoter and its concentration, and water content in the gel on the synthesis of B-rich analog of zeolite Beta, NCL-7, was studied thoroughly to understand the role of individual parameter. One parameter was changed at a time while keeping other parameters and addition sequence constant. The crystallization kinetics of the NCL-7 sample was studied for different molar gel composition and at different crystallization temperature. The samples were collected at regular interval of time and % crystallinity was calculated using the powder XRD patterns. After background subtraction, the sum of the areas under the five characteristic peaks of NCL-7 in the 2θ range of 6.44-9.44, 19.32-24.42, 26.30-27.52, 32.72-34.16 and 42.84-44.82 was taken as a measure of crystallinity, by comparison to a most crystalline and pure NCL-7 phase in the present study.

##### *2.3.2.1.1. Effect of temperature*

Influence of temperature on the phases formed and the proportion of B : A polymorphs in pure crystalline Beta phases was studied thoroughly in the range of 373-423 K. Table 2.2 presents the influence of temperature on the crystallization and the phase formed. The samples were collected at regular interval till the crystallization is completed. As evident, B-rich NCL-7 phase was obtained in the temperature range 373-413 K. When the synthesis was carried out at 423 K, the *BEA phase is formed (Table

2.2, Entry 7). As expected, decrease in the crystallization time for NCL-7 phase was observed with increase in temperature (Table 2.2, Entries 1-6).

**Table 2.2**

Influence of Temperature on Crystallization Time and Obtained Phase.

Molar gel composition $SiO_2$ : 0.68 TEAOH : 0.57 HF : 0.09 $HClO_4$ : 9.5 $H_2O$

| Entry No. | Temperature (K) | Duration (h) | Phase |
|---|---|---|---|
| 1 | 373 | 336 | NCL-7 |
| 2 | 383 | 228 | NCL-7 |
| 3 | 393 | 216 | NCL-7 |
| 4 | 403 | 144 | NCL-7 |
| 5 | 408 | 120 | NCL-7 |
| 6 | 413 | 108 | NCL-7 |
| 7 | 423 | 95 | *BEA |

The crystallization kinetics of the NCL-7 sample at different crystallization temperature is shown in Fig. 2.1. The % crystallinity of the NCL-7 sample was found to increase with crystallization time. The curves (a), (b), (c), (d), (e) and (f) refer to the crystallinity of the NCL-7 samples at various time interval synthesized at 373, 383, 393, 403, 408 and 413 K, respectively. As expected, the synthesis time to obtain fully crystalline NCL-7 decreased by increasing the crystallization temperature. There was no phase transformation of NCL-7 to *BEA or any other phase was seen even after 172 h of total crystallization time (curve e).

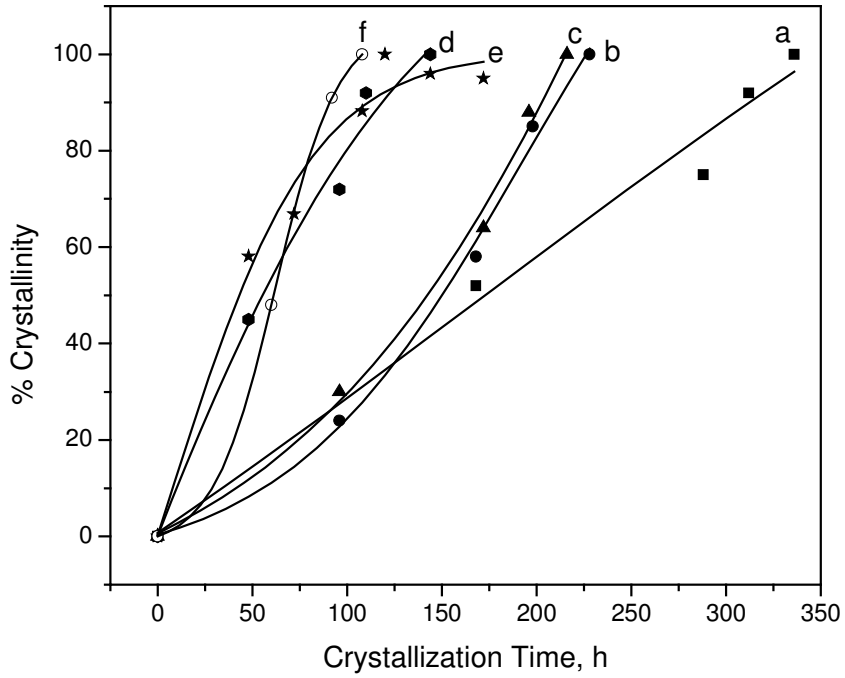


**Figure 2.1.** Crystallization kinetics as a function of crystallization temperature Curves (a) 373 K (b) 383 K (c) 393 K (d) 403 K (e) 408 K and (f) 413 K.

***2.3.2.1.2. Effect of seeding***

As synthesized sample of all silica NCL-7 was used as seed in order to understand its role on crystallization time and phase formation. The amount of seed was varied as 2.5 % and 5.0 % with respect to silica content in the gel. As it can be seen from the Fig. 2.2, the crystallization period deceases significantly to 86 and 72 h after addition of 2.5 and 5.0 % seed (based on silica content) in the initial synthesis gel. When the synthesis trial was conducted in absence of seed, the time required to obtain the NCL-7 phase was found to be 120 h. The addition of seed provides the larger surface area required for the

product to grow. This overcomes the necessity for such surfaces to be self generated by primary nucleation and thus reduces the crystallization time.

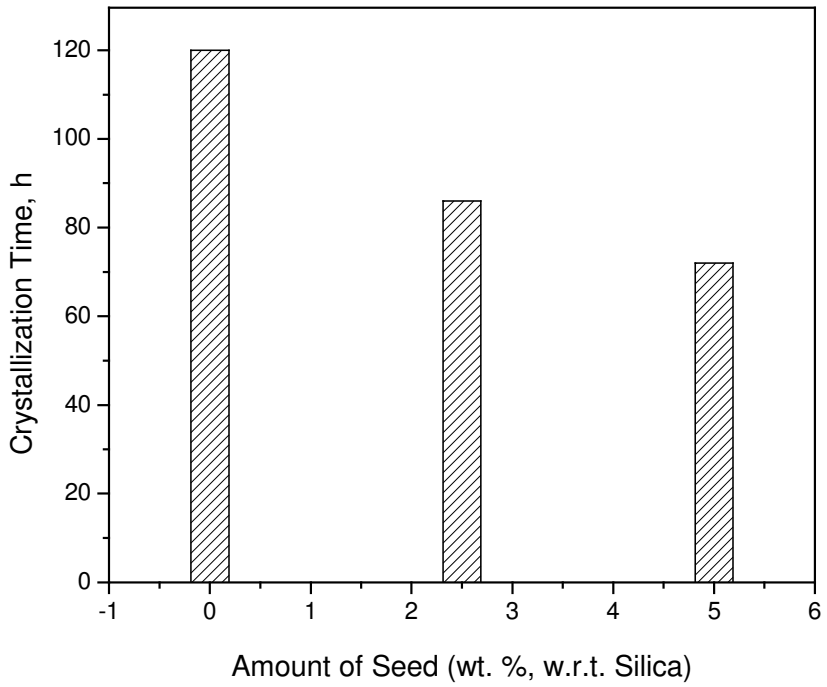


**Figure 2.2.** Effect of seeding on the crystallization of NCL-7 sample

***2.3.2.1.3. Effect of TEAOH concentration***

Effect of template (TEAOH) concentration on the crystallization of NCL-7 and phase obtained is tabulated in Table 2.3. Concentration of TEAOH was systematically varied in the range of the TEAOH/$SiO_2$ = 0.38-0.98 keeping other parameters constant. It was observed that NCL-7 phase was obtained in the range of TEAOH/$SiO_2$ = 0.68 to 0.98 (Table 2.3, Entries 3-6). However, when TEAOH/$SiO_2$ molar ratio was further decreased to 0.48 and 0.38, only *BEA phase was obtained. At the same time, the decrease in the crystallization time was observed from 120 h for (TEAOH/$SiO_2$ = 0.68) to 72 h for (TEAOH/$SiO_2$ = 0.98).

Figure 2.3 illustrates the crystallization kinetics of NCL-7 sample as a function of TEAOH concentration using the molar gel composition $SiO_2$ : x TEAOH : 0.57 HF : 0.09 $HClO_4$ : 9.5 $H_2O$ at 408 K, where the values of x varied in the range of 0.68 to 0.98 (Table 2.3, Entries 3-6). This could be attributed to the increase in pH due to presence of more $OH^-$ from TEAOH and amount of more $TEA^+$ cations available for nucleation as reported earlier.[16] Also, SDA contributes to the structure by formation of template-template bond and/or template-framework bond that leads to the different stabilizing interaction of the charge density of the framework and shape of the desired phase(s).

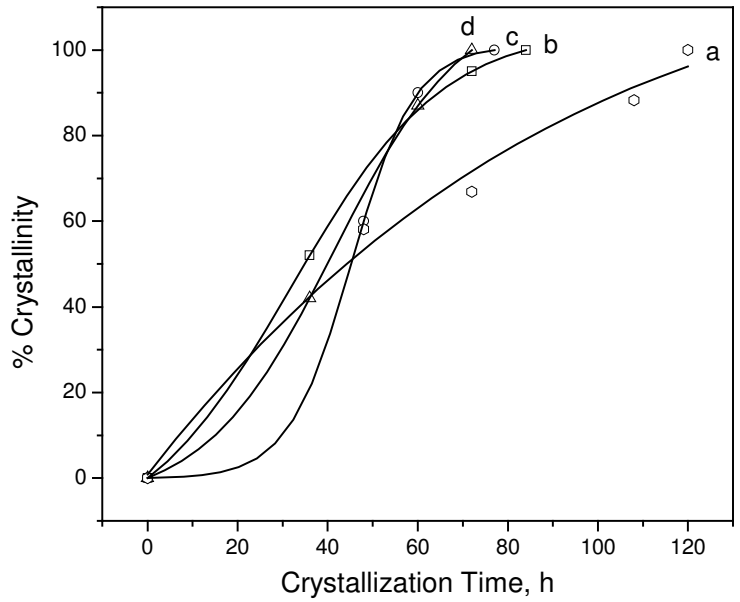


**Figure 2.3.** Crystallization kinetics as a function of TEAOH concentration in curves (a) TEAOH/$SiO_2$ = 0.68 (b) TEAOH/$SiO_2$ = 0.78 (c) TEAOH/$SiO_2$ = 0.88 (d) TEAOH/$SiO_2$ = 0.98

**Table 2.3**

Effect of TEAOH Concentration

Molar gel composition $SiO_2$ : x TEAOH : 0.57 HF : 0.09 $HClO_4$ : 9.5 $H_2O$, Temperature: 408 K

| Entry No. | x | Duration (h) | Phase |
|---|---|---|---|
| 1 | 0.38 | 170 | *BEA |
| 2 | 0.48 | 154 | *BEA |
| 3 | 0.68 | 120 | NCL-7 |
| 4 | 0.78 | 84 | NCL-7 |
| 5 | 0.88 | 77 | NCL-7 |
| 6 | 0.98 | 72 | NCL-7 |

***2.3.2.1.4. Effect of promoter concentration ($HClO_4/SiO_2$ molar ratio)***

Oxyanions such as perchlorate, phosphate and bromate act as a promoter for the enhancement of the nucleation and crystallization. It is reported that the polarizing ability (i.e. charge to radius ratio) plays a key role in enhancing crystallization rate and stabilizing the phases.[11,12] Table 2.4 outlines the effect of oxyacids, $HClO_4$ and $H_3PO_4$ and their concentration on the phase formation and duration required to obtain the crystalline phase. The concentration of $HClO_4$ as promoter was varied from 0.0 to 0.18 with stepwise increase, keeping $H_2O/SiO_2$ and $TEAOH/SiO_2$ molar ratio constant. It was observed that at lower $HClO_4$ concentration ($HClO_4/SiO_2$ = 0.0 to 0.045) *BEA was obtained (Table 2.4, Entry 1 and 9). At higher $HClO_4$ concentration ($HClO_4/SiO_2$ = 0.08

to 0.12), B-rich structure (NCL-7) was obtained (Table 2.4, Entry 2, 3 and 4). The crystallization kinetics of these NCL-7 samples is presented in Fig. 2.4. In this figure, curves (a), (b) and (c) refers to the crystallinity of the NCL-7 sample for $HClO_4/SiO_2$ = 0.08, 0.09 and 0.12, respectively. The crystallization curves exhibit sigmoidal nature indicating the different crystallinity of the sample at different crystallization time. Furthermore, when the $HClO_4$ concentration in the gel changed from $HClO_4/SiO_2$ = 0.08 to $HClO_4/SiO_2$ = 0.12 through 0.09, the synthesis time required to obtain the fully crystalline NCL-7 phase decreased from 126 to 115 h through 120 h (Table 2.4, Entry 2, 3 and 4). However, further increase in $HClO_4$ concentration (0.15 and 0.18), *BEA and *BEA containing MFI impurity (Table 2.4, Entry 5 and 6) was obtained. Similarly, when the synthesis trials were carried out using the $H_3PO_4$ as promoter (Table 2.4, Entry 7 and 8) the B-rich phase could not be obtained. This is due to the lower nucleation and crystallization energy of phosphoric acid as compared to perchloric acid. However, no B-rich phase was obtained for any synthesis trial conducted in the absence of promoter. Probably, the use of perchlorate oxyanion in concentrated fluoride medium (at moderate $H_2O/SiO_2$ molar ratio) may facilitate the overlapping of TEA-enclathrated oxo fluorosilicate species. Such overlapping forms composite species at the onset of crystallization process. Thus a kinetic effect seems to be responsible for the phase formation.

**Table 2.4**

Effect of Promoter

Molar gel composition $SiO_2$ : 0.68 TEAOH : 0.57 HF : x $HClO_4$ : y $H_3PO_4$ : 9.5 $H_2O$,

Temperature: 408 K

| Entry No. | x | y | Duration (h) | Phase |
|---|---|---|---|---|
| 1 | 0.045 | 0 | 160 | *BEA |
| 2 | 0.08 | 0 | 126 | NCL-7 |
| 3 | 0.09 | 0 | 120 | NCL-7 |
| 4 | 0.12 | 0 | 115 | NCL-7 |
| 5 | 0.15 | 0 | 102 | *BEA |
| 6 | 0.18 | 0 | 96 | *BEA + MFI impurity |
| 7 | 0 | 0.03 | 196 | *BEA |
| 8 | 0 | 0.09 | 148 | *BEA |
| 9 | 0 | 0 | 142 | *BEA |

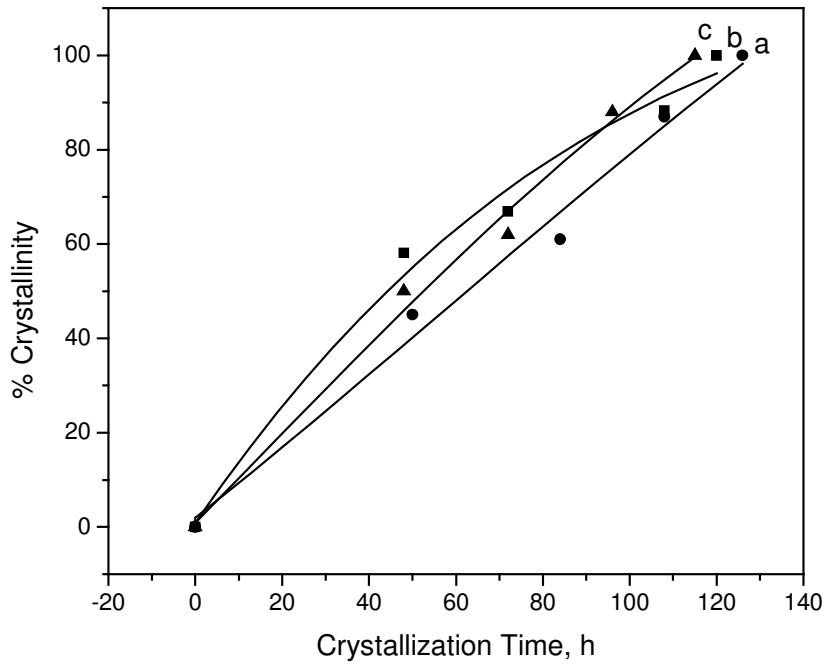


**Figure 2.4.** Crystallization kinetics of NCL-7 phase as a function of $HClO_4$ concentration in curves (a) $HClO_4/SiO_2 = 0.08$ (b) $HClO_4/SiO_2 = 0.09$ (c) $HClO_4/SiO_2 = 0.12$.

### *2.3.2.1.5. Effect of $H_2O$/ $SiO_2$ molar ratio*

Table 2.5 outlines the influence of $H_2O/SiO_2$ molar ratio in the range of 7.5 to 50 on crystallization keeping other synthesis parameters same. The minimum water concentration ($H_2O/SiO_2$ = 9.5) in the gel is already limited by the water content in the TEAOH (35 % aqueous solution), HF (40 % aqueous solution) and $HClO_4$ (70 % aqueous solution). Hence, without adding any extra water, the lower water gel compositions particularly $H_2O/SiO_2$ = 7.5 and 8.5 were achieved by removing the water from the

synthesis gel at room temperature under mild vacuum. The decrease in the water concentration ($H_2O/SiO_2$ = 7.5 to 9.5, Table 2.5, Entry 1-3) leads to the formation of the polymorph B-rich Beta phases namely NCL-5, NCL-6 and NCL-7 with *ca.* 60-65, 70-75 and 90-95 % enrichment of polymorph B. When the water concentration varied (up to $H_2O/SiO_2$ = 14 and 20, Table 2.5, Entry 4 and 5) pure *BEA phase was obtained and above this the obtained phase was a mixture of *BEA and MFI (Table 2.5, Entry 6 and 7).

The crystallization kinetics of NCL-5, NCL-6 and NCL-7 is presented in Fig. 2.5. The % crystallinity of the samples was calculated on the basis of area under the curves of powder XRD patterns recorded at different interval of time as mentioned earlier in section 2.3.2.1. Time required to obtain fully crystalline phase was found to be 96, 110 and 120 h, respectively for NCL-5, NCL-6 and NCL-7 samples (Table 2.5, Entry 1, 2 and 3). In order to investigate the stability of polymorph B-enriched structures, NCL-5, NCL-6 and NCL-7, the synthesis trials were conducted further for additional 48 h after obtaining the fully crystalline sample. However, polymorph B enriched structures were found to be quite stable and no phase transformation is observed even after continuing the synthesis trials for additional 48 h.

These observations described above can be related to the nucleation step and hence, is probably a kinetic effect. As all the synthesis trials are carried out in fluoride medium, the soluble species are more likely to be oxofluorosilicate around neutral pH. As the $H_2O/SiO_2$ ratio decreases the corresponding $F^-$ ion concentration increases which in turn is likely to increase the fluoride to oxygen ratio of the silicate species in the solution. As the crystallization takes place by condensation of silicate species in the solution, the

decrease in water content increases the concentration of occluded $F^-$ which requires higher concentration of SDA. Camblor *et al*. has reported that different phases such as ZSM-5 and ZSM-12 can be prepared by using the same template with varying the $H_2O/SiO_2$ ratio where the more metastable phases occur at more concentrated conditions (low $H_2O/SiO_2$ ratio).[17] Therefore, it could be concluded that water content in the gel plays an important role to obtain particular structure. The effect of water content in the synthesis mixture can modify to some extent the structure directing ability of the SDA and very different phases can be obtained using the same SDA. Transport properties within the gel and the viscosity of the reacting gel may also vary with the variation in the water content.

**Table 2.5**

Influence of Water Content

Molar gel composition $SiO_2$ : 0.68 TEAOH : 0.57 HF : 0.09 $HClO_4$ : x $H_2O$, Temperature: 408 K

| Entry No. | x | Duration (h) | Phase |
|---|---|---|---|
| 1 | 7.5 | 96 | NCL-5 |
| 2 | 8.5 | 110 | NCL-6 |
| 3 | 9.5 | 120 | NCL-7 |
| 4 | 14.0 | 144 | *BEA |
| 5 | 20.0 | 156 | *BEA |
| 6 | 25.0 | 168 | *BEA + MFI impurity |
| 7 | 50.0 | 190 | MFI + *BEA impurity |

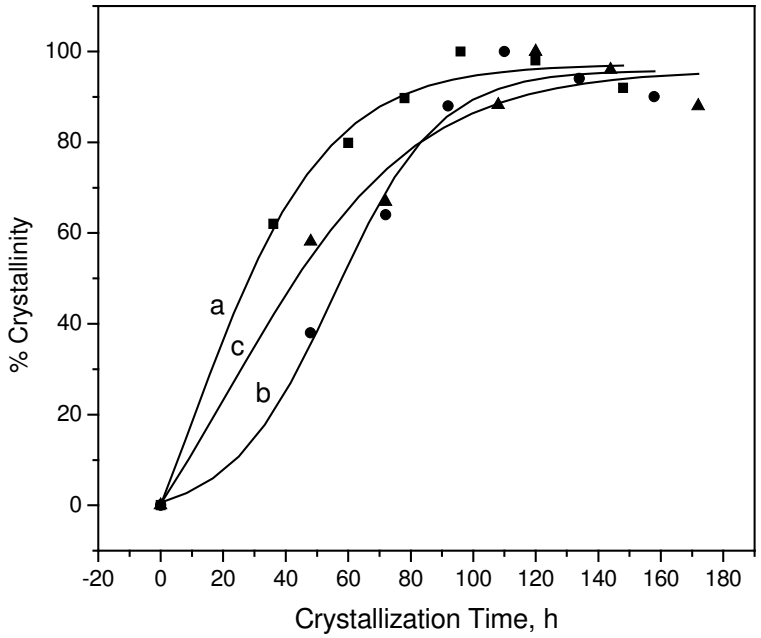


**Figure 2.5.** Crystallization kinetics of different polymorph B enriched analogs of zeolite Beta. Curve (a), (b) and (c) refers to the crystallization kinetics of NCL-5, NCL-6 and NCL-7 samples, respectively.

***2.3.2.2. Effect of Different Synthesis Parameters on NCL-5 (polymorph B : polymorph A = 90 : 10)***

The key factors responsible for the enrichment of polymorph B were low $H_2O/SiO_2$ molar ratio and presence of perchloric acid as promoter as reported in section 2.3.2.1 and elsewhere.[18] Taking in account these results, the synthesis parameters were further varied to improve the enrichment of polymorph B in the structure. Table 2.6 exhibits the gel composition and the resulting zeolite phases (polymorph intergrowth) obtained as a function of $H_2O/SiO_2$, $TEAOH/SiO_2$ and $HClO_4/SiO_2$ molar ratios in the gel.

When the water content in the gel was lowered (Table 2.6, Entries 1-3) from $H_2O/SiO_2$ = 9.5 to 7.5 through 8.5, the increase in polymorph B intergrowth resulting in the formation of NCL-5, NCL-6 and NCL-7 was observed. Although, the water content in the gel is limited by the use of aqueous solutions such as 35 wt % TEAOH, 40 wt % HF and 70 wt % $HClO_4$ the water content in the gel was further lowered ($H_2O/SiO_2$ = 6) by applying mild vacuum at room temperature to find out the effect of further decrease in water concentration (Table 2.6, Entry 5). This resulted in the formation of NCL-5 phase with slight reduction in crystallization time, as it can be seen by comparing entry 1 with entry 5 in Table 2.6. Attempts to further lower the $H_2O/SiO_2$ molar ratio to 4.5 by water removal yielded MFI phase. The above observations are in presumption that in fluoride medium more concentrated reaction mixtures will lead to the more metastable phases.[17] The concentration of the structure directing agent (SDA) plays vital role in the phase formation and crystallization kinetics. When concentration of SDA (TEAOH) was increased in the range from 0.68 to 0.88 through 0.78 (Table 2.6, Entries 1, 6 and 7), a

decrease in the crystallization time was observed from 96 to 84 h through 91 h, respectively. This can be attributed to the increasing amount of $OH^-$ ions with increasing concentration of TEAOH.[16] It is quite interesting to note that in the absence of perchloric acid, keeping all other compositional and synthesis parameters same, *BEA phase was obtained (Table 2.6, Entry 8). This underlines the crucial role played by oxyanion ($HClO_4$) in the synthesis of polymorph B enriched BEA zeolite phases.

The effect of different synthesis variables on crystallization of NCL-5 phase is presented in Fig. 2.6. Curve (a) explain the effect of decrease of water content in the gel from $SiO_2/H_2O$ = 7.5 to 6.0. As discussed above, the time required in obtaining NCL-5 phase decreases from 96 to 88 h. Effect of TEAOH concentration on crystallization of NCL-5 phase presented in curve (b) and (c) shows similar trend as observed in case of NCL-7 sample. The crystallization period is found to decrease with increase in TEAOH content in the gel. It is clear from Table 2.6 that each synthesis parameter plays an important role in the synthesis of desired phase.

The detailed study of crystallization kinetics of NCL-6 was not presented as the similar trend was obtained as in case of NCL-5 and NCL-7.

**Table 2.6**

Effect of Different Synthesis Parameters on Phase Formation

Molar gel composition $SiO_2$ : w TEAOH : 0.57 HF : x $HClO_4$ : y $H_3PO_4$ : z$H_2O$,

Temperature: 408 K

| Entry No. | w | x | y | z | Synthesis Time (h) | Phase |
|---|---|---|---|---|---|---|
| 1 | 0.68 | 0.09 | _ | 7.5 | 96 | NCL-5 |
| 2 | 0.68 | 0.09 | _ | 8.5 | 110 | NCL-6 |
| 3 | 0.68 | 0.09 | _ | 9.5 | 120 | NCL-7 |
| 4 | 0.68 | 0.09 | _ | 4.5 | 68 | MFI |
| 5 | 0.68 | 0.09 | _ | 6.0 | 88 | NCL-5 |
| 6 | 0.78 | 0.09 | _ | 7.5 | 91 | NCL-5 |
| 7 | 0.88 | 0.09 | _ | 7.5 | 84 | NCL-5 |
| 8 | 0.68 | _ | 0.09 | 7.5 | 114 | *BEA |

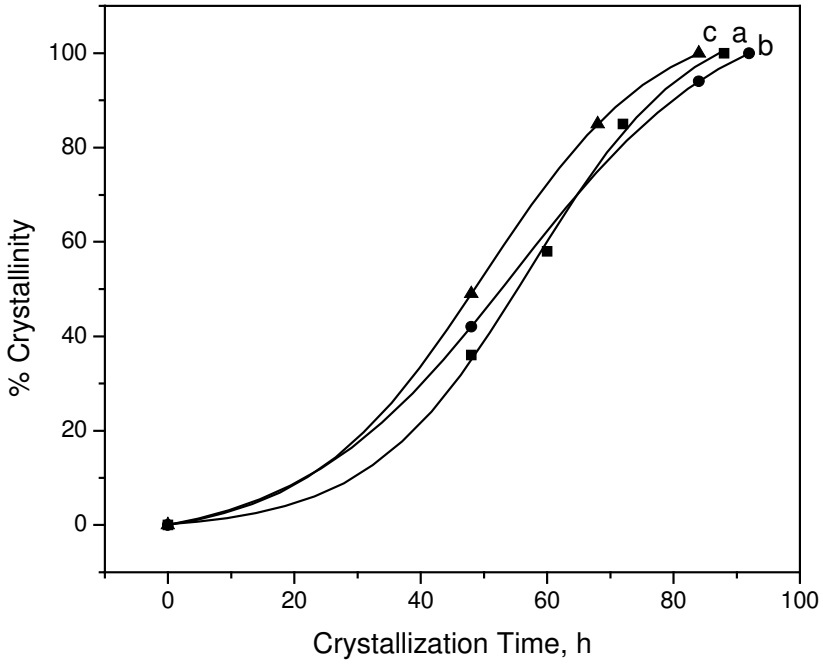


**Figure 2.6.** Effect of synthesis variables on crystallization kinetics of NCL-5 phase. Curve (a) represents the effect of lowering in water content in the synthesis gel ($SiO_2/H_2O$ = 6.0). Variation in the TEAOH concentration $SiO_2$/TEAOH = 0.78 and 0.88 is presented in curve (b) and (c).

## 2.4. SYNTHESIS OF Al-NCL-7

### 2.4.1. Experimental

#### *2.4.1.1. Synthesis of Al-NCL-7*

The synthesis of Al-NCL-7, a polymorph B enriched analog of zeolite Beta in the ratio of polymorph B : polymorph A as 65 : 35, was achieved using aluminum isopropoxide as Al-source and TEOS as Si-source. In a usual synthesis, 20.83 g TEOS and 28.61 g of tetraethylammonium hydroxide were mixed together. The gel was subjected to the complete hydrolysis and afterwards, 0.204 g of aluminum isopropoxide in 5 mL dry IPA was added to the synthesis mixture. The gel was stirred for 30 min. To this, 2.75 g of hydrofluoric acid was added as mineralizing agent. Finally, 1.29 g of $HClO_4$ was added and the stirring of the gel was continued till the homogenous reaction mixture was obtained. The resultant molar gel composition was found to be $SiO_2$ : 0.005 $Al_2O_3$ : 0.78 TEAOH : 0.55 HF : 0.09 $HClO_4$ : 9.5 $H_2O$. The gel was further crystallized at 408 K for 86 h. The obtained product was filtered with distilled water, followed by acetone and dried at 383 K for 4-6 h. The sample was further calcined at 833 K for 12-14 h in air.

#### *2.4.1.2. Synthesis of Al-impregnated NCL-7*

The synthesis of Al-impregnated NCL-7 was carried out for comparative study. In a typical synthesis, 3.0 g of calcined all silica NCL-7 sample was added to a solution of 0.102 g aluminum isopropoxide dissolved in 15.0 g isopropyl alcohol to prepare Al-impregnated NCL-7 with Si/Al = 100. The mixture was mixed thoroughly and heated to dryness. The dried impregnated sample was then calcined at 773 K for 8 h.

### 2.4.2. Results and Discussion

The synthesis of Al-NCL-7 was carried out under different synthesis conditions such as, varying the pH of the gel and Al content in the gel, in order to study their role on the crystallization period and phase formation.

#### *2.4.2.1. Effect of Al-Content*

The effect of Al-content on the phase formation and crystallization time is tabulated in Table 2.7. Synthesis of Al-NCL-7 was carried out in the range of Si/Al = 75 to 200 using the molar gel composition $SiO_2$ : x $Al_2O_3$ : 0.98 TEAOH : 0.57 HF : 0.09 $HClO_4$ : 9.5 $H_2O$ at 408 K. The synthesis of Al-containing polymorph B-enriched zeolite Beta (polymorphic proportions of polymorph B : polymorph A = 65 : 35), Al-NCL-7, was achieved in the range of Si/Al = 100 to Si/Al = 200 as specified in Table 2.7. Further increasing the Al-content in the gel to Si/Al = 75 (Table 2.7, Entry 1) leads to the formation of normal Beta. It is well known that the content of aluminum in the gel is one of the major factors for deciding the formation of phase in case of high silica materials as reported in the case of other zeolites.[19] At the same time, decrease in crystallization period is also observed with the lowering of Al-content in the gel.

**Table 2.7**

Effect of Al-Content in Gel on Phase Formation and Crystallization Time

Molar gel composition $SiO_2$ : x $Al_2O_3$ : 0.98 TEAOH : 0.57 HF : 0.09 $HClO_4$ : 9.5 $H_2O$, Temperature: 408 K

| Entry No. | x | Time (h) | Phase |
|---|---|---|---|
| 1 | 0.0066 | 96 | Al-Beta |
| 2 | 0.005 | 108 | Al-NCL-7 |
| 3 | 0.004 | 102 | Al-NCL-7 |
| 4 | 0.0033 | 94 | Al-NCL-7 |
| 5 | 0.0025 | 88 | Al-NCL-7 |

***2.4.3.2. Effect of pH***

Table 2.8 depicts the role of pH on the phase formation and crystallization time on the synthesis of Al-NCL-7. The pH of the gel was adjusted by varying the amount of tetraethylammonium hydroxide keeping all other synthesis variables constant. As seen from Table 2.8, the synthesis of Al-containing polymorph B-enriched zeolite Beta (Al-NCL-7, Si/Al = 100) can be achieved in the pH range of 8.0-10.0, which corresponds to the TEAOH/$SiO_2$ ratio = 0.78-0.98. At the lower TEAOH content i.e. TEAOH/$SiO_2$ = 0.58 and 0.68, the obtained phase was normal Beta with intergrowth of polymorph B : polymorph A = 55 : 45 (Table 2.8, Entry 1 and 2). It appears that the hydroxide concentration and amount of structure directing agent ($TEA^+$) in the gel is altering the crystallization time as well as changing crystallization phase.[20]

In case of Al-NCL-7 sample, lowering of crystallization period was observed from 120 to 108 h with the increase in the pH of the gel from 8.0 to 9.8 (Table 2.8, Entry 3-5). The decrease in the crystallization time may be attributed to greater amount of reactant dissolved in the alkali which in turn will lead to the growth of greater number of nuclei due to more numerous interactions between the more concentrated precursor species in the solution.

Moreover, aluminum is known to form tetrahedral co-ordination only in the basic pH in comparison with silica, which forms the tetrahedral phase all over the pH range. The solid-state $^{27}$Al MAS NMR study (Chapter 3, Section 3.3.2.4) shows that most of Al in Al-NCL-7 samples exhibit tetrahedral co-ordination showing a strong peak at 54 ppm and very small amount of aluminum is present in octahedral co-ordination.[21,22]

**Table 2.8**

Effect of pH on Synthesis of Al-NCL-7

Molar gel composition $SiO_2$ : 0.005 $Al_2O_3$ : x TEAOH : 0.57 HF : 0.09 $HClO_4$ : 9.5 $H_2O$; Temperature: 408 K

| Entry No. | x | pH | Time (h) | Phase |
|---|---|---|---|---|
| 1 | 0.58 | 7.0 | 90 | Al-Beta |
| 2 | 0.68 | 7.5 | 86 | Al-Beta |
| 3 | 0.78 | 8.0 | 120 | Al-NCL-7 |
| 4 | 0.88 | 8.7 | 112 | Al-NCL-7 |
| 5 | 0.98 | 9.8 | 108 | Al-NCL-7 |

## 2.5. SYNTHESIS OF Ti-NCL-7

### 2.5.1. Experimental

#### *2.5.1.1. Synthesis of Ti-NCL-7*

Ti-containing polymorph B enriched analog of zeolite Beta in the ratio of polymorph B : polymorph A as 65 : 35 (Ti-NCL-7) was carried out with the aid of titanium isopropoxide, TEOS as titanium and silica source, respectively. TEAOH and HF were utilized as structure directing agent and mineralizing agent. The molar gel composition in this case was $SiO_2$ : 0.01 $TiO_2$ : 0.68 TEAOH : 0.57 HF : 0.09 $HClO_4$ : 9.5 $H_2O$. The crystallization temperature of the gel was maintained at 408 K under autogeneous pressure and stirring condition (rpm = 100) using Parr autoclave. The time required to obtain fully crystalline Ti-NCL-7 phase was found to be 144 h.

#### *2.5.1.2. Synthesis of Ti-impregnated NCL-7*

Ti-impregnated NCL-7 sample with Si/Ti = 100 was prepared by the addition of 3.0 g of all siliceous NCL-7 to a mixture of 0.284 g of titanium isopropoxide in 15.0 g isopropyl alcohol. The mixture was stirred till homogenous slurry is obtained. The sample was further dried at 383 K and calcined at 773 K for 8 h.

### 2.5.2. Results and Discussion

Direct substitution of titanium in NCL-7 structure was studied using the molar gel composition $SiO_2$ : x $TiO_2$ : 0.68 TEAOH : 0.57 HF : 0.09 $HClO_4$ : 9.5 $H_2O$ at 408 K, where x = 0.013 to 0.005. As shown in Table 2.9, Ti-NCL-7 can be synthesized in the range of Si/Ti molar ratio = 100-200 (Table 2.9, Entry 2-5). When the synthesis trial was

conducted with increase in the Ti-content to 0.013, the obtained phase was found to be normal Beta without any enrichment of polymorph B in the structure despite of maintaining the key factors such as lower water content in the gel ($H_2O/SiO_2$ = 9.5) and presence of $HClO_4$ as promoter. Similar trend was observed during the synthesis of Al-NCL-7. Higher content of Ti and Al in the synthesis gel shows preference for the formation of normal Beta whereas the lower content of the same favours the formation of B-enriched NCL-7 structure.

**Table 2.9**

Effect of Ti-content on Ti-NCL-7

Molar gel composition $SiO_2$ : x $TiO_2$ : 0.68 TEAOH : 0.57 HF : 0.09 $HClO_4$ : 9.5 $H_2O$, Temperature: 408 K

| Entry No. | x | Time (h) | Phase |
|---|---|---|---|
| 1 | 0.013 | 120 | Ti-Beta |
| 2 | 0.01 | 144 | Ti-NCL-7 |
| 3 | 0.008 | 132 | Ti-NCL-7 |
| 4 | 0.0065 | 124 | Ti-NCL-7 |
| 5 | 0.005 | 115 | Ti-NCL-7 |

## 2.6. SYNTHESIS OF REFERENCE SAMPLES

### 2.6.1. Synthesis of Al-Beta

Al-Beta (Si/Al = 28) was synthesized using reported procedure[23] having molar gel composition as $SiO_2$ : 0.4 TEAOH : 0.08 $Na_2O$ : 0.033 $Al_2O_3$ : 25 $H_2O$. Tetraethyl-ammonium hydroxide, sodium aluminate (43.8 % $Al_2O_3$, 39 % $Na_2O$) and silica sol (40 % $SiO_2$) were employed as structure directing agent, Al- and Si-source, respectively. Sodium hydroxide was used as a base. The gel was crystallized at 413 K for 72 h to obtain the fully crystallized material. The solid product thus obtained was separated from mother liquor by filtration and washed thoroughly with distilled water. The product was dried at 383 K under vacuum for 2 h. The sample was further calcined at 833 K at a heating rate of 1 K per minute in order to remove the template. It was further subjected to repetitive ion exchange using 0.1 M aqueous ammonium nitrate solution at 353 K. After washing appropriately, the sample was finally dried followed by calcination at 833 K to obtain its protonic form.

### 2.6.2. Synthesis of Ti-Beta

The synthesis of hydrophobic Ti-Beta was carried out in fluoride medium using the molar composition: $SiO_2$ : 0.01 $TiO_2$ : 0.55 TEAOH : 0.55 HF : 7.5 $H_2O$, as reported in reference.[24] The typical synthesis gel was prepared by hydrolyzing 20.83 g of TEOS in 23.14 g of aqueous TEAOH solution. The mixture was kept under stirring until the complete evaporation of ethanol formed during hydrolysis of TEOS. To this, 0.340 g of titanium isopropoxide was added in 5 g of dry isopropyl alcohol. Finally, 2.75 g of 40 % HF added and the stirring was continued till the homogenous gel was obtained. The crystallization was carried out in 250 mL stainless steel Parr autoclave at 408 K with

rotation (~100 rpm) for 96 h. After required heating time, the autoclave was cooled and the solid was recovered by filtration and extensively washed with distilled water. Finally, the solid was dried at 383 K and calcined at 833 K.

### 2.6.3. Synthesis of Silicalite-1

The synthesis of Silicalite-1 was carried out by using TEOS as silica source and tetrapropylammonium hydroxide (TPAOH) as structure directing agent. In a classical synthesis, 20.83 g of TEOS was added to 33.35 g of 20 % aqueous solution of TPAOH. The gel was stirred around 1 h or till completion of hydrolysis. Finally, 18.16 g of water was added. The resultant molar gel composition $SiO_2$ : 0.33 TPAOH : 25 $H_2O$ was allowed to crystallize at 443 K for 36 h. The product thus obtained after crystallization was filtered, washed thoroughly with distilled water and acetone, and dried at ambient temperature under vacuum. Further, the sample was calcined in air at 813 K for 12 h.

### 2.6.4. Synthesis of Al-ZSM-5

The synthesis of Al-ZSM-5 was performed as per the procedure reported earlier.[25,26] Sodium silicate, aluminum sulphate, triethylbutylammonium bromide (TEBABr), sulphuric acid and distilled water were used as raw materials. The preparation of the synthesis gel was carried out in following steps.

i. In first step, sodium silicate solution was prepared by diluting 76.27 g sodium silicate with 35 g distilled water.

ii. In second step, 2.8 g triethylbutylammonium bromide salt was added in 17 g distilled water.

iii. In step three, acidified aluminum sulphate was prepared by adding 7.24 g sulphric acid and 52 g distilled water to 0.898 g aluminum sulphate.

The aluminosilicate gel was prepared by adding solution of TEBABr salt to the sodium silicate solution slowly over the period of 5-10 min. Finally, an acidified aluminum solution was added slowly to above mixture under vigorous stirring over the period of ~15 minutes. The gel so formed was kept under stirring at ambient temperature for 60 minutes and pH was maintained at 10.5 $\pm$ 0.2. The resultant molar gel composition was found to be $SiO_2$ : 0.0004 $Al_2O_3$ : 0.033 TEBABr : 0.23 $H_2SO_4$ : 26 $H_2O$. The gel was heated hydrothermally at 443 K for 24 h. The solid product obtained was separated by filtration and washed with copious amount of distilled water and dried overnight at 393 K. Further, the calcined sample was treated with 1 M aqueous ammonium nitrate (25 mL of ammonium nitrate for 1 g of sample) solution three times at 353 K. The sample was again washed thoroughly and calcined at 773 K to obtain the H-form of Al-ZSM-5.

**2.6.5. Synthesis of Si-MCM-41**

Synthesis of siliceous MCM-41 was carried out using cetyltrimethylammonium bromide (CTABr) as template and tetramethylammonium hydroxide (TMAOH) as base. In a typical synthesis procedure, 6 g fumed silica was added to a solution of 11.66 g TMAOH in 56.25 g $H_2O$ and stirred for 45 min. To this solution, 7.2 g of CTABr in 85 g $H_2O$ was added drop wise under stirring condition and stirring was continued for another 45 min. Finally, 75 g of $H_2O$ was added to the synthesis gel and further stirred for 30 min and autoclaved at 383 K for 36 h. The resultant molar gel composition was $SiO_2$ : 0.32

TMAOH : 0.2 CTABr : 125 $H_2O$. The product thus obtained after hydrothermal synthesis was filtered, washed thoroughly with distilled water and acetone, and dried at ambient temperature under vacuum. The sample was calcined at 813 K in presence of air for 7-8 h to remove the template.

### 2.6.6. Synthesis of Al-MCM-41

The synthesis of Al-MCM-41 sample was carried out using the reported procedure.[27] An aqueous solution of 0.47 g of $NaAlO_2$ was added to the mixture of 6 g fumed silica, 10.94 g TMAOH and 56.8 g water under stirring. To this, solution of 7.2 g of CTABr in 75 g $H_2O$ was added drop wise under stirring condition, stirring was continued for another 45 min. Finally, remaining amount of distilled water was added to the synthesis gel and crystallized at 383 K for 48 h. The product thus obtained after hydrothermal treatment was filtered, washed thoroughly with distilled water followed by acetone, and dried at ambient temperature under vacuum. Further, the sample was calcined at 813 K in presence of air for 8 h to remove the template. The H-form of Al-MCM-41 was obtained by treating the calcined samples with 0.5 M ammonium acetate solution (50 mL for 1.0 g sample) twice at room temperature, followed by calcination in air at 773 K for 6 h.

## 2.7. CONCLUSIONS

The new structures of BEA type topology with enrichment of polymorph B denoted as NCL-5, NCL-6 and NCL-7 were successfully synthesized. The synthesis parameters such as temperature, crystallization time, concentration of structure directing agent, different promoters, promoter concentration and water content in the gel were studied on polymorph B intergrowth of zeolite Beta entitled as NCL-5 and NCL-7 in detail. Synthesis of NCL-7 can be achieved in the temperature range 373-413 K, $TEAOH/SiO_2$ molar ratio 0.68-0.98, $HClO_4/SiO_2$ molar ratio 0.08 to 1.2 and $H_2O/SiO_2$ molar ratio 9.5. NCL-5 phase, with the enrichment of polymorph B *ca.* 90-95 %, can be synthesized in $TEAOH/SiO_2$ molar ratio 0.68-0.98 and $H_2O/SiO_2$ molar ratio 6.0-7.5 using $HClO_4$ as promoter. The key factors, which enabled to get preferentially higher concentration of polymorph B of zeolite Beta family, are the use of perchlorate as promoter oxyanion in fluoride medium and the $H_2O/SiO_2$ molar ratio. Furthermore, Al and Ti are incorporated in the structure of NCL-7 having the enrichment of polymorph B to 65 %.

## 2.8. REFERENCES


1. Wadlinger, R.; Keer, G. T.; Rosinski, E. J. U.S. Patent 3, 30, 8069, 1967.
2. Caputo, D.; Corbo, P.; Iucolano, F.; Migliardini, F.; Colella, C. *Separation Sci. Technology* **2004**, *39*, 1547.
3. Tabata, T.; Kokitsu, M.; Ohtsuka, H.; Okada, O.; Sabatino, L. M. F.; Bellussi, G. *Catal. Today* **1996**, *27*, 91.
4. Corma, A.; Palomares, A.; Marquez, F. *J. Catal.* **1997**, *170*, 132.
5. Hoefnagel, A.T.; Van Bekkum, H. *Appl. Catal. A* **1993**, *97*, 87.
6. Corma, A.; Garcia, H.; *Chem. Rev.* **2003**, *103*, 4307.
7. Kozhevnikova, E. F.; Quartararo, J.; Kozhevnikov, I. V. *Appl. Catal. A* **2003**, *245*, 69.
8. Taylor, R. J.; Petty, R. H. *Appl. Catal. A* **1994**, *119*, 121.
9. Newsam, J. M.; Treacy, M. M. J.; Koetsier, W. T.; De Gruyter, C. B. *Proc. R. Soc. London* **1988**, *A420*, 375.
10. Higgins, J. B.; LaPierre, R. B.; Schlenker, J. L.; Rohrman, A. C.; Wood, J. D.; Kerr, G. T.; Rohrbaugh, W. J. *Zeolites* **1988**, *8*, 446.
11. Kumar, R.; Bhaumik, A.; Ahedi, R. K.; Ganapathy, S. *Nature* **1996**, *298,* 381.
12. Kumar, R.; Mukherjee, P.; Pandey, R. K.; Rajmohanan, P.; Bhaumik, A. *Microporous Mesoporous Mater.* **1998**, *22*, 23.
13. Mukhopadhyay, K.; Ghosh, A.; Kumar, R. *Chem. Commun.* **2002**, *2404*.
14. Treacy, M. M. J.; Deem, M. W.; Newsam, J. M. *Computer Code DIFFaX, Version 1.807* NEC Research Institute, Inc.: Princeton, New Jersey, **2000**.
15. Treacy, M. M. J.; Newsam, J. M. *Nature* **1988**, *332,* 249.
16. Camblor, M. A.; Mifsud, A.; Perez-Periente, J. *Zeolites* **1991**, *11*, 792.
17. Camblor, M. A.; Corma, A.; Valencia, S. *Chem. Comm.* **1996**, 2365.
18. Kadgaonkar, M. D.; Kasture, M. W.; Bhange, D. S.; Joshi, P. N.; Ramaswamy, V.; Kumar, R. *Microporous Mesoporous Mater*. **2007**, *101*, 108.
19. Szostak, R. *Molecular Sieves-Principles of Synthesis and Identification* Blackie: London, **1998**.
20. Klinowski, J.; Thomas, J. M.; Fyfe, C. A.; Hartman, J. S. *J. Phys. Chem.* **1981**,

*85*, 2590.

21. Fyfe, C. A.; Gobbi, G. C.; Klinowski, J.; Thomas, J. M.; Ramdas, S. *Nature* **1982**, *296*, 530.
22. Casci, J. L.; Whittam, T. V.; Lowe, B. M. In *Proc. 6th Int.Conf. on Zeolites* Olson D. Bisio A. Eds Butterworth, **1984**, 894.
23. Kasture, M. W.; Niphadkar, P. S.; Sharanappa, N.; Mirajkar, S. P.; Bokade, V. V.; Joshi, P. N. *J. Catal.* **2004,** *227,* 375.
24. Blasco, T.; Camblor, M. A.; Corma, A.; Esteve, P.; Guil, J. M.; Martinez, A.; Perdigon-Melon, J. A.; Valencia, S. *J. Phys. Chem. B* **1998**, *102*, 75.
25. Shiralkar, V. P.; Joshi, P. N.; Eapen, M. J.; Rao, B. S. *Zeolites* **1991**, *11*, 511.
26. Kotasthane, A. N.; Shiralkar V. P. *Thermochimica Acta* **1986,** *102,* 31.
27. Kadgaonkar, M. D.; Laha, S. C.; Pandey, R. K.; Kumar, P.; Mirajkar, S. P.; Kumar, R. *Catal. Today* **2004**, *97*, 225.

## 3.1. INTRODUCTION

Information on structural and textural properties of zeolite is essential to understand sorption and catalytic applications.[1-3] Individual characterization technique gives information about particular aspect of the material. Therefore, it is necessary to apply different characterization tools in combination to thoroughly understand the complex structure of these materials and their possible utility as adsorbents and catalyst in different chemical processes.[4-6] Different characterization techniques utilized for characterizing zeolite and informations obtained from them are briefly described in Chapter 1(Section 1.8). Present chapter deals with the experimental details and the results of different characterization techniques used in the present dissertation. The techniques such as powder X-ray diffraction (PXRD), $N_2$ adsorption, diffuse reflectance UV-Vis, FTIR, solid state magic angle spinning (MAS) NMR and scanning electron microscopy (SEM) were used to characterize various mesoporous and microporous materials, synthesized as described in Chapter 2.

## 3.2. EXPERIMENTAL

### 3.2.1. X-Ray Diffraction

The powder X-ray diffractograms of as-synthesized and calcined samples were recorded on Rigaku Miniflex diffractometer using a Ni-filtered monochromatic Cu *K*α radiation (λ = 1.5406 Å). The microporous materials were scanned between 5-60° (2θ) whereas the diffractograms of mesoporous materials were recorded in the 2θ range 1.5-10°. The samples were prepared as thin layers on glass/aluminum slides, prior to scanning.

The polymorph B-enriched structures NCL-5, NCL-6 and NCL-7 were scanned on a Philips X'Pert Pro powder X-ray diffractometer using Co Kα radiation (λ = 1.7903 Å) on a flat sample stage in the reflection mode. The diffractometer was equipped with a Fe filter and X'celerator as detector, which uses the RTMS technique enhancing both intensity and resolution of the reflections. The samples were scanned in the range 5-60° 2θ at the rate of 0.01732 degrees/minute to increase the intensity of weak and overlapping reflections. The Rietveld refinement of the powder XRD pattern of NCL-5, NCL-6 and NCL-7 was attempted using the X'Pert Plus software. The polymorphic composition of polymorph A and B was also established using the Fortran-based code DIFFaX. Within the DIFFaX formalism, a crystalline solid is treated as a stacking of layers of atoms interconnected by stacking vectors: an approach that is ideally suited for layered materials and the diffraction intensities are computed layer by layer and integrated over an infinite or finite number of layers. By changing the layer composition or the stacking sequence, it is possible to build in different types of disorder into the lattice and compute the changes in the pattern.

### 3.2.2. Adsorption Measurements

The specific surface area, pore size and pore volume of calcined samples were determined by BET method from $N_2$ adsorption isotherms using a commercial volumetric adsorption apparatus (Omnisorb 100 CX, Coulter Corporation, USA). Prior to measurement, sample was degassed for 12 h under vacuum at 573 K. The specific surface areas were determined by BET method.

### 3.2.3. Diffuse Reflectance UV-Vis Spectroscopy

The diffuse reflectance UV-Vis spectra were recorded in the range 200-600 nm wavelength using Shimadzu UV-2101 PC spectrometer equipped with a diffuse reflectance attachment using solid sample holder. The base line correction was made using barium sulfate as the reference standard.

### 3.2.4. Fourier Transform Infrared (FTIR) Spectroscopy

The IR spectra for the framework vibrations were recorded on Nicolet-740 instrument with a resolution of 2 $cm^{-1}$ using KBr wafer technique. Prior to measurement, the calcined samples were dried thoroughly under vacuum at 423 K. For preparing KBr pallets, 1 mg of sample was ground with 99 mg of KBr and pressed into a disc of 1 cm diameter. As many as 300 scans were co-added for plotting each spectrum.

### 3.2.5. Nuclear Magnetic Resonance (NMR) Spectroscopy

Solid-state $^{29}Si$ MAS NMR and $^{27}Al$ MAS NMR spectra were recorded on Bruker MSL-300 NMR spectrometer at 59.595 MHz. The finely powdered calcined samples were placed in zirconia rotor and spun at 4 kHz. The chemical shifts were referred with respect to tetraethylorthosilicate ($\delta$ = -82.4 ppm from TMS) and $Al(H_2O)_6^{3+}$ ($\delta$ = 0.0 ppm) as reference compounds for recording $^{29}Si$ MAS NMR and $^{27}Al$ MAS NMR, respectively.

### 3.2.6. Scanning Electron Microscopy (SEM)

The SEM micrographs of the samples were obtained on JEOL JSM-5200 scanning electron microscope. The samples were loaded on stubs and sputtered with thin

gold film to prevent surface charging and also to protect from thermal damage from the electron beam, prior to scanning.

## 3.3. RESULTS AND DISCUSSION

### 3.3.1. Polymorph B-Enriched Structures: NCL-5, NCL -6 and NCL -7

#### *3.3.1.1. X-Ray Diffraction*

Powder X-ray diffraction technique has been used as preferential tool to investigate the phase purity and polymorphic composition of polymorph B-enriched structures NCL-5, NCL-6 and NCL-7. Two different approaches, Rietveld refinement and DIFFaX code, were used to elucidate the structure and polymorphic proportion in NCL-5, NCL-6 and NCL-7 structures. Comparison of these two techniques is depicted below.

##### *3.3.1.1.1. Rietveld refinement*

Rietveld refinement is a technique investigated by Hugo Rietveld and commonly used in the characterization of crystalline materials.[7] Introduction of this technique was a significant step forward in the diffraction analysis of powder samples. The neutron and X-ray diffraction of powder samples results in a pattern characterized by peaks in intensity at certain positions. The height, width and position of these peaks can be used to determine many structural aspects of the material structure. The Rietveld method uses a least square approach to refine a theoretical line profile until it matches the measured profile.

Figure 3.1 depicts the powder XRD patterns of calcined NCL-5, NCL-6, NCL-7 and *BEA samples along with simulated pattern of pure polymorph B. The X-ray profile consists of mainly sharp reflections and some broad peaks indicative of the inherent faulting characteristic of the *BEA. In comparison to the reported powder patterns of

zeolite Beta, the samples synthesized in the present study yielded fairly good powder patterns indicating the predominant phase of polymorph B. Similar values of the ratio of the relative intensity of the first two peaks (110 and $11\bar{1}$) in the low angle region of NCL-5 (1.42) and the simulated pattern of polymorph B (1.45) also supports the synthesis of polymorph B rich sample. The similarities between the experimental pattern of NCL-5 and simulated pattern of polymorph B confirm its successful synthesis for the first time. Although, the Rietveld refinement of powder patterns of disordered zeolite Beta is not appropriate for structural studies, yet the refinement method was used to derive the phase composition and also possible structural refinement till the model was steady. Coordinates for polymorphs A and B were taken from the reported data by Higgins *et al.*[8]

The Rietveld refinement was started with the correction of scale, zero shift and background employing a polynomial with six refinable variables using the X'Pert Plus software. The scale was refined through out the refinement. The shapes of the profiles were refined using a Pseudo-Voigt function. During the initial stages of the refinement of the profile parameters, only the lattice parameters of the three phases were refined. Various refinement strategies were used which involved use of a single polymorph for refinement, combination of two polymorphs at a time and finally simultaneous refinement of all the three polymorphs at a time. Because of negative effect of the polymorph C in samples, further refinement was done using only polymorph A and B. After refining the lattice parameters of both the polymorphs, the overlapping reflections from the two phases could be identified and the refinement converged well to give a reasonably good fit between the calculated and the observed profiles enabling us to get the relative contribution of polymorph A and B in all the three samples viz. NCL-5, NCL-6 and NCL-7. During the course of the refinement the pattern was checked for the

chemical and structural sensibility of the models, at regular intervals. The refinement of the structural parameters was done till the model was stable. The R values could not be improved further because the atoms could not be stably refined due to the inherent disorder present in the samples. This led to the differences in the intensities in the calculated and experimental patterns. However, the refinement strategy is largely helpful in determining the phase composition in our samples. The Rietveld refinement plots of a typical polymorph B rich sample along with the difference plot are given in Fig. 3.2. Detailed crystallographic data obtained from Rietveld refinement is given in Table 3.1. A model generated on the basis of the refined crystallographic data of typical polymorph B rich sample is shown as an inset in Fig. 3.2.

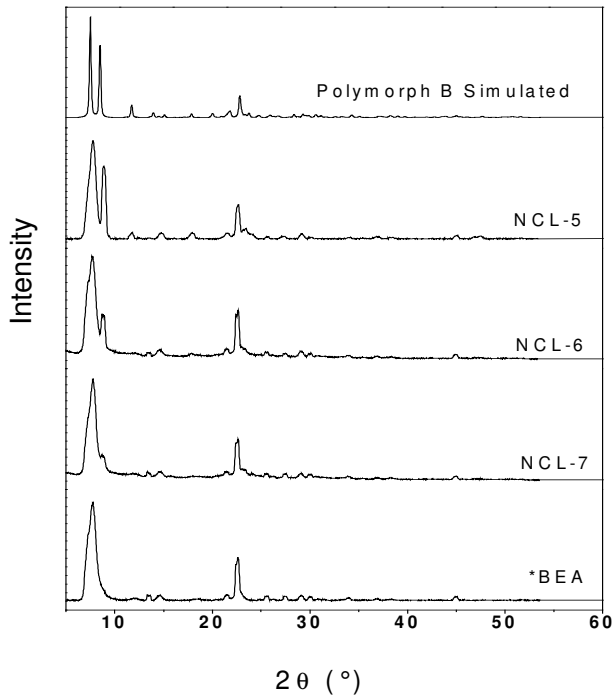


**Figure 3.1.** The powder XRD patterns of simulated polymorph B and experimentally obtained NCL-5, NCL-6 and NCL-7 and *BEA (standard Si-Beta).

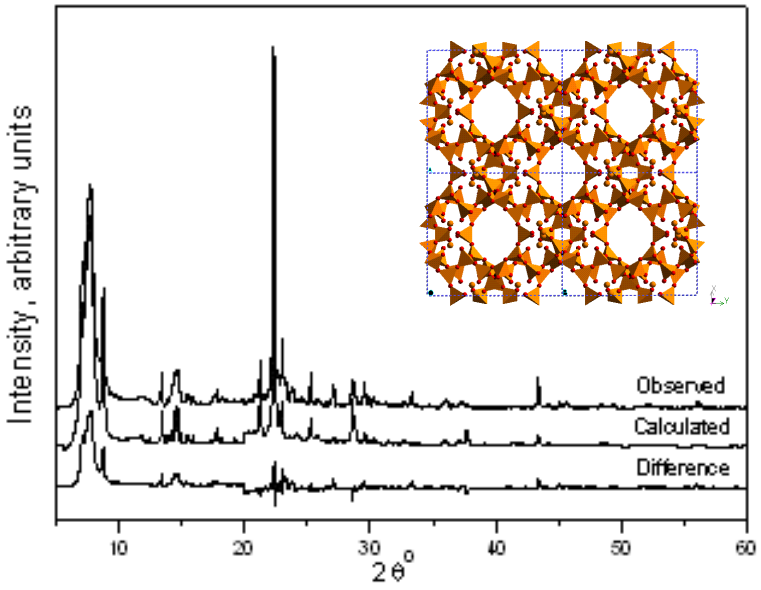


**Figure 3.2**. The observed, calculated and the difference profiles of a typical polymorph B-rich Beta sample (NCL-5), inset shows the structural model generated from the refined crystallographic data.

**Table 3.1**

Crystallographic Data Obtained from Rietveld Refinement of NCL-5 Sample

| | | | |
|---|---|---|---|
| Diffractometer | | Philips X-pert Pro | |
| Radiation | | Cu Kα (λ = 1.5406 Å) | |
| Detector | | X'celerator | |
| Mode of scanning | | Reflection geometry, rotation | |
| Step size | | 0.02°, 10s /step | |
| | | Polymorph A | Polymorph B |
| Space group | | $P4_122$ | C2/c |
| Lattice parameters | a (Å) | 12.661(4) | 17.821(4) |
| | b (Å) | 12.661(4) | 17.614(3) |
| | c (Å) | 26.406(3) | 14.424(3) |
| | β (°) | 90 | 114.41(1) |
| | V (Å$^3$) | 4232.90 | 4122.87 |
| % Contribution | | 2.3 (7) | 97.7 (7) |
| Rietveld Refinement Parameters | | | |
| $R_{Exp}= (N-P) / \sum x_i y_{io}^2$ | | 0.082 | |
| $R_p=\sum [y_{io} - y_{ic}]/ \sum y_{io}$ | | 0.260 | |
| $R_{wp}= [ \sum w_i (y_{io} - y_{ic})^2 / \sum w_i y_{io}^2 ]^{1/2}$ | | 0.347 | |

#### *3.3.1.1.2. DIFFaX*

DIFFaX is a FORTRAN based computer program that calculates diffraction intensities from crystals that contain coherent planar defects, such as twins and stacking faults. DIFFaX uses the recurring patterns found in randomized stacking sequences to compute the average interference wave function scattered from each layer type occurring in a faulted crystal. It is then a simple step to calculate the incoherent intensity contribution at *hkl*. General uses and methodology used in the implementation of DIFFAX code was carried out as summarized in the manual.[9]

Since, the Rietveld refinement of the powder pattern of disordered zeolite Beta is not appropriate for structural studies and the R values could not be improved since the atoms could not be stably refined due to the inherent disorder present in the sample, the Rietveld refinement is precluded for the faulty structures such as zeolite Beta. Hence, the simulations of powder patterns of zeolite Beta for different ratios of polymorphs A and B have been carried out using DIFFaX code.[9] This program is particularly useful to describe one-dimensional disorder of structures, which can be constructed by stacking layer-like building units along one direction. The stacking direction $c'$ is perpendicular to the $a'$ $b'$ plane of the layer. For comparison with the observed patterns of NCL-5, NCL-6 and NCL-7, the intensity values of simulated patterns for random intergrowths of polymorphs A and B were normalized. On comparison of the simulated patterns with the experimental patterns of NCL-5 (Fig. 3.3), NCL-6 (Fig. 3.4) and NCL-7 (Fig. 3.5), the best agreement was found with 90-95 %, 70-75 % and 60-65 % of polymorph B composition, respectively. The powder X-ray diffractogram of Si-Beta (with polymorphic proportions polymorph B : polymorph A = 55 : 45) is compared with the simulated

patterns of zeolite Beta with the intergrowth of polymorph B as 60 and 50 vis-à-vis polymorph A in Fig. 3.6. Broadening in the reflections of the observed patterns is due to the heavy faulting/disorder in the material. From the use of DIFFaX code to derive the polymorphic concentration of different materials NCL-5, NCL-6 and NCL-7 one can unambiguously affirm that these materials composed of intergrowth of polymorph B and polymorph A in B : A ratio of *ca.* 95 : 05, 75 : 25 and 65 : 35, respectively.

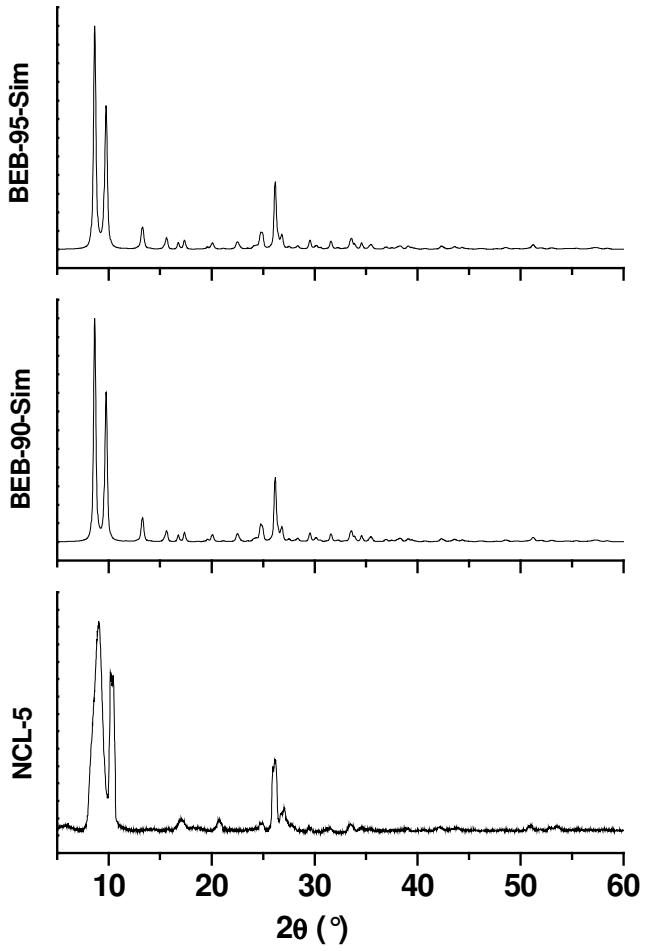


**Figure 3.3.** Comparison of the powder XRD pattern of NCL-5 with the simulated patterns of BEB-90-Sim and BEB-95-Sim consisting of the intergrowth of polymorph B : polymorph A ratio of 90 :10 and 95 : 05, respectively.

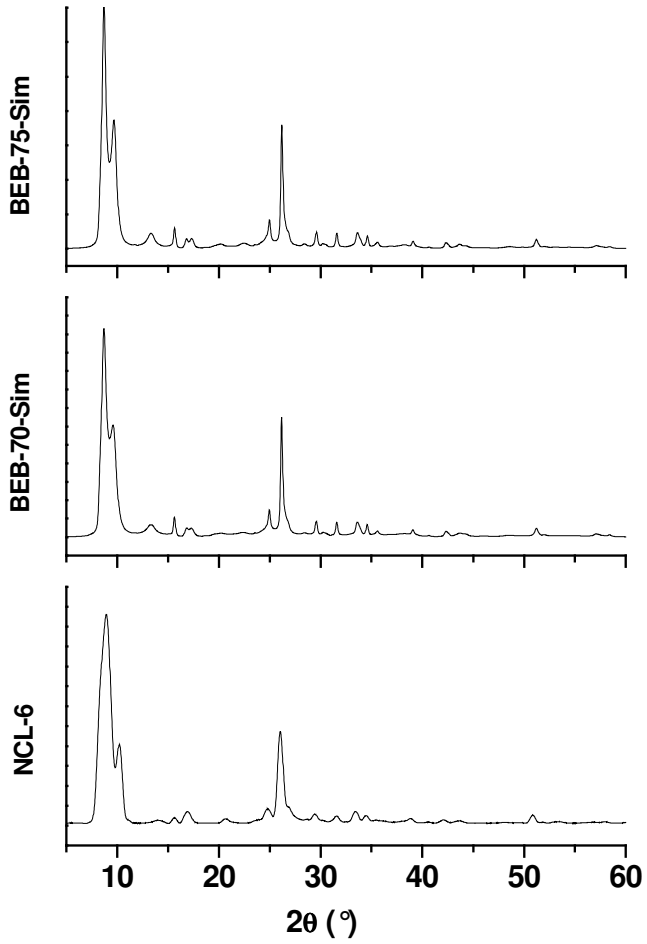


**Figure 3.4.** Comparison of the powder XRD pattern of NCL-6 with the simulated patterns of BEB-70-Sim and BEB-75-Sim consisting of the intergrowth of polymorph B : polymorph A ratio of 70 : 30 and 75 : 25, respectively.

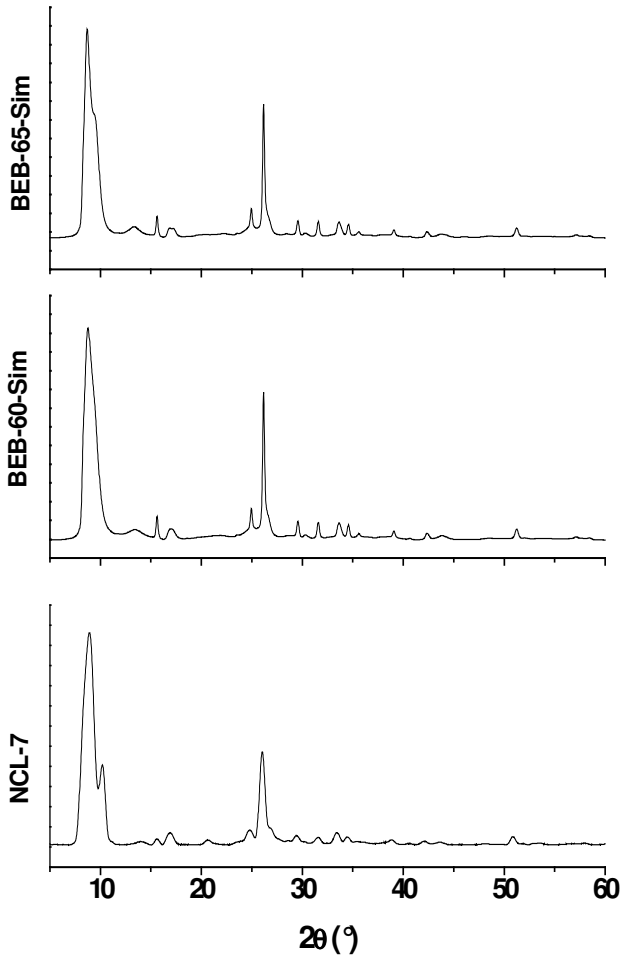


**Figure 3.5.** Comparison of the powder XRD pattern of NCL-7 with the simulated patterns of BEB-60-Sim and BEB-65-Sim consisting of the intergrowth of polymorph B : polymorph A ratio of 60 : 40 and 65 : 35, respectively.

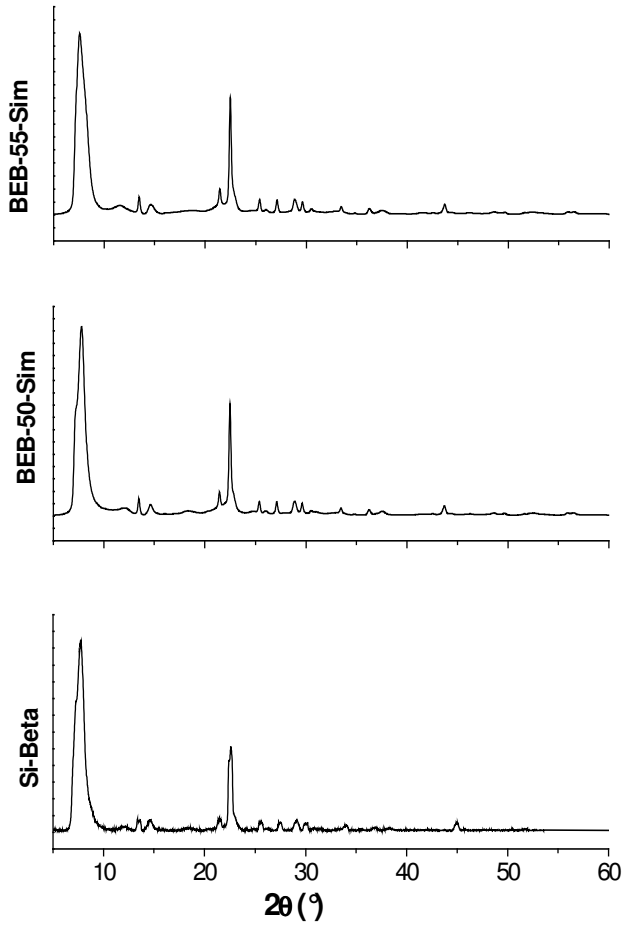


**Figure 3.6.** Comparison of the powder XRD pattern of Si-Beta with the simulated patterns of BEB-50-Sim and BEB-55-Sim consisting of the intergrowth of polymorph B : polymorph A ratio of 50 : 50 and 55 : 45, respectively.

### *3.3.1.2. $N_2$ Adsorption*

Table 3.2 outlines the low temperature $N_2$ adsorption-desorption isotherms for NCL-5, NCL-6 and NCL-7 samples in comparison Si-Beta. The surface area of the samples NCL-5, NCL-6, NCL-7 and Si-Beta calculated using the BET method was found to be 621, 589, 560 and 590 $m^2g^{-1}$, respectively. The representative adsorption-desorption isotherm of NCL-5, NCL-7 and Si-Beta is shown in Fig. 3.7. The pore diameter, calculated using HK method, of polymorph B-enriched analogs of all siliceous NCL-5, NCL-6 and NCL-7 samples was found to be 0.82, 0.76 and 0.77 nm, respectively, in comparison with 0.67 nm for Si-Beta having the polymorphic compositions as polymorph B : polymorph A in the ratio 55 : 45. However, the pore volume of all the samples found to have almost similar ~0.22 mL $g^{-1}$. The inherent faulting in zeolite Beta does not affect the accessible pore volume significantly, yet it influences the pore connectivity along c-direction. The enrichment of polymorph B in the sample leads to the increase in tortuousity. This may, in turn, influence the adsorption properties of polymorph B-rich samples.[10]

**Table 3.2**

Low Temperature $N_2$ Adsorption-Desorption Studies

| Sample Name | Polymorph Composition B : A | Surface Area[a] $m^2 g^{-1}$ (± 5 %) | Pore Diameter[b] (nm) | Pore Volume[c] mL/g (± 2 %) |
|---|---|---|---|---|
| NCL-5 | 90 : 10 | 621 | 0.82 | 0.22 |
| NCL-6 | 75 : 25 | 589 | 0.76 | 0.23 |
| NCL-7 | 65 : 35 | 560 | 0.77 | 0.23 |
| Si-Beta | 55 : 45 | 590 | 0.67 | 0.22 |

a = From $N_2$ adsorption measurement at 77 K

b = As per the HK formulation

c = As per t-method

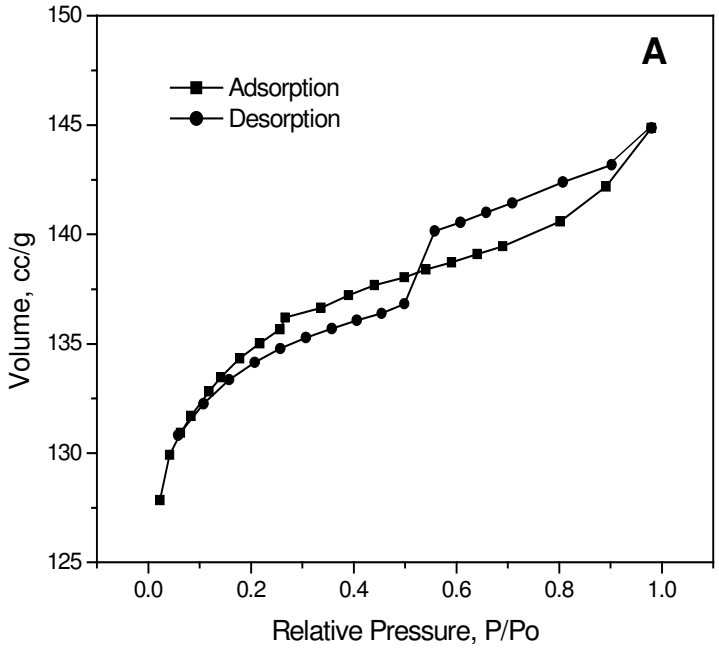
A
Adsorption
Desorption
Volume, cc/g
Relative Pressure, P/Po
150
145
140
135
130
125
0.0
0.2
0.4
0.6
0.8
1.0

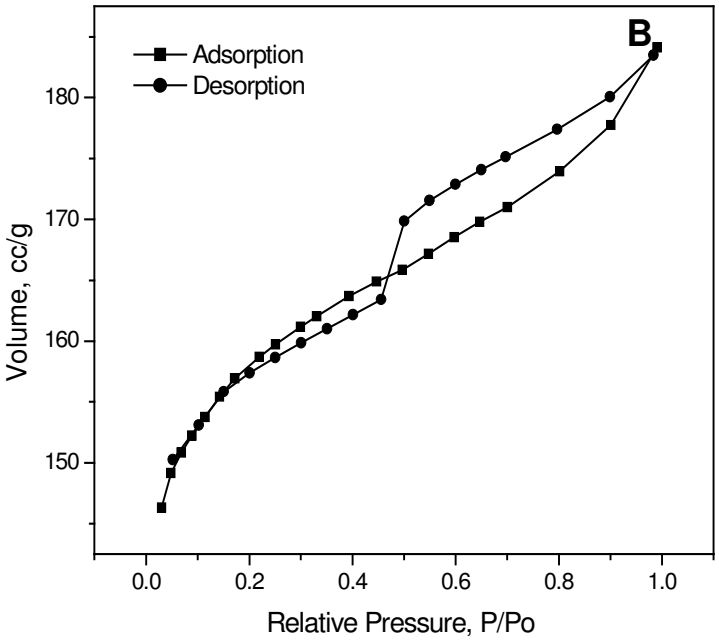
B
Adsorption
Desorption
Volume, cc/g
Relative Pressure, P/Po
180
170
160
150
0.0
0.2
0.4
0.6
0.8
1.0

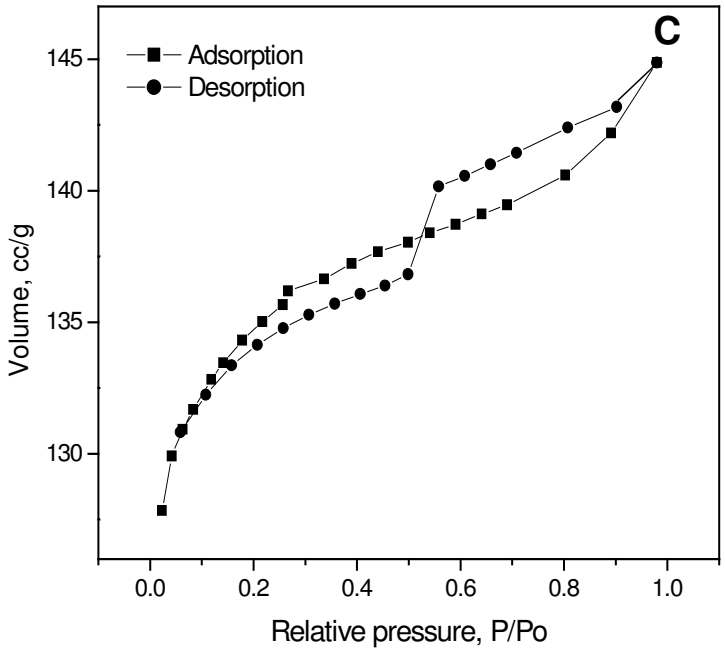


**Figure 3.7.** $N_2$ adsorption-desorption isotherm for NCL-5 (A), NCL-7 (B) and Si-Beta (C).

### *3.3.1.3. Framework FTIR Spectroscopy*

Curves a, b, c and d in Fig. 3.8 show the framework FTIR spectra of NCL-5, NCL-6, NCL-7 and Si-Beta, respectively, prepared in $F^-$ medium. The position of the FTIR vibrations for NCL-5, NCL-6 and Si-Beta are in good agreement with those reported earlier indicating the formation of fully crystalline BEA-type topology.[11-13] A band at 423 $cm^{-1}$ in all the samples show the characteristic feature of pore opening in zeolite Beta whereas band at 560 $cm^{-1}$ reflects the double ring vibrations. As postulated, the polymorph B compared to all Si-Beta (with polymorphic proportions as polymorph B

: polymorph A = 55 : 45) has more tortuous channel structure.[10] This should be reflected by the larger strain on Si-O bond thereby giving higher frequency vibrations. Because of this, the two prominent bands of almost equal intensity at around 1097 and 1018 $cm^{-1}$ (Fig. 3.8, curve d) in the TO asymmetric stretching region can be assigned to the Si-O stretching bands of polymorph B and A, respectively in all Si-Beta sample. However, in the case of NCL-5 (Fig. 3.8, curve a), the relative intensity of 1097 $cm^{-1}$ band increases significantly vis-à-vis 1018 $cm^{-1}$ band, which is almost absent. The relative intensity of these bands ($I_{1097}/I_{1018}$) follows the trend as NCL-5 (Fig. 3.8, curve a) > NCL-6 sample (Fig. 3.8, curve b) > NCL-7 (Fig. 3.8, curve c) > Si-Beta sample (Fig. 3.8, curve d). As shown in XRD patterns, the IR results are well align with the above postulate where the enrichment of polymorph B is found to be 90, 75 and 65 %, respectively in NCL-5, NCL-6 and NCL-7 samples. In the similar way, the pair of bands at 460 and 423 $cm^{-1}$ may also arise due to the presence of polymorph B and A, respectively in *BEA. Hence, the significantly higher intensity of 460 $cm^{-1}$ band (vis-à-vis 423 $cm^{-1}$ band) further supports the predominance of polymorph B in NCL-5.

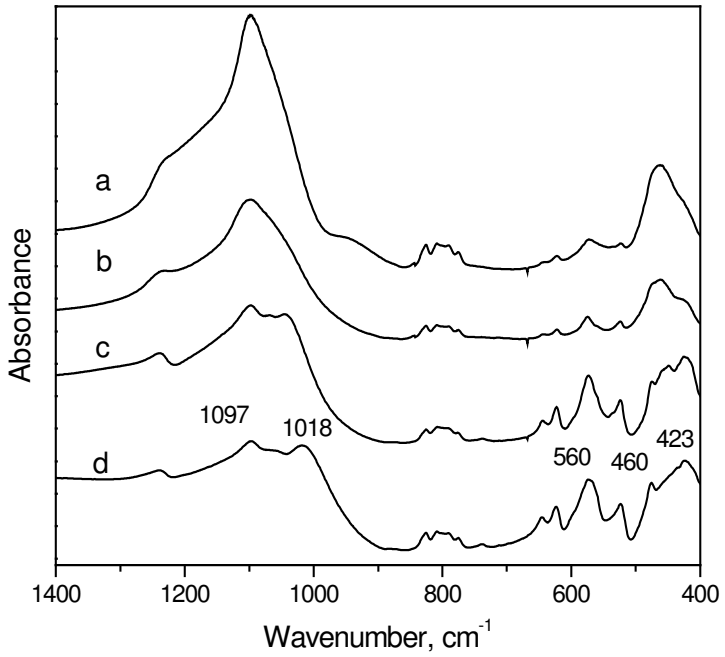


**Figure 3.8.** Framework FTIR spectra for NCL-5 (Curve a), NCL-6 (Curve b), NCL-7 (Curve c) and Si-Beta (Curve d).

### *3.3.1.4. $^{29}$Si MAS NMR Spectroscopy*

$^{29}$Si MAS NMR spectra of calcined all silica Si-Beta, NCL-7, NCL-6 and NCL-5 samples are presented in Fig. 3.9. All four samples do not show any distinctive peaks in the range of 95-100 ppm, due to the absence of $Q^3$ silicate species, which is in general agreement that relatively defect-free structure can be obtained by fluoride-mediated syntheses under mentioned conditions. The near absence of $Q^3$ species for the materials synthesized in fluoride medium can be attributed mainly to the pH of the gel and charge balance by $F^-$, where the synthesis is carried out at around the neutral pH as the charge balance is generally achieved by the occlusion of $F^-$.[14] Furthermore, the synthesis at lower

pH favors more complete condensation of silica. The $^{29}$Si MAS NMR spectra of the calcined samples were deconvoluted in 5 different T sites in the range of -111.46 to 115.98 ppm, which have been assigned to $Q^4$ sites.[15] The data for different $Q^4$ site population for these samples are provided in Table 3.3.

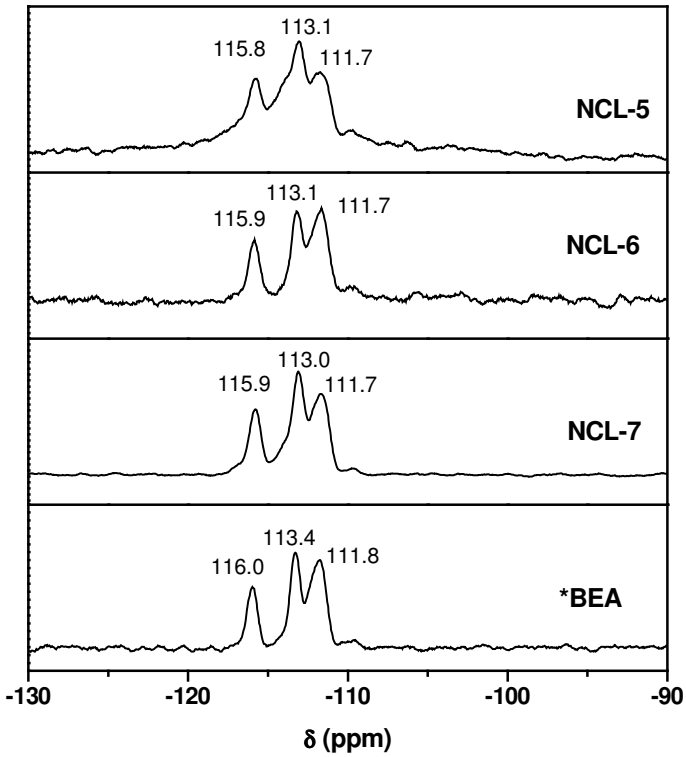


**Figure 3.9.** $^{29}$Si MAS NMR spectrum for Si-Beta (*BEA), NCL-7, NCL-6 and NCL-5 samples.

**Table 3.3**

$^{29}$Si MAS NMR Data for $Q^4$ Site Distribution in BEA Samples With Different Proportions of Polymorph B : Polymorph A

| Sample Name | Lattice Site $T_A$ (-111.58 ± 0.2 ppm) | | | Lattice Site $T_B$ (-112.20 ± 0.2 ppm) | | | Lattice site $T_C$ (-113.15 ± 0.2 ppm) | | | Lattice Site $T_D$ (-113.9 ± 0.2 ppm) | | | Lattice Site $T_E$ (-115.88 ± 0.1 ppm) | | |
|---|---|---|---|---|---|---|---|---|---|---|---|---|---|---|---|
| | Cs[a] | Lw[b] | P[c] | Cs[a] | Lw[b] | P[c] | Cs[a] | Lw[b] | P[c] | Cs[a] | Lw[b] | P[c] | Cs[a] | Lw[b] | P[c] |
| *BEA | 111.72 | 0.76 | 34.82 | 112.39 | 0.51 | 12.07 | 113.27 | 0.49 | 27.94 | 113.74 | 0.80 | 4.12 | 115.98 | 0.58 | 21.06 |
| NCL-5 | 111.55 | 1.39 | 25.34 | 112.15 | 1.03 | 7.06 | 113.09 | 0.79 | 25.34 | 114.04 | 1.16 | 14.73 | 115.79 | 1.26 | 27.52 |
| NCL-6 | 111.62 | 1.00 | 37.14 | 112.22 | 0.54 | 6.76 | 113.17 | 0.60 | 27.25 | 114.07 | 0.45 | 2.52 | 115.89 | 1.08 | 26.32 |
| NCL-7 | 111.46 | 0.68 | 21.72 | 112.06 | 0.68 | 12.71 | 113.08 | 0.65 | 34.52 | 113.96 | 1.08 | 8.87 | 115.81 | 0.75 | 22.17 |

[a] Chemical Shift Assignment in ppm [b] LW= Line width in ppm [c] Relative population of lattice sites in the sample (normalized to 100) in ppm.

### *3.3.1.5. Scanning Electron Microscopy (SEM)*

Figure 3.10 shows the SEM images of Si-Beta, NCL-7 and NCL-5 samples. As the samples were synthesized in the fluoride medium, the crystal size of these materials was found to be comparatively bigger. The morphology and the size of the crystals are found to be influenced strongly by the synthesis medium as reported earlier.[15-17] The Si-Beta sample shows the truncated square morphology in most of the particles.

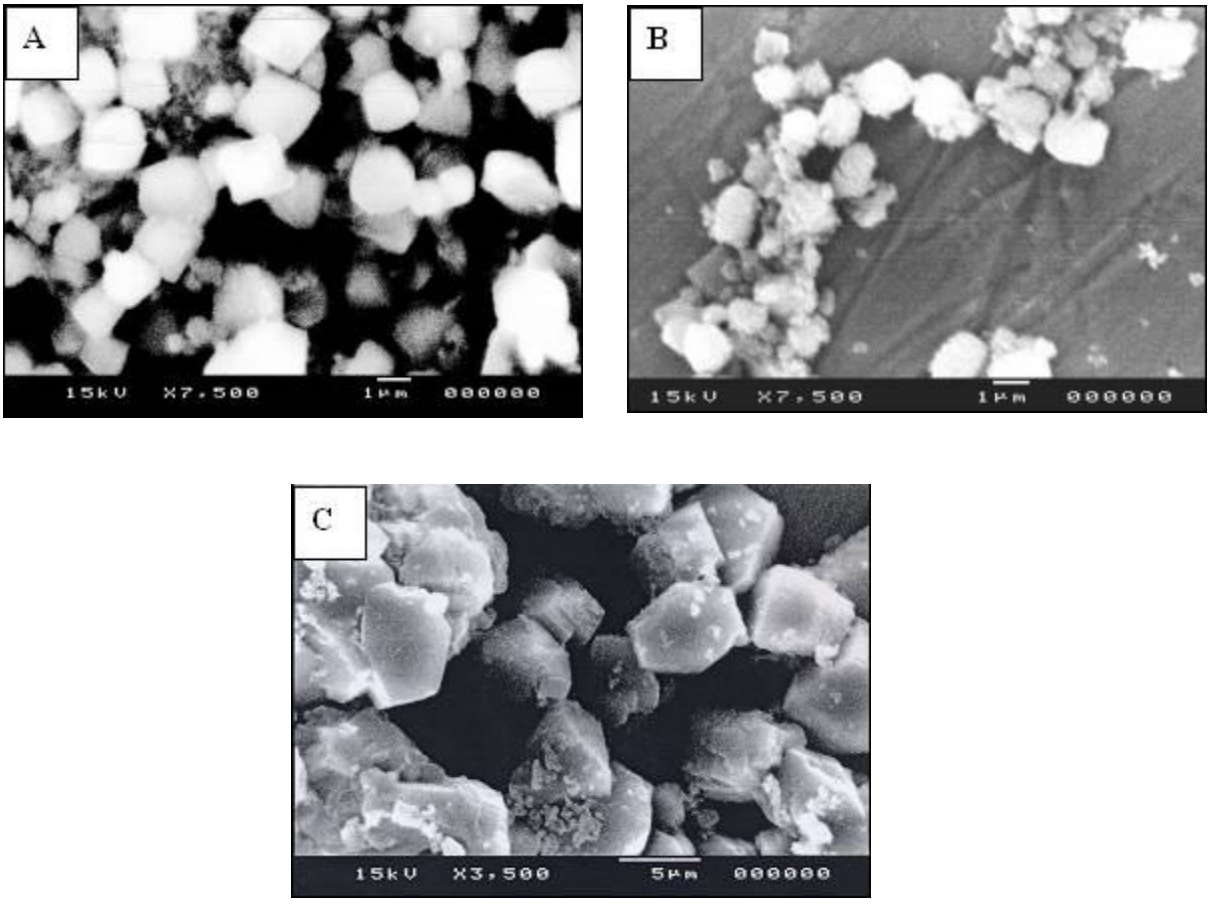


**Figure 3.10.** Scanning Electron Micrographs (SEM) of Si-Beta (A), NCL-7 (B) and NCL-5 (C).

The size of Si-Beta varied from 0.5-2.0 μm. Polymorph B enriched sample, NCL-7, showed round shaped particles along with truncated square morphology as shown in image B. In this case, the particle size of the sample varied from 0.5-2.0 μm. However, in case of NCL-5 sample comparatively large particle size, around 5.0 μm was observed as shown in image C.

### 3.3.2. Al-NCL-7 and Ti-NCL-7

#### *3.3.2.1. X-Ray Diffraction*

Figure 3.11 depicts the comparison of the powder X-ray diffraction patterns of the calcined Al-NCL-7 (curve b) and Ti-NCL-7 (curve c) samples with pure siliceous NCL-7 in curve (a). The XRD patterns shown in Fig. 3.11 matches well in term of width and relative intensity of different lines with the Si-NCL-7 sample. All the samples showed characteristics Bragg's reflection (302) around $2\theta = 22.6^\circ$ (d-spacing = 4.57) along with other five weak reflections, 004, 300, 304, 008 and 308, as indexed by Higgins *et al*.[8] At the same time, a split is observed in broad reflection at lower $2\theta$ value (110 and $11\bar{1}$ reflections) indicating the enrichment of polymorph B in Al-NCL-7 and Ti-NCL-7. Furthermore, slight increase in the d-spacing Al-NCL-7 and Ti-NCL-7 sample in 110 and $11\bar{1}$ Bragg's reflections supports the direct incorporation of aluminum and titanium in NCL-7 structure. The increase in the d-spacing for Al-NCL-7 and Ti-NCL-7 samples can be attributed to larger size of $Al^{3+}$ and $Ti^{4+}$ compared to $Si^{4+}$ as reported for different microporous and mesoporous materials reported earlier.[20-22] The increase in the d-spacing for 110 and $11\bar{1}$ Bragg's reflections is shown in Table 3.4.

The polymorphic proportion in Al-NCL-7 was determined using the DIFFaX formulation as described in detail for Si-NCL-7 sample in section 3.3.1 and elsewhere.[18-19] For comparison with the experimental patterns of Ti-NCL-7 and Al-NCL-7 obtained in the present study, the intensity values of simulated patterns for random intergrowths of polymorphs A and B were normalized. The obtained experimental patterns of Al-NCL-7 and Ti-NCL-7 were compared with the simulated patterns of zeolite Beta (obtained from DIFFaX code) with polymorphic compositions of polymorph B : Polymorph A as 60 : 40 and 65 : 35. In both the samples the enrichment of *ca.* 65 % in polymorph B was observed.

**Table 3.4**

Comparative d-spacing of Si-NCL-7, Al-NCL-7 and Ti-NCL-7 samples.

| Sample Name | d-spacing of Bragg's reflections | |
|---|---|---|
| | 110 | $11\bar{1}$ |
| Si-NCL-7 | 12.96 | 11.24 |
| Al-NCL-7 | 13.20 | 11.37 |
| Ti-NCL-7 | 13.37 | 11.53 |

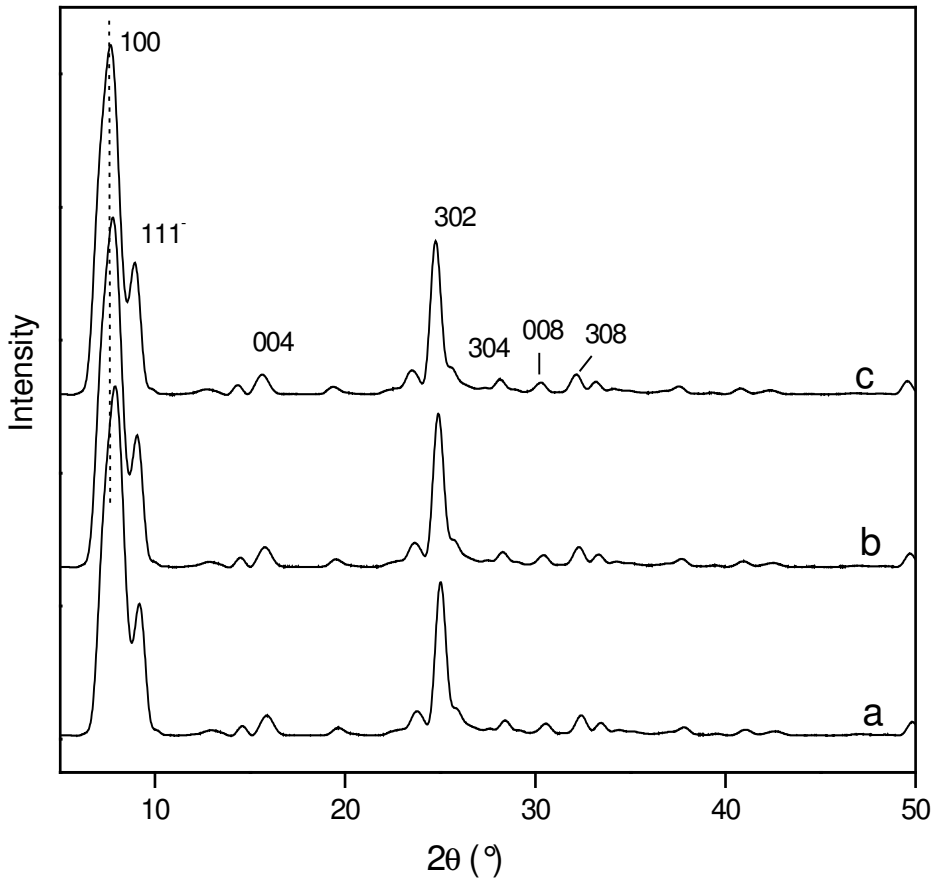


**Figure 3.11.** Comparison of the powder XRD pattern of Si-NCL-7 (curve a), Al-NCL-7 (curve b) and Ti-NCL-7 (curve c).

### *3.3.2.2. $N_2$ Adsorption*

Table 3.5 depicts the low temperature $N_2$ adsorption-desorption isotherms for Al-NCL-7 and Ti-NCL-7 samples with different content of aluminum and titanium along with Si-NCL-7. The surface area of Al-NCL-7 samples with Si/Al ratio as 100, 125 and 150 calculated using the BET method was found to be 528, 539 and 590 $m^2g^{-1}$, respectively. The pore diameter of these materials, calculated employing HK method, was found to be 0.69, 0.72 and 0.73 nm, respectively in comparison with 0.77 nm for Si-NCL-7. As seen from the Table 3.5, a decrease in the surface area was observed with increase aluminum content in the sample. The pore diameter and pore volume of the samples decreases with increase in aluminum content. Similar trend was observed in case of Ti-NCL-7 (Table 3.5, entries 5-7). The decrease in pore volume is generally obtained with incorporation of heteroatom such as Al and Ti.[10]

**Table 3.5**

Low Temperature $N_2$ Adsorption-Desorption Studies on Al-NCL-7 and Ti-NCL-7

| Entry No. | Sample Name | Si/Al or Si/Ti | Surface Area[a] $m^2 g^{-1}$ (± 5 %) | Pore Diameter[b] (nm) | Pore Volume[c] mL/g (± 2 %) |
|---|---|---|---|---|---|
| 1 | Si-NCL-7 | – | 560 | 0.77 | 0.23 |
| 2 | Al-NCL-7 | 100 | 528 | 0.69 | 0.21 |
| 3 | Al-NCL-7 | 125 | 539 | 0.72 | 0.22 |
| 4 | Al-NCL-7 | 150 | 590 | 0.73 | 0.24 |
| 5 | Ti-NCL-7 | 100 | 538 | 0.68 | 0.20 |
| 6 | Ti-NCL-7 | 125 | 558 | 0.70 | 0.23 |
| 7 | Ti-NCL-7 | 150 | 582 | 0.74 | 0.22 |

a = From $N_2$ adsorption measurement at 77 K

b = As per the HK formulation

c = As per t-method

### *3.3.2.3. Diffuse Reflectance UV-Vis Spectroscopy*

The diffuse reflectance UV-Vis spectroscopy is known to be a very sensitive probe for the identification and characterization of metal ion coordination and its existence in the framework and/or in the extra-framework position of metal containing zeolites. Curves a-d in Fig. 3.12 shows the diffuse reflectance UV-Vis spectra of calcined

Ti-NCL-7 samples containing Si/Ti ratio 100, 125, 150 and 200, respectively. All the samples show a strong ligand to metal charge transfer band around 220 nm. This is attributed to the tetrahedrally isolated $Ti^{4+}$ species in the framework position of Ti-NCL-7 samples. Similar observations are reported for other Ti-containing zeolites.[23,24] Curves a-c in this figure also shows a weak absorption edge in the range of 260-280 nm. This may be due to penta-coordination of titanium in the sample. However, its presence is negligible compared to tetrahedral species. It may be recalled the titanium content in the sample presented in curves a-c is higher as compared to curve d (Table 2.9, Entry No. 2-5). The absence of any absorption band at *ca*. 330 nm rules out the presence of anatase in Ti-NCL-7 samples.

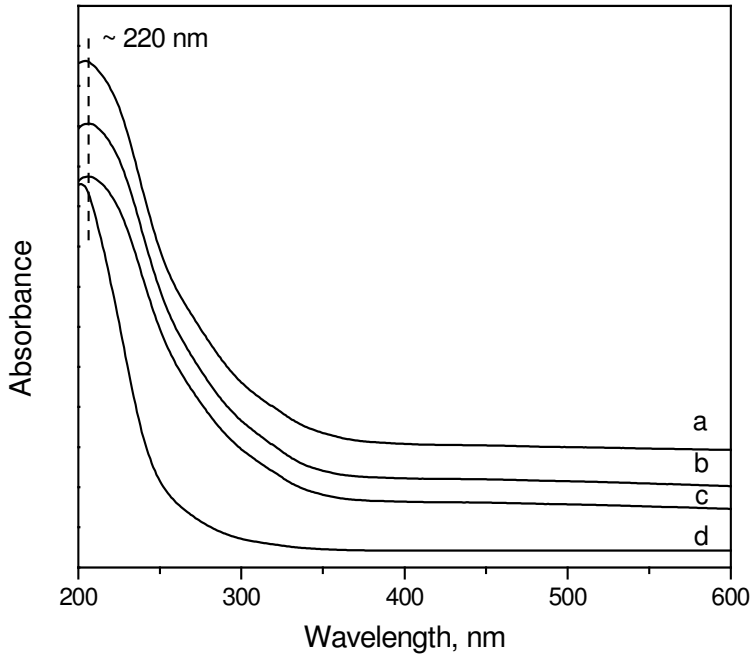


**Figure 3.12.** Diffuse reflectance UV-Vis spectra of calcined (a) Ti-NCL-7 (Si/Ti = 100), (b) Ti-NCL-7 (Si/Ti = 125), (c) Ti-NCL-7 (Si/Ti = 150) and (d) Ti-NCL-7 (Si/Ti = 200).

### *3.3.2.4. $^{27}$Al MAS NMR Spectroscopy*

The solid-state $^{27}$Al MAS NMR spectra of Al-NCL-7 with Si/Al ratio 100, 125, 150 and 200 are presented in curves a-d of Fig. 3.13. All the samples exhibit a strong and sharp band at 54 ppm. This can be assigned to the tetrahedrally coordinated Al in NCL-7 sample. Weak signal was observed at 0 ppm indicates the presence of very little amount of Al in octahedral coordination.[25] As seen from the curves a-d in this figure the signal at 0 ppm decreases with decrease in Al-content in the sample from Si/Al = 100 to Si/Al = 200. However, it is pertinent to mention that the intensity of the signal of 0 ppm is very subtle, compared to strong band at 54 ppm.

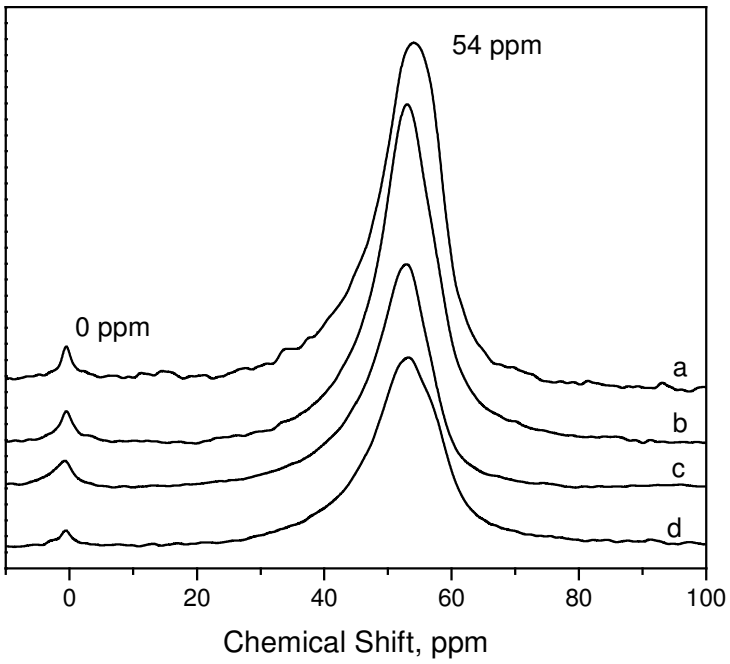


**Figure 3.13.** $^{27}$Al MAS NMR spectra of Al-NCL-7 sample (a) Al-NCL-7 (Si/Al = 100), (b) Al-NCL-7 (Si/Al = 125), (c) Al-NCL-7 (Si/Al = 150) and (d) Al-NCL-7 (Si/Al = 200).

### *3.3.2.5. Scanning Electron Microscopy (SEM)*

Figure 3.14 illustrates the SEM images of Al-NCL-7 and Ti-NCL-7 sample synthesized in fluoride medium. As seen in case of Si-Beta and other polymorph B enriched phases, NCL-5, NCL-6 and NCL-7, the crystal size of these materials was found to be comparatively larger due to its synthesis in fluoride medium. The Al-NCL-7 sample shows the crystal size in the range of 2-4 μm whereas the same varied in the range of 3-5 μm in case of Ti-NCL-7 sample. Both the samples show truncated square morphology in most of the particles as reported in the literature for BEA type structures.[15-17]

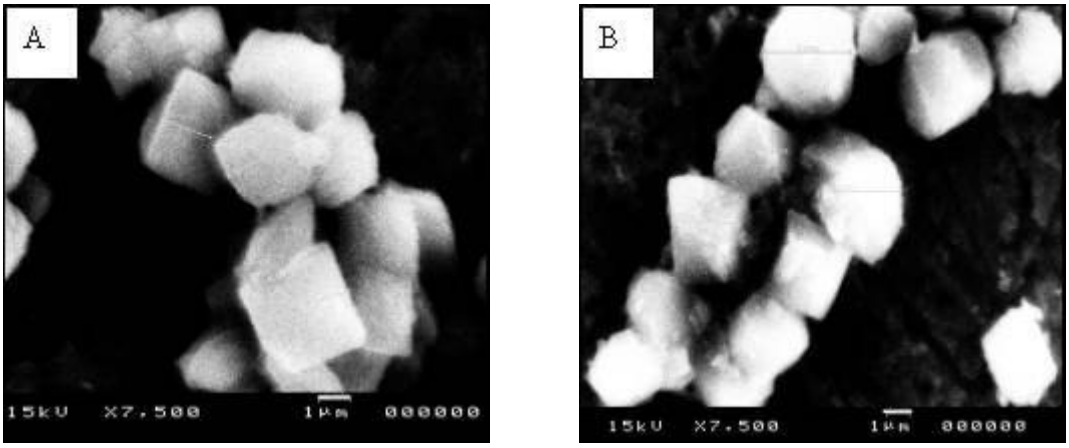


**Figure 3.14.** Scanning Electron Micrographs (SEM) of Al-NCL-7 (A) and Ti-NCL-7 (B).

### 3.3.3. REFERENCE MATERIALS

Along with polymorph B enriched structures NCL-5, NCL-6 and NCL-7, Silicalite-1, Al-ZSM-5, Si-Beta, Al-Beta, Si-MCM-41 and Al-MCM-41 have been used as the standard materials in the present work for comparison purpose. The physico-chemical characterization of these materials is discussed below.

Figure 3.15 depicts the powder X-ray diffraction pattern of the Silicalite-1 and Al-ZSM-5 samples. As seen from the Fig. 3.15, both the sample match very well in terms of width and relative intensity of different lines of MFI topology reported in the literature for orthorhombic symmetry with a space group $p_n m_a$. The major characteristic peaks of MFI topology were observed at 3.87, 3.73 and 3.66 d values corresponding to 610, 611 and 540 Bragg's reflections.[26] Similarly, in case of Al-ZSM-5 sample (Fig. 3.15, curve b) in the peak at $2\theta = 46.8°$ splits into two peaks centered at $2\theta$ value, 45.0 and 45.5°. The spacing between the two peaks at *ca.* 45.0 and 45.5 ° (Cu K$\alpha$ radiation) was reported to reduce with increase in Al content of Al-ZSM-5.[27] The intensities of these two peaks fall and they broaden considerably as the Al content increases. The surface area and pore volume of Al-ZSM-5 calculated using the BET equation and HK method was estimated to be 440 $m^2g^{-1}$ and 0.16 mL/g. In case of Silicalite-1 sample, the surface area was found to be 416 $m^2g^{-1}$ whereas the pore volume remains same, 0.16 mL/g.

Curves a and b in Fig. 3.16 show the powder XRD patterns of Si-Beta and Al-Beta samples. A broad reflection peaking at $2\theta$ value of $7.75^{\circ}$ and a sharp line at $2\theta = 22.6^{\circ}$ (d = 4.57) in curve (b) of this figure are the characteristic features of zeolite Si-Beta with an intergrowth of the two polymorphs in almost equal proportion.[8,10,28] A marginal increase in the d-spacing is observed in case of Al-Beta (curve a), as reported earlier.[6]

Also, Bragg's reflections marked in Fig. 3.16 (curves a and b) matches with the reported XRD data of Al-Beta and Si-Beta zeolites, composed of polymorphs B and A in a ratio ~55 : 45. The surface area of Si-Beta and Al-Beta was found to be 590 and 554 $m^2g^{-1}$, respectively. Pore volume of Si-Beta was found to be higher (0.22 mL/g) in comparison with Al-Beta, 0.17 mL/g.

The powder X-ray diffraction patterns of Si-MCM-41 and Al-MCM-41 are presented in curve a and b of Fig. 3.17. The powder XRD pattern of these materials shows four Bragg's reflection corresponding to *hkl* = 100, 110, 200 and 210.[29] The BET surface area of Si-MCM-41 and Al-MCM-41 was found be 1210 and 1161 $m^2g^{-1}$. Both the sample exhibited typical type IV isotherms having inflection around P/Po = 0.3-0.45, characteristic of MCM-41 type ordered mesoporous materials.[30]

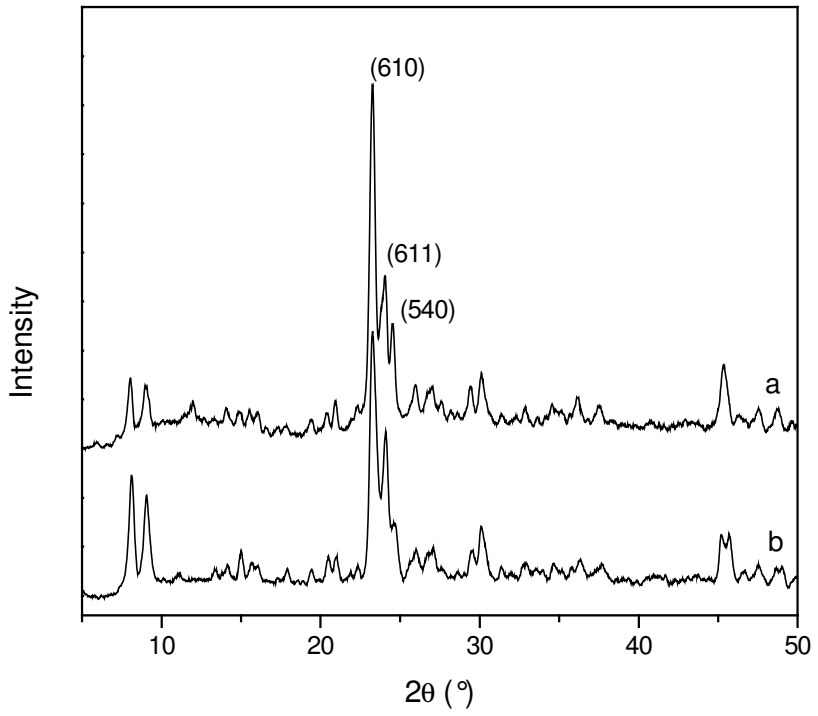


**Figure 3.15.** Powder X-ray diffraction patterns of (a) Silicalite-1 and (b) Al-ZSM-5.

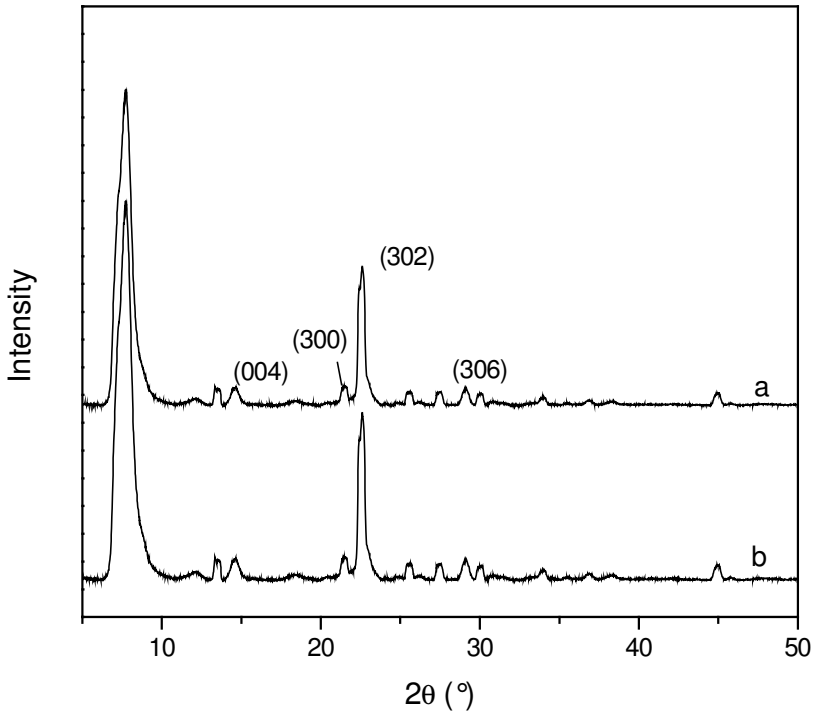


**Figure 3.16.** Powder X-ray diffraction patterns of (a) Si-Beta and (b) Al-Beta.

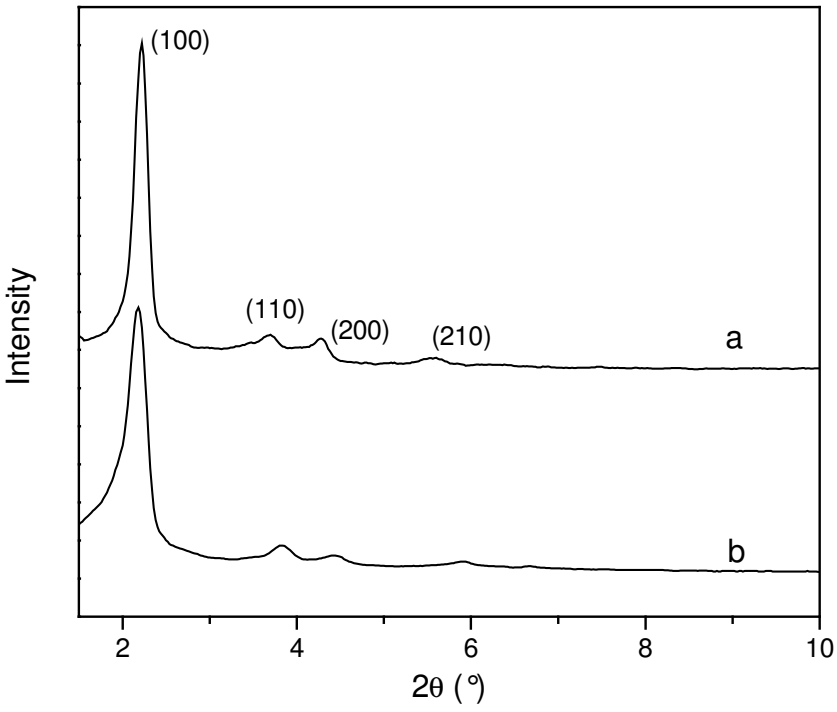


**Figure 3.17.** Powder X-ray diffraction patterns of (a) Si-MCM-41 and (b) Al-MCM-41.

**Table 3.6**

Physico-Chemical Properties of Different Reference Samples

| Sample Name | Si/Al | Surface Area, $m^2g^{-1}$ | Pore Volume, mL/g |
|---|---|---|---|
| Silicalite-1 | _ | 416 | 0.16 |
| Al-ZSM-5 | 28.5 | 440 | 0.16 |
| Si-Beta | _ | 590 | 0.22 |
| Al-Beta | 30 | 554 | 0.17 |
| Si-MCM-41 | _ | 1210 | 0.68 |
| Al-MCM-41 | 27 | 1161 | 0.68 |

## 3.4. CONCLUSIONS

The enrichment of polymorph B in newly synthesized NCL-5, NCL-6 and NCL-7 structures was figured out using Rietveld refinement and DIFFaX. The later is preferred over Rietveld refinement due to inherent stacking present in the structure. The structure elucidation and polymorphic composition, deduced using DIFFaX code, unambiguously reveal that there is *ca.* 95, 75 and 65 % enrichment of polymorph B in NCL-5, NCL-6 and NCL-7 zeolites, respectively. $^{29}$Si MAS NMR shows absence of $Q^3$ species for the samples. The framework FTIR spectral analysis of NCL-5, NCL-6, NCL-7 and Si-Beta samples supported the postulate that there is an increase in tortuousity of the channel system with increase in polymorph B in zeolite Beta as reflected in the relative intensities

of 1097 and 1018 $cm^{-1}$ vibrations. This was also corroborated by the similar trend in low frequency bands at 460 and 423 $cm^{-1}$.

$^{27}Al$ MAS NMR study reveals that most of aluminum in Al-NCL-7 is present in tetrahedral coordination. Similar observations were obtained in case of Ti-NCL-7 samples using diffuse reflectance UV-Vis spectroscopy where all the Ti-NCL-7 samples shows a strong ligand to metal charge transfer band around 220 nm due to tetrahedral coordination of titanium.

## 3.5. REFERENCES


1. Bergeret, G. In *Handbook of Heterogeneous Catalysis*, *Vol. 2*; Ertl G., Knozinger, H.; Weitkamp, Eds.; J. Wiley-VCH: Weinheim 1997, p 464.
2. *Introduction to zeolite science and practice*; Bekkum, H. V.; Flanigen, E. M.; Jacobs, P. A. Eds.; Elsevier: Amsterdam, 2001.
3. Corma, A. *Cat. Rev. Sci. Engg*. **1985**, *27*, 29.
4. Corma, A.; Garcia, H. *Chem. Rev.* **2003**, *103,* 4307.
5. Kokotailo, G. T.; Fyfe, C. A. *J. Phys. Chem. Solid* **1989,** *50,* 441.
6. Corma, A. *Chem. Rev.* **1997**, 97, 2373.
7. Rietveld, H. M. *J. Appl. Crystallogr.* **1969**, *2*, 65.
8. Higgins, J. B.; LaPierre, R. B.; Schlenker, J. L.; Rohrman, A.C.; Wood, J. D.; Kerr, G. T.; Rohrbaugh, W. J. *Zeolites* **1988**, *8*, 446.
9. Treacy, M. M. J.; Deem, M. W.; Newsam, J. M. *Computer Code DIFFaX, Version 1.807* NEC Research Institute, Inc.: Princeton, New Jersey, **2000**.
10. Newsam, J. M.; Treacy, M. M. J.; Koetsier, W. T.; De Gruyter, C. B. *Proc. R. Soc. London* **1988**, *A420*, 375.
11. Brigden, C. T.; Williams, C. D. *Microporous Mesoporous Mater.* **2007**, *105*, 118.
12. Eapen, M. J.; Reddy, K. S. N.; Shiralkar, V. P. *Zeolites* **1994***, 14,* 295.
13. Pariente, J. P.; Martens, J. A.; Jacobs, P. A. *Appl. Catal.* **1987**, *31*, 35.
14. Fyfe C. A.; Strobl H.; Kokotailo G. T.; Pasztor C. T.; Barlow G. E.; Bradley S. *Zeolites* **1988**, *8*, 132.
15. Larlus, O.; Valtchev, V. P. *Chem. Mater.* **2005**, *17*, 881.
16. Yongzhong, Z.; Yuntong, N.; Jaenicke, S.; Chauh, G. –K. *J. Catal.* **2005**, *229*, 404.
17. Treacy, M. M. J.; Newsam, J. M. *Nature* **1988**, *332,* 249.
18. Kadgaonkar, M. D.; Kasture, M. W.; Bhange, D. S.; Joshi, P. N.; Ramaswamy, V.; Gupta, N. M.; Kumar, R. *Microporous Mesoporous Mater.* **2007**, *105*, 82.
19. Kadgaonkar, M. D.; Kasture, M. W.; Bhange, D. S.; Joshi, P. N.; Ramaswamy V.; Kumar, R. *Microporous Mesoporous Mater.* **2007**, *101*, 108.

20. Chaudhari, K.; Das, T. K.; Chandwadkar, A. J.; Sivasankar, S. *J. Catal.* **1999,** *183,* 281.
21. Borade, R. B.; Clearfield, A. *Catal. Lett.* **1995**, *31*, 267.
22. Tanev, P. T.; Chibwe, M.; Pinnavaia, T. J. *Nature* **1994**, *368*, 321.
23. Reddy, J. S.; Kumar, R.; Ratnasamy, P. *Appl. Catal.* **1990**, *58*, L1.
24. Srinivas, D.; Manikandan, P.; Laha, S. C.; Kumar, R.; Ratnasamy, P. *J. Catal.* **2003**, *217*,160.
25. Kasture, M. W.; Niphadkar, P. S.; Sharanappa, N.; Mirajkar, S. P.; Bokade, V. V.; Joshi, P. N. *J. Catal.* **2004**, *227,* 375.
26. Breck, D. W. In *Zeolite Molecular Sieves*; John Wiley: New York, 1974, p 373.
27. Bibby, D. M.; Aldridge, L. P.; Milestone, N. B. *J. Catal*. **1981**, *72*, 373.
28. Camblor, M. A.; Corma, A.; Valencia, S. *J. Mater. Chem.* **1998**, *8*, 2137.
29. Beck, J. S.; Vartulli, J. C.; Roth, W. J.; Leonowicz, M. E.; Kresge, C. T.; Schmitt, K. D.; Chu, C. T. -W.; Olson, D. H.; Sheppard, E. W.; McCullen, S. B.; Higgins, J. B.; Schlenker, J. L. *J. Am. Chem. Soc*. **1992**, *114*, 10834.
30. Chen, X.; Huang, L.; Li, Q. *J. Phys. Chem. B* **1997**, *101*, 8460.

## 4.1. INTRODUCTION

Catalytic properties of the zeolites originate from their capacity to adsorb different molecules. However, direct information about the nature of adsorbed molecules in zeolite is available rather scantly.[1-3] The proper understanding of the fundamental processes involved in the transport of reactant and product molecules and the nature of their interactions inside the zeolite channels are one of the most important aspects of zeolite chemistry. It is also vital to understand the behavior of different molecules inside the cavities. The transport of guest molecule in the host matrix of zeolite is influenced considerably due to its interaction with zeolite framework sites, extra-framework cations and hydroxyl groups. Additionally, the inter-molecular interactions in the reactants and products occluded in the zeolite cages may further influence the transport processes and catalytic behavior of a particular zeolite. The adsorption and encapsulation of small molecules in microporous and mesoporous silicates have therefore been the subject of dedicated research ever since the discovery of the zeolites in nineteen sixties.[4-10]

Adsorption and diffusion of hydrocarbons, especially benzene, have been investigated using zeolites of different pore characteristics and chemical compositions. Various techniques such as Fourier transform infrared spectroscopy (FTIR), Fourier transform Raman spectroscopy (FT Raman), microcalorimetry, nuclear magnetic resonance (NMR), quasielastic neutron scattering (QENS) have been employed to study these interactions. The adsorption of benzene has been investigated over Silica and FAU, MFI, EMT and BEA type zeolites using IR technique.[11-15] FTIR spectroscopy is preferred over other characterization tools because of the sensitivity of the benzene IR bands to the geometrical and chemical nature of the adsorbent zeolite. The transport properties and the

binding states of benzene molecules are studied generally by monitoring the in-plane C-H/C-C stretches (3100-3000 $cm^{-1}$), out-of-plane C-H vibrations (2000-1800 $cm^{-1}$) and fundamental $\nu_{19}$ C-C stretch (1479 $cm^{-1}$) vibrations of the benzene molecules. Among these, in-plane C-H/C-C stretches and fundamental $\nu_{19}$ vibrations of adsorbed benzene are found to match with the IR bands of liquid benzene. However, out-of-plane C-H bending vibrations, combination band at 1960 $cm^{-1}$ ($\nu_5 + \nu_{17}$ vibrations) and 1815 $cm^{-1}$ ($\nu_{10} + \nu_{17}$) for liquid benzene splits into overlapping bands on adsorption in zeolitic cavities. This splitting has been commonly attributed to the interaction of zeolites with π-cloud electron of benzene. A brief account on the benzene adsorption in zeolites is presented in chapter 1.[15-23] Similarly Gupta *et al*. reported an alternative explanation to the splitting in out-of-plane region on the basis of pore size/volume rather than electronic bonding of benzene molecules with the framework.[24-28]

In the light of above observations, the present chapter deals with the adsorption of benzene in BEA type zeolite as a function of the subtle structural and chemical changes resulting due to change in polymorphic composition of zeolite Beta (polymorph A and B) and presence of aluminum, respectively. Benzene, a non-polar molecule of dimensions matching that of the channels and pore openings of zeolite samples under study, has been chosen as a probe molecule. In order to further discern the nature of the guest-host interaction, hexadeuterated benzene ($C_6D_6$) was also employed as adsorbate. Al-Beta with Si/Al ratio 28, Si-Beta and polymorph B enriched structures NCL-5 (polymorph B : polymorph A = 90 : 10), NCL-6 (polymorph B : polymorph A = 75 : 25) and NCL-7 (polymorph B : polymorph A = 65 : 35) were used as host matrices.

Similar experiments were carried out on the MFI and M41S type topology for comparison purposes.

## 4.2. MATERIALS AND CHARACTERIZATION

The synthesis of Al-Beta (Si/Al = 28), Si-Beta and polymorph B rich structures, NCL-5, NCL-6 and NCL-7, is described in detail in chapter 2. The synthesis of all silica MCM-41, Al-MCM-41 (Si/Al = 25), Silicalite-1 and Al-ZSM-5 (Si/Al = 18) is also outlined in Chapter 2. The physico-chemical and textural properties of these materials are illustrated in Chapter 3.

## 4.3. INSTRUMENTATION AND METHODOLOGY

The high-temperature, high-pressure stainless steel IR cell used in this study was equipped with $CaF_2$ windows and permitted evacuation of a sample and its pretreatment under the desired atmosphere as well as temperature conditions. Figure 4.1 depicts the schematic diagram of IR cell used in the present study. The detail description of the cell is described elsewhere.[34,35] A Thermo Nicole (model-Nexus 870) FT-IR equipped with a DTGS detector was employed for recording of the IR spectra in transmission mode. The self-supporting wafers (~70 mg, 25 mm diameter) were heated *in-situ* for 8-10 h at a temperature of 573 K under vacuum (~$1 \times 10^{-3}$ Torr), followed by cooling to room temperature and recording of their background spectrum. The samples were then dosed with successive pulses of gas mixture containing nitrogen and benzene vapor (each pulse ~0.1 mmol of benzene $g^{-1}$ adsorbent), and the pressure in the cell was monitored at each stage by using a digital manometer. For the benzene loading in the range of 0.1- to 0.6

mmol $g^{-1}$, the pressure in the cell varied from 50 to 250 mm. Spectra were recorded after an equilibration time of 10 to 15 min. following each pulse, and were compensated for the IR bands of corresponding unexposed sample. The figures in the text represent the absorbance bands due to the species formed in adsorption process. Spectra were also recorded on post-exposure evacuation of the cell and on step-wise elevation of sample temperature subsequent to the saturation coverage of benzene. 300 scans were co-added at a resolution of 4 $cm^{-1}$ for plotting of each spectrum. The numbers given in parentheses in some of the figures represent the corresponding absorbance values. For inter-comparison, the absolute intensity of selected IR bands was estimated from the integrated area under different peaks. Spectra were also recorded for un-adsorbed gaseous and liquid forms of benzene and deuterated benzene to serve as reference.

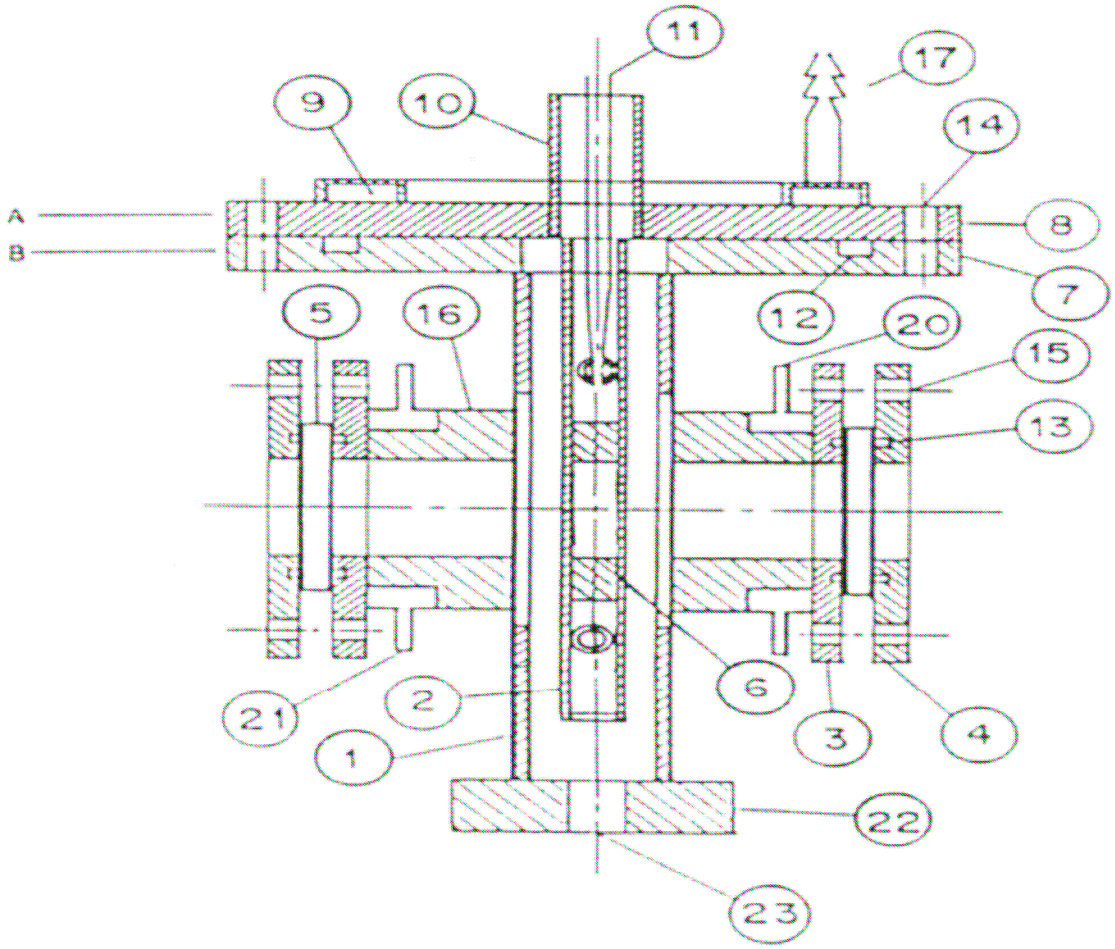


**Figure 4.1.** A cross sectional view of IR cell for *in-situ* study.

A - Top flange with heater block and thermocouple connection; B - Cell body; 1- Rectangular stainless body; 2, 6 - sample holder block; 3, 4, 7, 8 - Flanges; 5 - Optical window; 9, 16 - Water jackets; 10- Thermocouple feed through; 11 - Thermocouple connections; 12 - Teflon O-ring; 13 - Viton O-ring; 14, 15 - Screws; 17, 20, 21 - Water inlet/outlets; 22 - Stainless steel base with bakelite lining; 23 - Screws for bakelite lining.

## 4.4. ADSORPTION AND BINDING STATE OF BENZENE AND DEUTERATED BENZENE IN BEA TYPE TOPOLOGY

### 4.4.1. Results

#### *4.4.1.1. Adsorption of Benzene ($C_6H_6$) in Al-Beta*

##### *4.4.1.1.1. Out-of-plane combination (C-H) bending vibrations (2050 -1750 $cm^{-1}$)*

Spectra a-d in Fig. 4.2 show the combination bands of out-of-plane C–H bending vibrations when an Al-Beta zeolite wafer, activated *in-situ* under vacuum, was exposed to successive pulses of benzene vapor at ambient temperature. The accumulated amount of dosed benzene ranged between 0.1 to 0.6 mmol $g^{-1}$. On comparison with the spectra recorded under identical condition for liquid and vapor states of benzene (curves e and f), it is evident that the spectra (a-d) do not match with either of these two phases of benzene. In place of C-H out-of-plane combination band at 1960 $cm^{-1}$ ($\nu_5 + \nu_{17}$ vibrations) for liquid benzene (Fig. 4.2, curve e) at least two overlapping bands were observed with frequency maxima at 1971 and 1956 $cm^{-1}$ (Fig. 4.2, curves a-d). Similarly, the corresponding lower frequency out-of-plane combination band at 1815 $cm^{-1}$ ($\nu_{10} + \nu_{17}$) splits into two overlapping bands around 1830 and 1812 $cm^{-1}$ (spectroscopic notations used in the present work are as per Refs. 36, 37). Further, between these two pairs of bands mentioned above, the intensity of the absorption bands appearing at 1956 and 1815 $cm^{-1}$ registered a slower rate of growth for the first few injections of benzene before reaching an equilibrium value. In other words, the adsorbed benzene gave rise to the pair of higher frequency bands to begin with (curves a, b), followed by satellite bands having frequency values close to those of liquid benzene on increased loading (curves c, d).

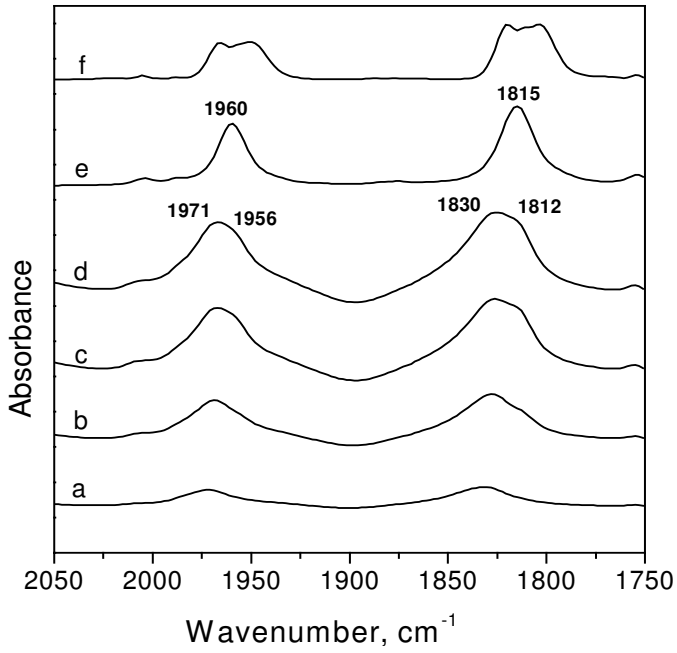


**Figure 4.2.** C-H out-of-plane vibrational bands for (a) 0.1 (b) 0.2 (c) 0.3 and (d) 0.6 mmol benzene ($C_6H_6$) loading per gram of Al-Beta sample. Curves (e) and (f), respectively show IR spectra of liquid and vapor forms of benzene.

Curves a-c in Fig. 4.3 present the IR spectra of Al-Beta zeolite exposed to 0.6 mmol $g^{-1}$ of benzene (curve a), followed by step-wise elevation of sample temperature (curves b, c). The intensity of both the pair of bands mentioned above decreases to almost similar extent with increasing sample temperature. Also, spectrum (c) in Fig. 4.3 shows that a considerable amount of benzene remained trapped even after annealing at an elevated temperature of 473 K. Similar resistance to removal of occluded benzene was noticed on post-exposure pumping of a sample. Again, the intensity of all the IR bands decreased during the pumping and both the sets of IR bands could be observed even after two hours of pumping, though with a marginal change in their relative intensity. Curves

(d) and (e) in Fig. 4.3 show representative spectra plotted after the post-exposure evacuation of a sample at room temperature for 2 min. and 1 h, respectively.

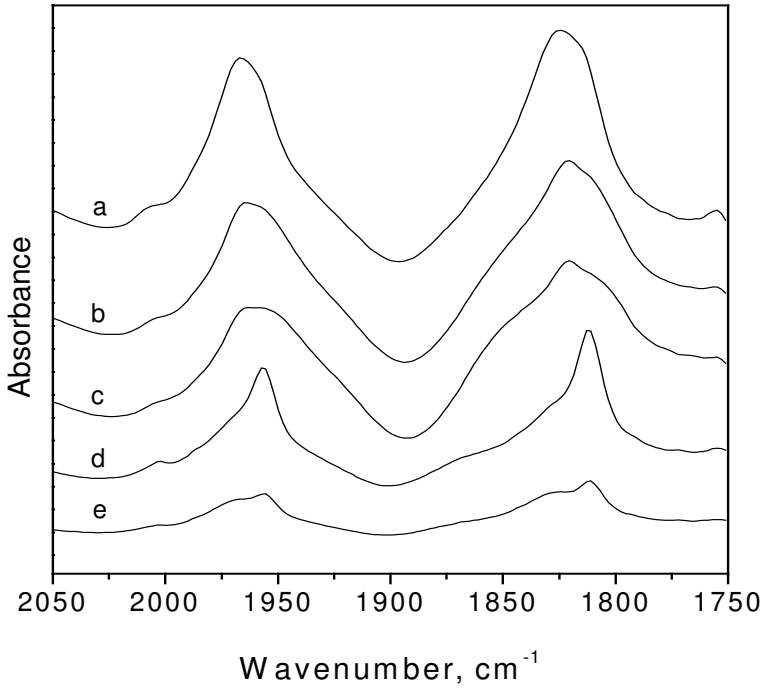


**Figure 4.3.** C-H out-of-plane vibrational bands of benzene for loading of 0.6 mmol $g^{-1}$ benzene in Al-Beta followed by annealing at (a) 323 (b) 398 and (c) 473 K. Curves (d) and (e) show IR spectra of benzene loaded Al-Beta subjected to subsequent evacuation for 2 and 60 min., respectively.

#### *4.4.1.1.2. In-plane C-H/C-C stretch combination bands (3150 -2950 $cm^{-1}$)*

No splitting was observed in the IR bands in 3150-2950 $cm^{-1}$ region, arising due to fundamental C-H stretching ($\nu_{20}$) and combination C-C stretching in-plane vibrations of benzene, under the loading conditions of this study. Figure 4.4 exhibits an overlay of the typical IR bands observed in this region (curves a-d), along with the representative spectra of un-adsorbed benzene in liquid and vapor states (curves e, f). The absorbance

bands in curves a-d exhibit features similar to that of the liquid phase benzene (curve e), with almost no shift in the frequency of different bands in this region. As in the case of 2050-1750 $cm^{-1}$ region bands described above, the growth of these bands was found to occur in two steps, initially at a rate proportional to the pressure and later only marginal. A stage of saturation was observed after adsorption of ~0.3 mmol $g^{-1}$ of benzene. This trend is shown by plot in the inset of Fig. 4.4, for the loading dependent growth of 3037 $cm^{-1}$ IR band. It was also seen that the IR bands associated with the adsorbed species have much smaller half width (full-width at half intensity, $\Delta\, \nu_{1/2}$), compared to those of the liquid benzene (Table 4.1).

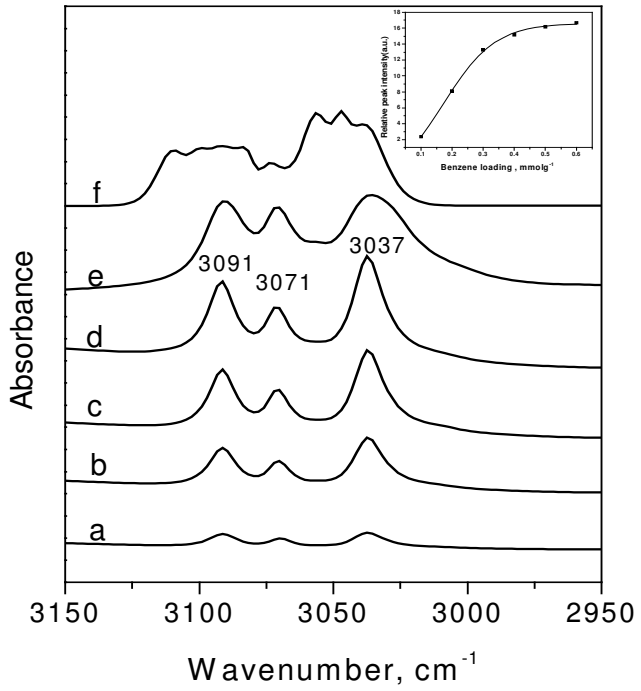


**Figure 4.4.** C-H stretching ($\nu_{20}$) and combination C-C ($\nu_1 + \nu_6 + \nu_{19}$ and $\nu_{19} + \nu_8$) stretch vibrations of benzene adsorbed in Al-Beta at different doses: Curve (a) 0.1, (b) 0.2, (c) 0.3 and (d) 0.6 mmol $g^{-1}$. Curves (e) and (f), respectively show the IR spectra in this region for liquid and vapor states of benzene. The inset shows the loading dependent growth of 3037 $cm^{-1}$ IR band.

**Table 4.1**

Comparative width of in-plane C-C stretch vibrational band ($\nu_{19}$) at 1479 $cm^{-1}$ of benzene on adsorption in different BEA type zeolites and the intensity ratios of selected in-plane vibrational bands

| Sample Name | [a] Band width of $\nu_{19}$ vibrational band ($cm^{-1}$) | [b] Peak ratio $I_{1479}/I_{1528}$ | [b] Peak ratio $I_{1479}/I_{3037}$ |
|---|---|---|---|
| Al-Beta | 7.2 | 28.0 | 1.8 |
| Si-Beta | 10.5 | 7.2 | 1.3 |
| NCL-7 | 10.8 | 8.2 | 1.2 |
| NCL-6 | 9.7 | 8.5 | 1.4 |
| NCL-5 | 9.4 | 7.2 | _ |
| Benzene Liquid | 21.0 | 3.4 | 0.7 |
| Benzene Vapor | 33.7 | _ | 0.5 |

[a] Full Width at half maximum (FWHM)

[b] Estimated from areas under respective IR bands for a loading of 0.2-0.3 mmol $g^{-1}$

#### *4.4.1.1.3. Fundamental $\nu_{19}$ C -C stretching vibration (1479 $cm^{-1}$)*

The intensity and the shape of the $\nu_{19}$ vibrational band (1479 $cm^{-1}$) were influenced considerably on adsorption of benzene in Al-Beta. Curves a-d in Fig. 4.5 presents these data for the different amounts of benzene adsorbed. Curves (e) and (f) in the inset of this

figure show again the comparative spectra in this region for benzene in its liquid and vapor forms.

Following are the important observations:

I. The frequency of this band shows no shift in the adsorbed state and matches well with the spectrum of liquid benzene (Fig. 4.5, inset).

II. The width of this IR band is found to decrease considerably after adsorption of $C_6H_6$ in zeolite Beta, the value of half width ($\Delta \nu_{1/2}$) changing only marginally as a function of loading. These representative data are presented in Table 4.1.

III. The apparent peak intensity of $\nu_{19}$ C-C stretching band increases considerably on adsorption in Al-Beta, as compared to other bands. Thus, the relative intensity of 1479 and 1528 $cm^{-1}$ bands is very different from the corresponding bands observed for liquid $C_6H_6$ in this region. (Fig. 4.5, curve e). In fact, the intensity of the 1528 $cm^{-1}$ band appears to be negligibly small in spectra (a-d) of Fig. 4.5, presumably because of its broadening, being an out-of-plane combination band. A similar trend is noticed in the intensity ratio of 1479 and 3037 $cm^{-1}$ ($\nu_1 + \nu_6 + \nu_{19}$ combination) band also. The relative intensities of the representative IR peaks are listed in Table 4.1.

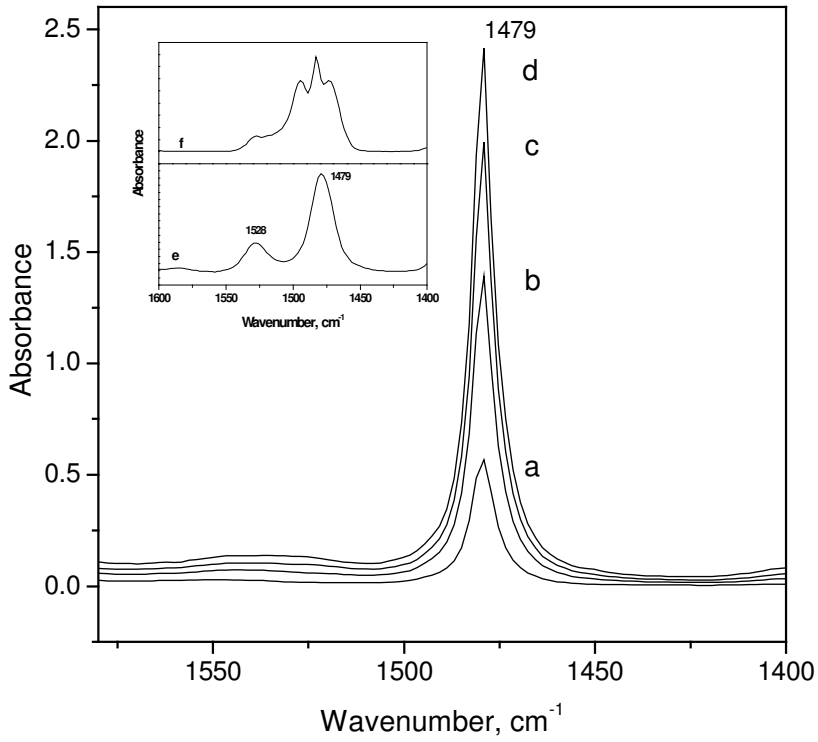


**Figure 4.5.** In-plane C-C stretching ($\nu_{19}$) vibrations of benzene for adsorption at different loadings in Al-Beta Curve (a) 0.1, (b) 0.2, (c) 0.3 and (d) 0.6 mmol $g^{-1}$. The inset figure shows the comparative spectra of benzene in (e) liquid and (f) vapor form.

### *4.4.1.2. Adsorption of $C_6H_6$ in Si-Beta and Polymorph B-Enriched Structures (NCL-7, NCL-6 and NCL-5): A Comparison*

The spectral features were quite different for benzene adsorption in Si-Beta and also in polymorph B enriched structures samples, as compared to the vibrational bands described above. For all these samples, two intense bands at around 1955 and 1811 $cm^{-1}$, similar to that of liquid benzene besides a shift in the frequency to a lower value by ~5 $cm^{-1}$ were observed compared to the overlapping two pair of bands seen in Fig. 4.2. The intensity of these bands was found to increase with loading, reaching a saturation stage

after adsorption of ~0.3 mmol of benzene $g^{-1}$ of sample. For instance, Fig. 4.6 shows the growth of out-of-plane combination (C-H) bending vibrations (2050-1750 $cm^{-1}$) of benzene after adsorption at different loadings in a pre-activated Si-Beta sample. A comparison of the out-of-plane combination bands of benzene, observed typically for adsorption of 0.3 mmol $g^{-1}$ benzene over Al-Beta, Si-Beta and polymorph B enriched samples, NCL-7, NCL-6 and NCL-5 is presented in Fig. 4.7. As seen in this figure, the intensity of the pair of bands at 1971 and 1830 $cm^{-1}$ observed for Al-Beta (curve a) is negligibly small as compared to curves b, c, d and e of this figure, pertaining to adsorption in Si-Beta and other siliceous intergrowth of zeolite Beta, NCL-7, NCL-6 and NCL-5 samples, respectively.

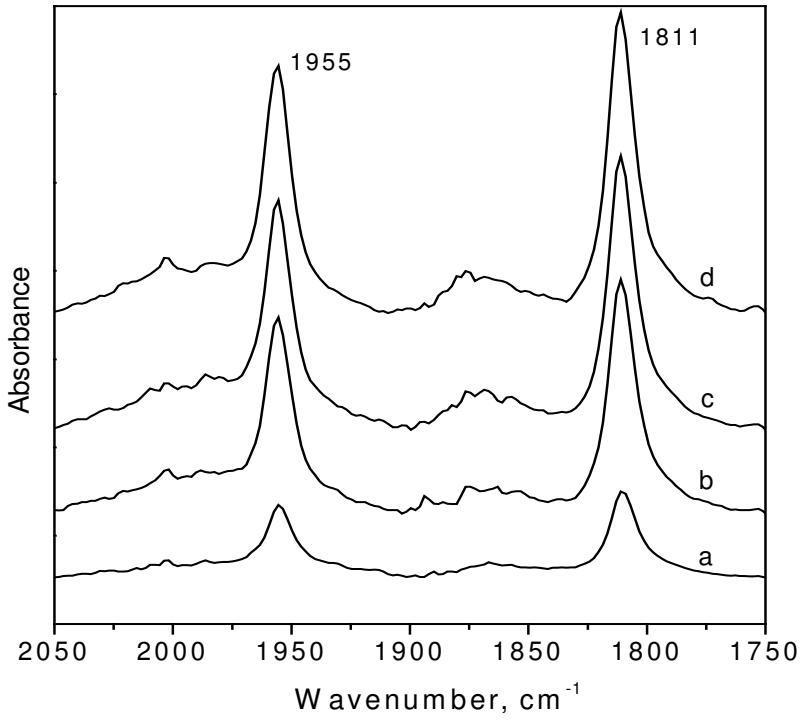


**Figure 4.6.** C-H out-of-plane vibrational bands of benzene for adsorption in Si-Beta at different loadings: curve (a) 0.1, (b) 0.2, (c) 0.4 and (d) 0.6 mmol $g^{-1}$.

As in the case of Al-Beta, no shift was observed in the frequency of in-plane C-H/C-C stretch combination bands and also the fundamental C-C stretching vibration ($\nu_{19}$) of benzene, whereas the amount of benzene adsorbed at saturation coverage was normally smaller for NCL-7, NCL-6 and NCL-5 as compared to Si-Beta. Figure 4.8 exhibits the growth behavior of 1479 $cm^{-1}$ ($\nu_{19}$) band as a function of benzene loading in Si-Beta. Again, a comparison with Fig. 4.5 reveals an increased width of this band and also an increase in the peak intensity of 1521 $cm^{-1}$ band (observed at 1528 $cm^{-1}$ in Fig. 4.5). The relative values of the bandwidth and the intensity ratio of the 1479 and 1521 $cm^{-1}$ bands are listed in Table 4.1. Once again this shows the difference in behavior of out-of-plane combination bands ($\nu_{10} + \nu_{11}$) of benzene for adsorption in Al-Beta and all siliceous analogs of zeolite Beta. Furthermore, while the growth pattern of the 1479 $cm^{-1}$ band remained the same the amount of benzene adsorbed at saturation coverage was normally smaller in the case of NCL-5 as compared to Si-Beta. Saturation coverage follows the order Si-Beta > NCL-7 > NCL-6 > NCL-5. Figure 4.9 (A) shows the comparative intensity (peak area) of 1479 $cm^{-1}$ band for the adsorption of benzene in Si-Beta, NCL-7, NCL-6 and NCL-5 in the curves a-d, respectively. Similarly, Fig. 4.9 (B) presents corresponding data on the intensity of 1329 $cm^{-1}$ band for adsorption of $C_6D_6$ for similar host matrices.

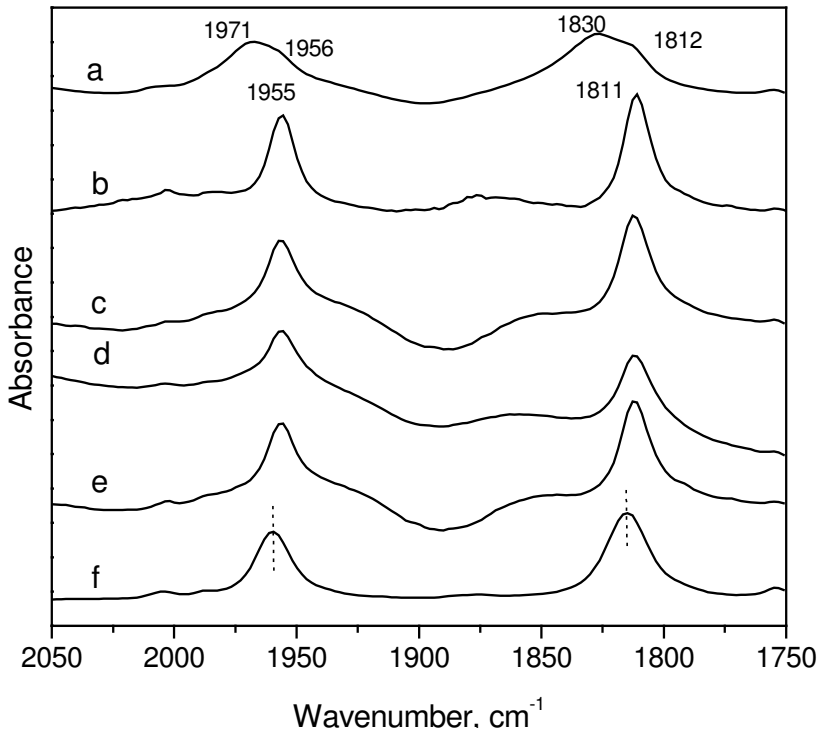


**Figure 4.7.** A comparison of the C-H out-of-plane IR bands of $C_6H_6$ for a loading at 0.3 mmol $g^{-1}$ in different BEA type samples: curve (a) Al-Beta, (b) Si-Beta, (c) NCL-7, (d) NCL-6 and (e) NCL-5. The spectrum of liquid benzene in this region is shown in curve (f).

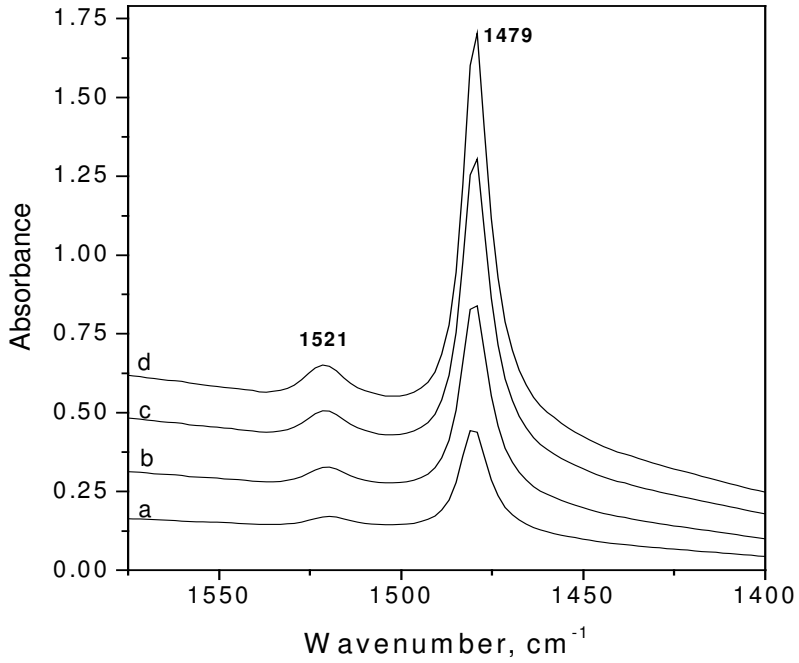


**Figure 4.8.** In-plane C-C stretching ($\nu_{19}$) vibrational bands of benzene for adsorption in Si-Beta at different loadings: curve (a) 0.1, (b) 0.2, (c) 0.3 and (d) 0.5 mmol $g^{-1}$.

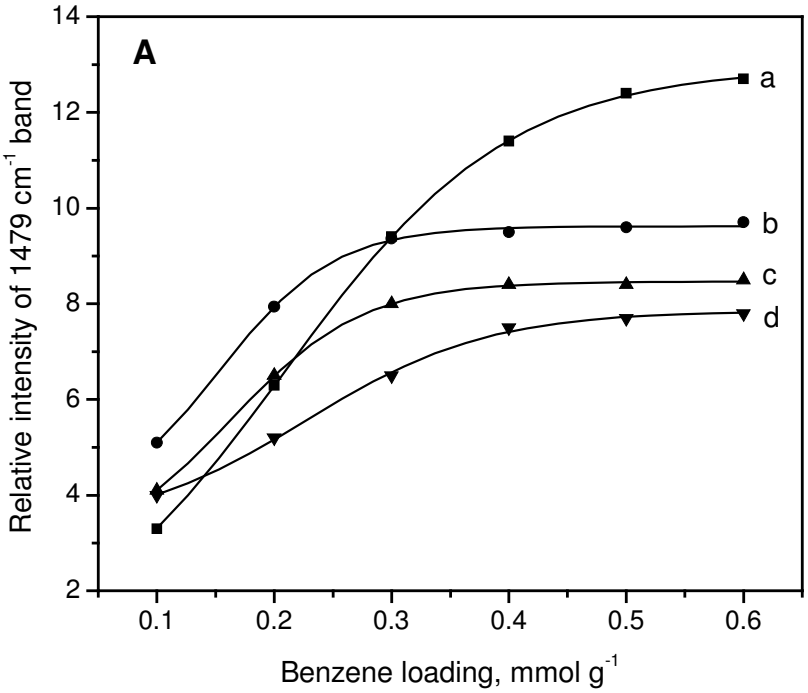

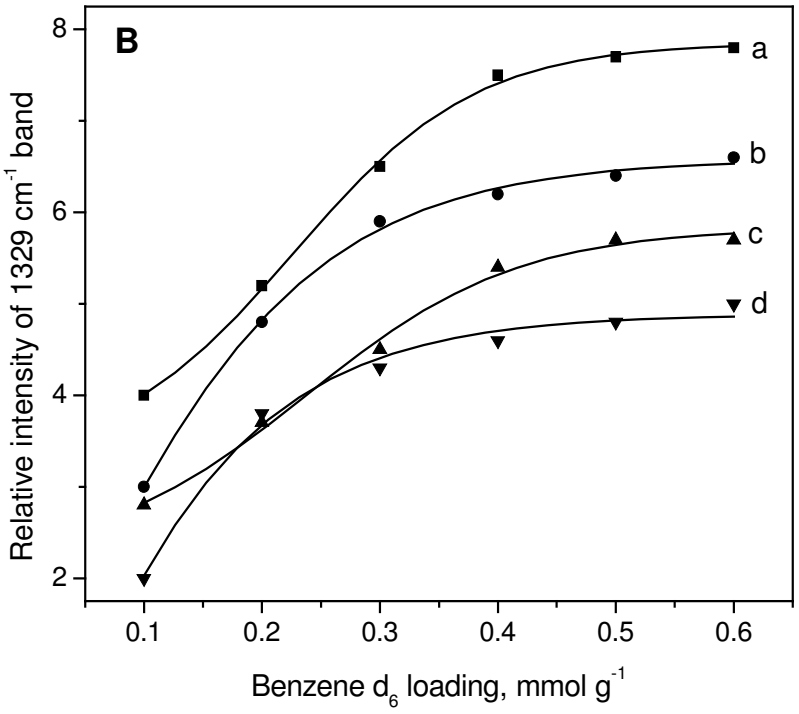


**Figure 4.9. (A)** A comparison of dose dependent variation in intensity of fundamental $\nu_{19}$ band (1479 $cm^{-1}$) of benzene on adsorption in Si-Beta (curve a), NCL-7 (curve b), NCL-6 (curve c) and NCL-5 (curve d). **(B)** Comparative dose dependent variation in intensity of fundamental $\nu_{19}$ band (1329 $cm^{-1}$) of benzene $d_6$ on adsorption in Si-Beta (curve a), NCL-7 (curve b), NCL-6 (curve c) and NCL-5 (curve d).

#### *4.4.1.3. Adsorption of Hexadeuterobenzene ($C_6D_6$)*

The IR bands formed on adsorption of benzene-$d_6$ ($C_6D_6$) exhibited almost similar dose dependent growth and splitting pattern as described above for $C_6H_6$. In brief, the bands arising due to fundamental vibrations and due to combinations of vibrations, which are in the plane of benzene ring, remained unchanged in frequency. On the other hand, the bands due to combinations of out-of-plane vibrations undergo splitting and frequency shift, depending again on the presence of Al in a sample and the pore characteristics. Curves a-e in Fig. 4.10 show the comparative out-of-plane region bands on adsorption of $C_6D_6$ over the sample Al-Beta, Si-Beta, NCL-7, NCL-6 and NCL-5, respectively. Curve (f) in this figure is for liquid $C_6D_6$. As observed in curve (a), the 1453 $cm^{-1}$ band due to combination $\nu_{10} + \nu_{17}$ out-of-plane stretching vibrations of $C_6D_6$, corresponding to 1815 $cm^{-1}$ band due to $\nu_{10} + \nu_{17}$ vibration of $C_6H_6$ (cf. Fig. 4.2), undergoes splitting and the relative intensities of the split bands appearing at 1450 and 1460 $cm^{-1}$ in Fig. 4.10 is found to be very different in Al-Beta, Si-Beta and polymorph B enriched samples (cf. Figs. 4.2 and 4.7). As in case of Fig. 4.7, in place of a single band at 1453 $cm^{-1}$ for liquid benzene (curve d), two almost equally intense bands at 1460 and 1450 $cm^{-1}$ were observed in the case of $C_6D_6$ adsorption in Al-Beta (Curve a). Also, as in case of $C_6D_6$ experiments, the 1460 $cm^{-1}$ band is very weak in curves (b) and (c) of Fig. 4.10, a trend similar to that observed in case of $C_6H_6$ experiments.

No splitting was observed in the $\nu_{19}$ stretching band (1330 $cm^{-1}$) or in the C-D stretch band at 2281 $cm^{-1}$. In order to make a comparison, curves a, b, c, d and e in Fig. 4.11 present the $\nu_{20}$ CD stretch vibrational band at 2281 $cm^{-1}$ for $C_6D_6$ adsorbed (0.3 mmol $g^{-1}$) in Al-Beta, Si-Beta, NCL-7, NCL-6 and NCL-5 samples, respectively

(notations as per Ref. 37). As depicted in Fig. 4.5 showing corresponding $C_6H_6$ data, IR spectra in Fig. 4.11 match in the frequency with that of the liquid $C_6D_6$ (curve f) with no measurable shift. It may be referred that the weak combination C-D stretching in-plane vibrational bands in frequency region 2400-2300 $cm^{-1}$ also match well with that of the liquid benzene (Fig. 4.11, curve f). A difference is however noticeable in the relative peak intensities of the bands in Fig. 4.11, the intensity ratio $I_{2281}/I_{2270}$ follow a trend Al-Beta > Si-Beta > NCL-7 > NCL-6 > NCL-5 > liquid benzene.

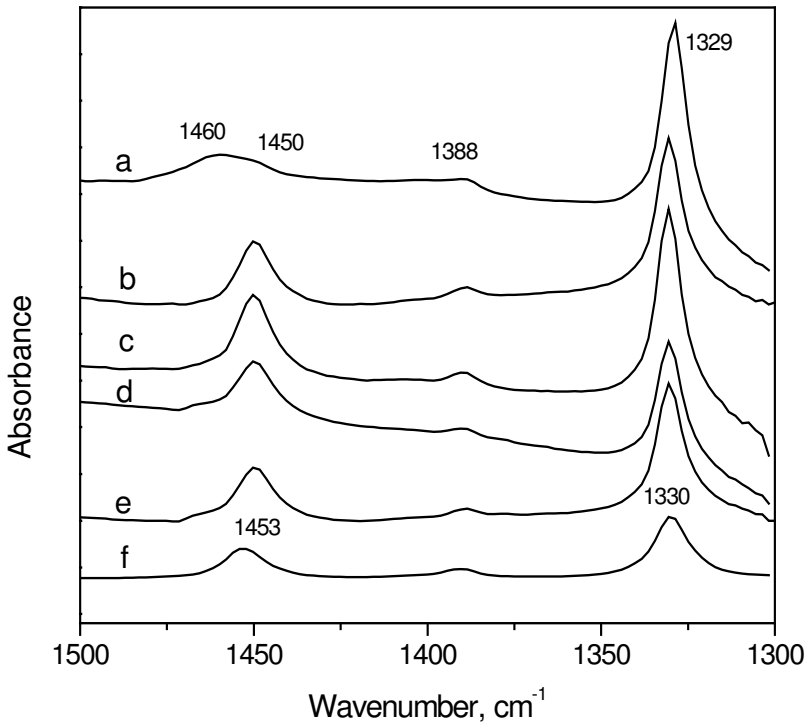


**Figure 4.10.** A comparison of C-H out-of-plane region IR bands for adsorption of 0.3 mmol of $C_6D_6$ per gm of different BEA type samples (a) Al-Beta, (b) Si-Beta, (c) NCL-7, (d) NCL-6 and (e) NCL-5. Curve (f) presents IR spectrum of $C_6D_6$ in liquid form.

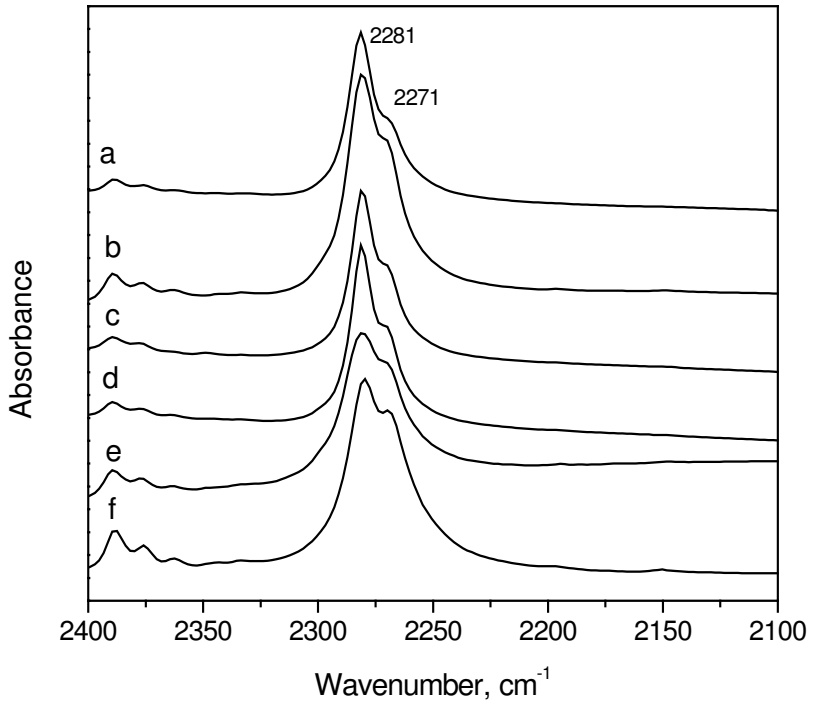


**Figure 4.11.** Comparison of C-C/C-H in-plane vibrational bands of $C_6D_6$ for loading at 0.3 mmol $g^{-1}$ in different BEA type zeolitic samples: curve (a) Al-Beta, (b) Si-Beta, (c) NCL-7, (d) NCL-6 and (e) NCL-5. Curve (f) is corresponding spectrum of liquid $C_6D_6$.

### *4.4.1.4. OH/OD Stretching Bands*

Curve (a) in Fig. 4.12 represents the OH region IR spectrum of zeolite Al-Beta activated *in-situ* at 573 K and with no exposure to benzene. A strong sharp peak at 3735 $cm^{-1}$ and a shoulder band at 3742 $cm^{-1}$ represent characteristic ν(OH) vibrations of zeolite Beta, attributed respectively to the silanols and the hydroxy groups associated with framework aluminum sites. The presence of a weak shoulder band at a lower frequency of ~3675 $cm^{-1}$ is also indicated in this spectrum, which is normally ascribed to the bridge-

bonded Bronsted acid sites. These bands were removed instantly on dosing of the first benzene pulse (0.1 mmol $g^{-1}$), using both $C_6H_6$ and $C_6D_6$. The peaks pointing downwards (negative absorbance) in spectrum (b) of Fig. 4.12 represent this feature for the adsorption of the first pulse of mixture of $C_6H_6 + N_2$. The intensity of the negative bands changed on exposure of a sample to successive pulses of benzene vapor till about 0.3 mmol $g^{-1}$ (Fig. 4.12, curves c, d), after which it remained constant, corresponding to saturation observed in the benzene bands (cf. Figs. 4.4 and 4.5). The removal of these 3750-3650 $cm^{-1}$ region bands ($\Delta\nu_{1/2}$ ~20 $cm^{-1}$) was accompanied with the development of a new broad band ($\Delta\nu_{1/2}$ ~100 $cm^{-1}$) centered at 3615 $cm^{-1}$. Again, the intensity of this band increased progressively as a function of benzene loading, reaching saturation on dosing of *ca.* 0.3 mmol $g^{-1}$of benzene. In addition to the relatively broad 3615 $cm^{-1}$ band, two broad bands are also discernible in the 3400-3200 $cm^{-1}$ region. When $C_6D_6$ was used for loading, more or less same behavior was observed besides a very weak new peak at ~3050 $cm^{-1}$. No peaks were observed in the O-D region, indicating only a negligible isotopic exchange at room temperature between the OH groups of the matrix and the adsorbed deuterated benzene

Figure 4.13 shows the changes in the OH and CH region bands on post-exposure thermal activation of an Al-Beta sample at different temperatures. As seen 3735 $cm^{-1}$ band progressively becomes more and more positive with increase in temperature (as reflected in the absorbance values mentioned in the parentheses) but never goes back to zero, as it should, if the wafer returns to the original condition. Similarly, the benzene C-H and C-C stretch bands also show the presence of residual benzene even after annealing of the sample at 523 K (curves c, d). The other important features of Fig. 4.13 is the

progressive decrease in the intensity and almost complete removal of the 3615 $cm^{-1}$ peak at the annealing temperatures of 423 K and above (curves c, d).

Almost similar changes in *v*(OH) bands were observed when an Al-Beta wafer exposed to $C_6D_6$ was subjected to thermal treatments. These results are presented in Fig. 4.14. The appearance of two new bands at 2747 and 2681 $cm^{-1}$ is an important feature of this figure. The intensity of the 2681$cm^{-1}$ *v*(OD) band, corresponding to *v*(OH) band at 3608 $cm^{-1}$, increases initially with the rise in temperature to 423 K (curves c-e) and then it registers a considerable decrease (curves f and g). At the same time, a positive shift is also observed in the frequency of this band. On the other hand, the intensity of the 2747 $cm^{-1}$ peak, corresponding to the 3735 $cm^{-1}$ *v*(OH) peak in the blank sample, increases continuously with the rise in sample temperature. A marginal increase in the intensity of the weak band appearing at 3052 $cm^{-1}$ was observed in this figure.

As expected, the intensity of the ν(OH) region bands was very small for in case of Si-Beta, NCL-7, NCL-6 and NCL-5 samples, because of their synthesis in the fluoride medium. Exposure of these samples also gave rise to a weak broad band at ~3610 $cm^{-1}$ accompanied with the removal of the 3735 $cm^{-1}$ band, the intensity of these bands following a trend similar to that shown in Fig. 4.12.

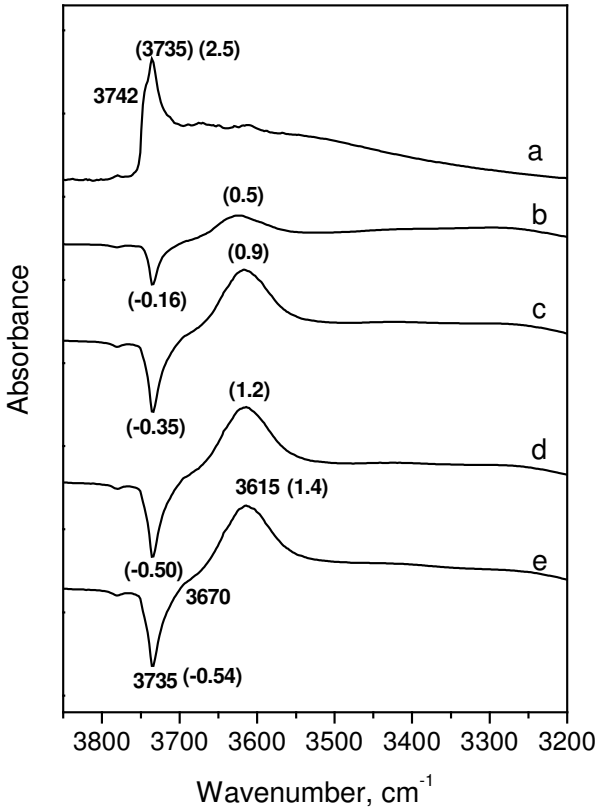


**Figure 4.12.** Difference IR spectra of Al-Beta in $\nu$(OH) region as a function of $C_6H_6$ loading at room temperature. Benzene loading: Curve (a) Nil, (b) 0.1, (c) 0.2, (d) 0.3 and (e) 0.6 mmol $g^{-1}$.

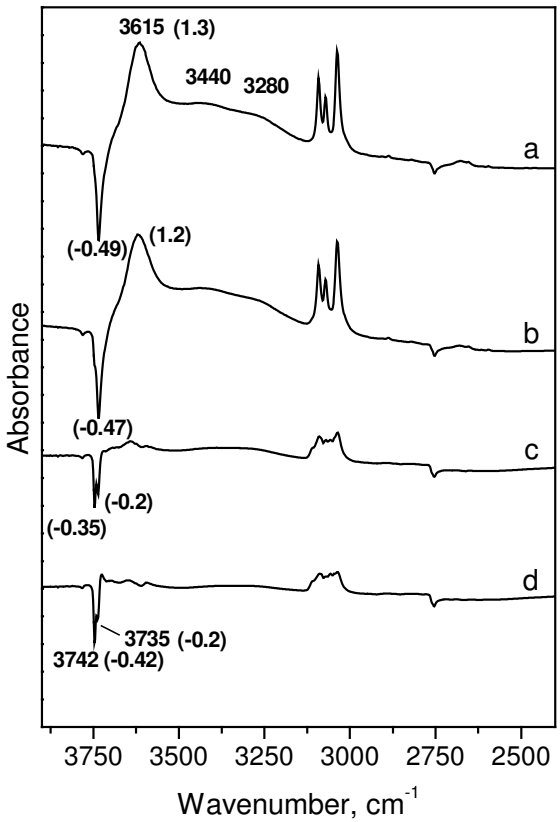


**Figure 4.13.** Effect of annealing on the $\nu$(OH) and C–H region IR bands when Al-Beta sample dosed with $C_6H_6$ to saturation was subjected to heat treatment at (a) 323, (b) 353, (c) 423 and (d) 523 K.

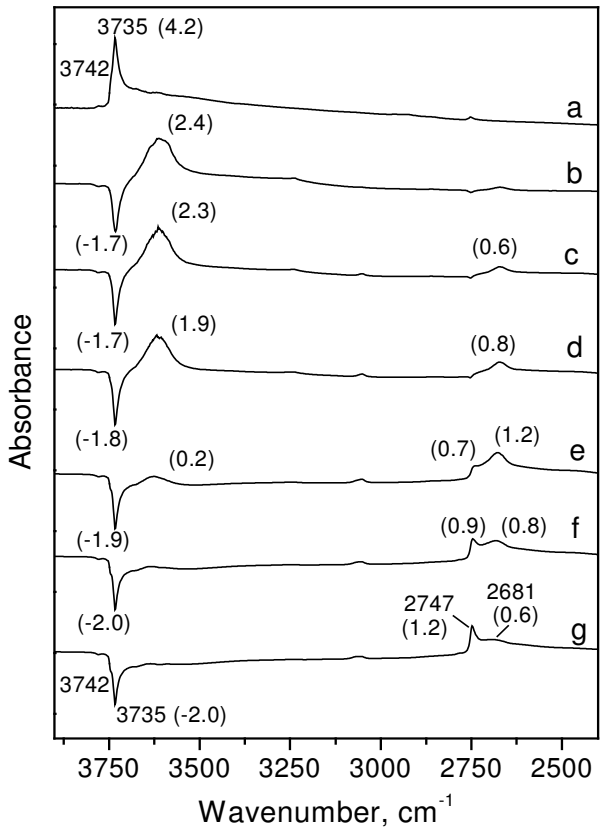


**Figure 4.14.** Effect of annealing on the $\nu$(OH) and $\nu$(OD) region IR bands when a Al-Beta sample dosed with $C_6D_6$ to saturation was subjected to a heat treatment at (b) nil, (c) 323, (d) 353, (e) 423, (f) 473 and (g) 523 K. Curve (a) shows IR spectrum before benzene adsorption.

### 4.4.2. Discussion

The three-dimensional 12-membered ring channel system with elliptical openings of 7.6 × 6.4 Å is the only site available in zeolite Beta for the entry of the molecules such as benzene. Therefore, the data in Figs. 4.2, 4.7 and 4.10, showing doubling of the out-of-plane combination vibrational bands, can not be explained on the basis of the entrapment

of benzene molecules at two different locations in the BEA channel system. The effect of annealing or evacuation of a sample subsequent to saturation benzene coverage, as shown in Fig. 4.3, is in agreement with this conclusion. Similar splitting of out-of-plane vibrations has been reported earlier for adsorption of benzene in microporous aluminosilicates including zeolite Beta, and these observations have been generally attributed to the interaction of benzene molecules with framework cations through the π-electron cloud.[12,16,38-40] However, such adsorption mechanism is expected to result in considerable perturbation and hence the frequency shift of in-plane C-H/C-C stretching vibration as well, which is contrary to the observations of this study (Figs. 4.4, 4.5, 4.8 and 4.11). At the same time, multiple vibrational bands were observed for the adsorption of $C_6H_6$ and $C_6D_6$ in the case of Si-Beta and polymorph B-rich samples NCL-7, NCL-6 and NCL-5 samples without aluminum, albeit with different relative intensities (Fig. 4.10). Therefore, the direct bonding of benzene molecules at zeolitic sites, such as $Al^{3+}$ or charge balancing cations, is not likely to be responsible for the splitting of IR bands in this region. The increase in number of bands in overtone/combination region can also arise from the loss of symmetry of benzene molecules in adsorbed state leading to the splitting of the combination modes of degenerate vibrations and the appearance of certain forbidden bands. But this is also unlikely because none of the in-plane degenerate fundamentals are found to split, thus ruling out the lowering of molecular symmetry in the adsorbed state of benzene. As has been described earlier in detail,[25,26] the selective splitting of only out-of-plane vibrational bands can also arise because of a highly compressed state of benzene molecules (dimers, trimers etc.) confined in the narrow zeolite cavities. It is to be noted that the narrowing of all the in-plane modes and

particularly the $v_{19}$ C-C stretching band (Table 4.1), variation in the relative intensity of different absorption bands (Table 4.1), and the splitting of out-of-plane vibrations, as observed in our study, are the well-reported features associated with transformation of benzene molecules to a highly condensed state, i.e. from the liquid to a solid-like state where even the reorientational motion present in liquids are highly restricted.[41,42]

The narrowing of the bands provides an evidence for the strong solid-like property of the adsorbed state. As is well known, the loss of free rotational motion (quantized rotational levels) during transformation from gas to liquid state causes the loss of PQR structure in liquid phase spectrum. However, the molecule still undergoes partial rotation, and the rotational correlation function is a measure of the free rotation before collisions overtake the rotational motion. The correlation time is inversely proportional to the half width and the short correlation times due to collisions cause the broadening of the vibrational bands in the liquid state. On the other hand, in solid state, all collisional/reorientational processes are reduced to a large extent and any broadening arises from restricted rotation, phonon interactions, or crystal splitting. The narrowing of the bands (including in-plane C-H stretch) thus clearly show that all the reorientational motions are lost in the adsorbed state of benzene molecules, indicating the existence of a highly condensed solid-like state. It may also be noted that the IR active in-plane fundamentals are doubly degenerate modes with their transition moments perpendicular to the symmetry axis. In liquid benzene, the rotation about the symmetry axis is relatively easy compared to the tumbling motion, giving broad bands for in-plane modes and sharp bands for out-of-plane modes. The fact that the in-plane modes are much narrower in the

adsorbed state (Table 4.1), further confirms that the adsorbed benzene is highly restricted in its rotational motion, very close to a solid-like condition.

A comparison of the results presented in Table 4.1 and Figs. 4.2 and 4.6 reveals that the narrowing of the bands is more prominent in case of Al-Beta samples. Similarly, the changes in the relative intensities of different IR bands are influenced considerably by $Al^{3+}$ ions present in zeolite Beta. It can be concluded that even though the $Al^{3+}$ sites are not likely to be involved in the direct bonding of benzene molecules, the electrostatic charge associated with these cations may promote the clustering process to a significant extent. Further, the trend observed in uptake capacity of benzene in all siliceous samples is Si-Beta > NCL-7 > NCL-6 > NCL-5 (Fig. 4.9). It can be explained only on the basis of marginal difference in the pore characteristics of these materials. As discussed earlier, the polymorphic proportions of polymorph B : polymorph A in Si-Beta, NCL-7, NCL-6 and NCL-5 samples are 55 : 45, 65 : 35, 75 : 25 and 90 : 10, respectively. Thus, the higher restricted sorption of benzene in NCL-5 compared to NCL-6, NCL-7 and Si-Beta may be attributed to its constrictive channels because of higher polymorph B content. Although, the inherent faulting of the zeolite Beta structure does not affect the accessible pore volume significantly, it increases the tortuous nature of the pore system considerably. Since the sample NCL-5 is *ca.* 90 % B polymorph intergrowth as compared to *ca.* 75, 65 and 55 in NCL-6, NCL-7 and Si-Beta, it is expected that there could be more constraints in the adsorption of gas molecules in NCL-5 as compared to the other host matrices compared above. It may be recalled that the straight channels of polymorph B are more elliptical compared to that of Si-Beta.[29,31] The loading-dependent changes in the width and the intensity ratio of various out-of-plane and in-plane vibrational bands as compared

to that of liquid benzene, as described above, further demonstrate that the density of the benzene clusters occluded in zeolite-BEA may eventually depend upon a combination of several factors, such as presence of $Al^{3+}$ (and also the charge balancing cations), pore size, and the pore structure of the confining medium; following an overall trend Al-Beta > Si-Beta > NCL-7 > NCL-6 > NCL-5.

The OH stretching bands observed in curve (a) in Fig. 4.12 represents the well-reported hydroxyl groups in zeolite Beta, silanol OH (3735 $cm^{-1}$), two kinds of Al-OH groups (3745, 3782 $cm^{-1}$) and a bridging Si-OH-Al (~3675 $cm^{-1}$). The frequency and the relative intensity of these vibrational bands are found to vary with the Si/Al ratio, method of preparation, and the pretreatment given to a sample.[43-48] The disappearance of the 3800 -3650 $cm^{-1}$ region ν(OH) bands and simultaneous formation of a relatively broad band at ~3615 $cm^{-1}$, as depicted in curves b-e of Fig. 4.12, is a well documented observation for room temperature adsorption of benzene in microporous aluminoslicates, including zeolite Beta.[24,30,31] This behavior has been attributed normally to the interaction of benzene π-electron cloud with the surface OH groups. The interaction of π-electron cloud with surface hydroxyl groups is likely to change the frequencies of the benzene vibrations and may also lead to increase in the *ν*(OH) frequencies, due to the increased electron density along the bond. Therefore, the 3615 $cm^{-1}$ band (Figs. 4.12 and 4.13) can not be attributed to electronic interaction between the benzene molecules and the hydroxyl groups of zeolite. More likely, this band may arise from a weak hydrogen bonding between the two adjacent OH groups. This can happen if we assume that the benzene clusters occluded in the pores displace the –OH groups physically, resulting in their

tilting towards the zeolite walls and thus facilitating a Van-der Waal's type interaction between themselves. This is shown pictorially in scheme 1.

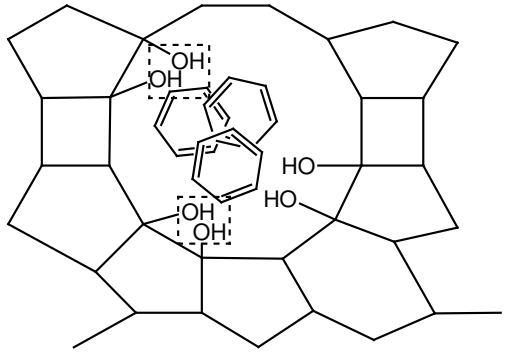


**Scheme 4.1**. The picture representing perturbation of some of the hydroxy groups in zeolitic cavities due to entrapment of benzene clusters, resulting in the hydrogen bonding between two tilted OH groups and the lowering of ν(OH) frequency.

It is to be noted that such configurations where OH groups are mutually hydrogen bonded to each other may cause practically no change in the vibrational frequencies of adsorbed benzene (Figs. 4.4 and 4.5), other than that can happen on its condensation (Fig. 4.2). At the same time, the hydrogen bonding between two OH groups will give rise to the band broadening and the shift in their frequency to lower side, as observed in Fig. 4.12. As described above, the adsorption of $C_6D_6$ also results in similar changes in the *ν*(OH) bands, giving rise to a 3615 $cm^{-1}$ band (Fig. 4.14, curve a). As seen in Fig. 4.12, the positive absorbance of ~2.5 for silanol peak at 3735 $cm^{-1}$ in curve (a) gives rise to a negative peak with absorbance of only ~0.5 after saturation coverage, indicating that only a fraction of the silanols get perturbed in the sorption process. This is understandable, since the OH groups present inside the channel system will be affected on benzene

adsorption, as depicted in Scheme 1. This is further confirmed by the results on $C_6D_6$ experiments (Fig. 4.14), where an initial absorbance of ~4.2 in the un-exposed sample (curve a) gives rise to a negative band with an absorbance value of ~1.7 on benzene adsorption (curve b). Furthermore, the presence of very weak bands in 3500-3300 $cm^{-1}$ in Figs. 4.12-4.14 indicates that a small fraction of hydroxyl groups may also convert to water molecules during the occlusion of the benzene clusters in zeolite pores, as described above.

The results in Fig. 4.14 further reveal that H-D isotopic exchange may take place between the adsorbed benzene molecules and the surface hydroxyl groups, even at a low temperature of 323 K, giving rise to a weak band at 3052 $cm^{-1}$ ($C_6D_5H$) (Fig. 4.14, curve b). The extent of this isotopic exchange increases with the rise in sample temperature, giving rise to the formation of more OD and $C_6H_5D$ species, as seen from the increase in the 3660 $cm^{-1}$ band. The hydrogen-bonded O-D peaks at 2681 $cm^{-1}$ was observed in Fig. 4.14, corresponding to 3615 $cm^{-1}$ band in Fig. 4.12, the intensity of which increases because of more isotopic exchange with rise in temperature (Fig. 4.14, curves b-d) and then decreases subsequently because of the release of the occluded benzene molecules (Fig. 4.14, curves e, f). A similar trend may be noticed in the intensity of 3615 $cm^{-1}$ band as a function of sample temperature (Fig. 4.13).

Figure 4.13 shows that even though the intensity of 3615 $cm^{-1}$ band decreases drastically on thermal activation, the intensity of the sharp negative band at 3735 $cm^{-1}$ change only partially and it does not revert to its original value in the matrix, in which case a flat, zero baseline can be anticipated. This may be attributed to the restricted release of benzene clusters on thermal activation, as evident from the results of Figs. 4.3

and 4.13, where the residual molecules will continue to perturb the hydroxyl groups. Loss of a part of the OH groups in formation of water (HDO for $C_6D_6$) also contributes to the decrease of the silanol band. This is confirmed by the $C_6D_6$ adsorption, where the reversal of the intensity of 3735 $cm^{-1}$ band is found to be negligibly small but at the same time the growth of a sharp band at 2747 $cm^{-1}$ due to free -OD groups was observed (Fig. 4.14). It is apparent that the $C_6D_6$ molecules face a greater resistance to removal from the narrow pores of zeolite Beta as compared to $C_6H_6$.

### 4.4.3. Conclusions

*In-situ* FTIR spectroscopy has been employed in this study to monitor the binding states of $C_6H_6$ and $C_6D_6$ molecules in the zeolites of BEA family, for the loadings of 0.1- to 0.6 mmol $g^{-1}$ at room temperature. Different samples of zeolite Beta, varying from each other in Si/Al ratio and comprising of polymorphs B and A in different proportions, were used as adsorbent in these experiments. In all the cases, the frequency of the in-plane C–C/C–H stretch vibrations of adsorbate molecules matched with the vibrational spectrum of liquid phase benzene, irrespective of the loading. The bands arising from out-of-plane bending vibrations on the other hand were found to undergo splitting, and the frequencies and the relative intensities depended strongly on the presence of $Al^{3+}$ cations and the polymorphic composition. The loading-dependent changes in the width and relative intensity of these two kinds of absorbance bands suggest that the benzene molecules trapped in the zeolitic channels existed in a highly condensed (clustered) state. The electrostatic field associated with the $Al^{3+}$ cations and the pore characteristics of the host matrix are found to have considerable influence on the physical state of occluded

benzene. Thus, the increase in the polymorph B content in a sample from 55 % ($^{*}$BEA, zeolite Beta) to 90 % (NCL-5) resulted in the constrained transport and adsorption of benzene molecules in the channels of NCL-5, attributed to the more tortuous pore characteristics of the B polymorph. The results of this study also provide strong evidence for the physical perturbation to OH/OD groups by occluded benzene, leading possibly to their tilt towards the zeolite wall. The reoriented hydroxy groups in turn experience a weak hydrogen bonding between themselves, resulting in the broadening of ν(OH) bands and in the lowering of their frequency. A fraction of the hydroxy groups may also convert to water molecules in this process. Furthermore, the entrapped benzene and OH groups are found to undergo reversible H/D isotopic exchange and the process is promoted on rise in temperature. In conformity with earlier studies on this subject, no specific interaction is envisaged between the π-bonds of the benzene molecules and the surface hydroxy groups/zeolitic framework sites.

## 4.5. ADSORPTION AND BINDING STATES OF BENZENE AND DEUTERATED BENZENE IN MFI AND M41S TYPE MATERIALS: A COMPARATIVE STUDY

A comparative study was carried out using all siliceous and Al-containing ZSM-5 and MCM-41 structures, in order to ascertain the effect of chemical nature (due to presence of Al) and particularly that of the structural features of these materials on adsorption of $C_6H_6$ and $C_6D_6$ molecules. Among these, ZSM-5 is a medium pore zeolite, having wide applications in the petroleum industries and in the synthesis of fine chemicals. It constitutes a complex 3 dimensional pore structure comprising of elliptical straight channels (5.1 × 5.6 Å) and near circular interconnecting zigzag channels (5.4 × 5.6 Å) with an intersection dimension of ~ 8 Å (4 intersections per unit cell). These structural parameters offer shape selectivity for different catalytic processes involving the hydrocarbons. MCM-41 is a mesoporous material having the hexagonal structure and well-defined pore size of 20-100 Å. High surface area (>700 $m^2$ $g^{-1}$) and the control of pore sizes are among the many desirable properties that have made these materials the focus of great interest. All the three host matrices used in the present study is pictorially represented in following scheme.

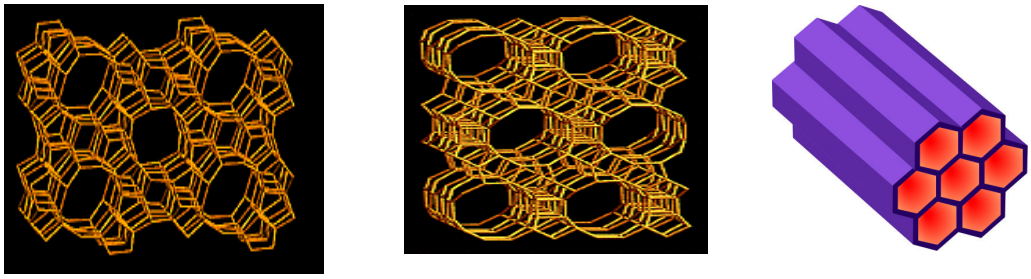

**ZSMM-5** **BETA** **MCM-41**

**Scheme 4.2.** Structural representation of ZSM-5, Beta and MCM-41.

Adsorption of Benzene and deuterated benzene on MFI and M41S structures was studied by using the methodology described above. As described in section 4.4, the in-plane C-H/C-C and C-D/C-C stretches, out-of-plane C-H and C-D vibrations and fundamental $\nu_{19}$C-C stretch vibrations of $C_6H_6$ and $C_6D_6$ are monitored systematically so as to study the binding state of these guest molecules in the porous materials having different pore characteristics and structural features.

### 4.5.1. Results

#### *4.5.1.1. Adsorption of Benzene ($C_6H_6$) in Al-ZSM-5 and Al-MCM-41*

##### *4.5.1.1.1. Out-of-plane combination (C-H) bending vibrations (2050 -1750 $cm^{-1}$)*

Adsorption of benzene on Al-ZSM-5, Al-Beta and Al-MCM-41 was studied for the loading in range of 0.1- to 0.6 mmol $g^{-1}$. Curves a, b and c in Fig. 4.15 present the comparative spectra of out-of-plane C-H bending vibrations when 0.3 mmol $g^{-1}$ of benzene was dosed on Al-ZSM-5, Al-Beta and Al-MCM-41 samples, respectively. Curves (d) and (e) represent the spectra for liquid and vapor phase benzene. On comparison, it is apparent that the spectrum of benzene adsorbed in Al-ZSM-5 (curve a) does not match with either of these two phases of benzene (curves d, e). In place of C-H out-of-plane combination band at 1960 $cm^{-1}$ ($\nu_5 + \nu_{17}$ vibrations) for liquid benzene (Fig. 4.15, curve c), at least four overlapping bands with frequency maxima 2006, 1986, 1971 and 1956 $cm^{-1}$ are noticeable in curve (a) of Fig. 4.15. Similarly, 1815 $cm^{-1}$ band is found to split into four bands with frequency maxima at 1873, 1852, 1830 and 1810 $cm^{-1}$. As described in section *4.4.1.1.1,* in case of Al-Beta sample, the lower frequency out-of-plane combination band at 1815 $cm^{-1}$ splits into two overlapping bands at around 1830

and 1812 $cm^{-1}$ and at least two bands are observed with the frequency maxima of 1971 $cm^{-1}$ and 1956 $cm^{-1}$ in place of higher frequency band at 1960 $cm^{-1}$. On the other hand, the spectral features of benzene adsorbed in Al-MCM-41 sample were quite different as compared to the vibrational bands described in case of Al-ZSM-5 and Al-Beta (Fig. 4.15, curves a, b). Two intense bands around 1972 and 1830 $cm^{-1}$ were observed in Al-MCM-41, similar to that of liquid benzene. At the same time, a small shift in the frequency to a lower value by ~15 $cm^{-1}$may also be noticed in curve (c).

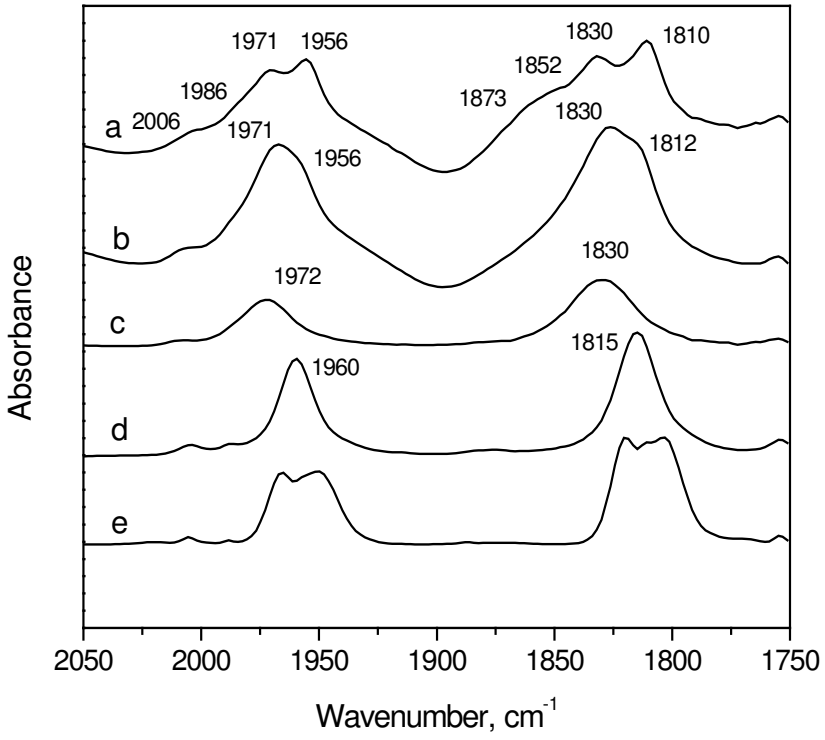


**Figure 4.15.** C-H out-of-plane vibrational bands for benzene loading of 0.3 mmol $g^{-1}$ in curve (a) Al-ZSM-5, (b) Al-Beta and (c) Al-MCM-41. Curves (d) and (e) show IR spectra of liquid and vapor forms of benzene, for comparison.

***4.5.1.1.2. In-plane C-H/C-C stretch combination bands (3150 - 2950 cm$^{-1}$)***

In-plane C-H/C-C stretch combination bands (3150-2950 cm$^{-1}$) of benzene after adsorption over Al-ZSM-5, Al-Beta and Al-MCM-41 are shown in Fig. 4.16. Curve (d) in Fig. 4.16 presents comparative spectra of in-plane C-H stretching ($\nu_{20}$) and combination C-C ($\nu_1 + \nu_6 + \nu_{19}$ and $\nu_{19} + \nu_8$) bands of liquid phase benzene. Curves a, b and c in this figure refer to corresponding spectrum of benzene when adsorbed in Al-ZSM-5, Al-Beta and Al-MCM-41 at room temperature.

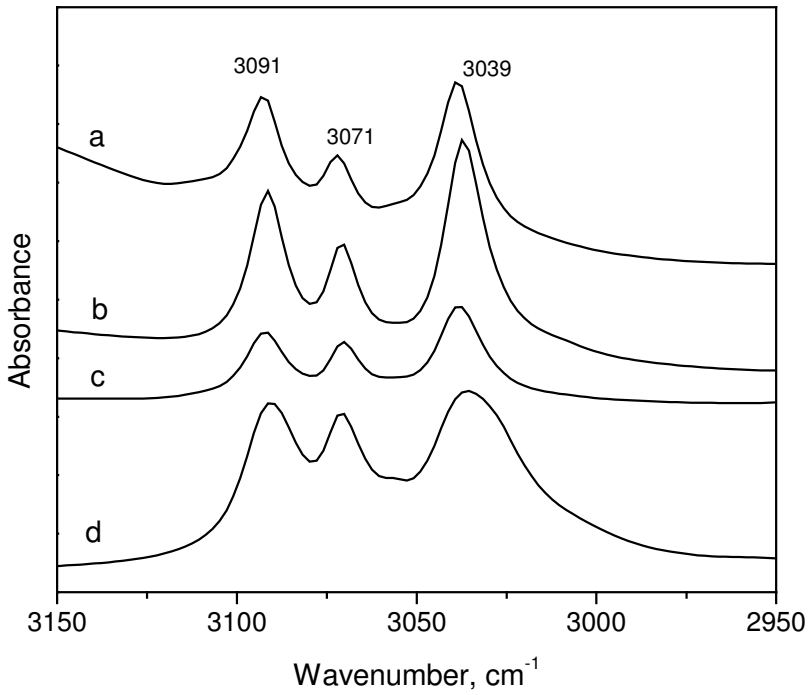


**Figure 4.16.** Comparison of C-C/C-H in-plane vibrational bands of $C_6H_6$ for loading at 0.3 mmol g$^{-1}$ in different zeolitic samples: curve (a) Al-ZSM-5, (b) Al-Beta and (c) Al-MCM-41. Curve (d) represents spectrum of liquid phase $C_6H_6$.

As it can be seen from the Fig. 4.16, benzene on adsorption in Al-ZSM-5, Al-Beta and Al-MCM-41 give rise to three prominent bands at 3091, 3071 and 3039 $cm^{-1}$ in the in-plane C-C/C-H vibrational region, which show complete absence of PQR branches of vapor phase. The IR bands in the curves a, b and c match quite well with the spectrum of liquid benzene in this region (Fig. 4.16, curve d).

#### *4.5.1.1.3. Fundamental $\nu_{19}$ C-C stretching vibration (1479 $cm^{-1}$)*

Curves a, b and c of Fig. 4.17 shows fundamental $\nu_{19}$ C-C stretching vibration of benzene, when adsorbed in Al-ZSM-5, Al-Beta and Al-MCM-41, respectively at 0.3 mmol $g^{-1}$ benzene loading. The liquid phase spectrum of benzene is plotted in curve (d) for comparison. The spectrum of all the three samples, Al-ZSM-5, Al-Beta and Al-MCM-41, show likeness with the spectrum of liquid phase (curve d). Similar behavior was observed in case of Al-Beta as described in detail in section 4.4.1.1.3. The half width (full-width at half intensity $\triangle\nu_{1/2}$) was found to be much smaller as compared to liquid benzene. It is also noteworthy to mention that the half width of Al-containing samples (Table 4.2, entry 1-3) was found to be smaller than all siliceous samples (Table 4.2, entry 4-6).

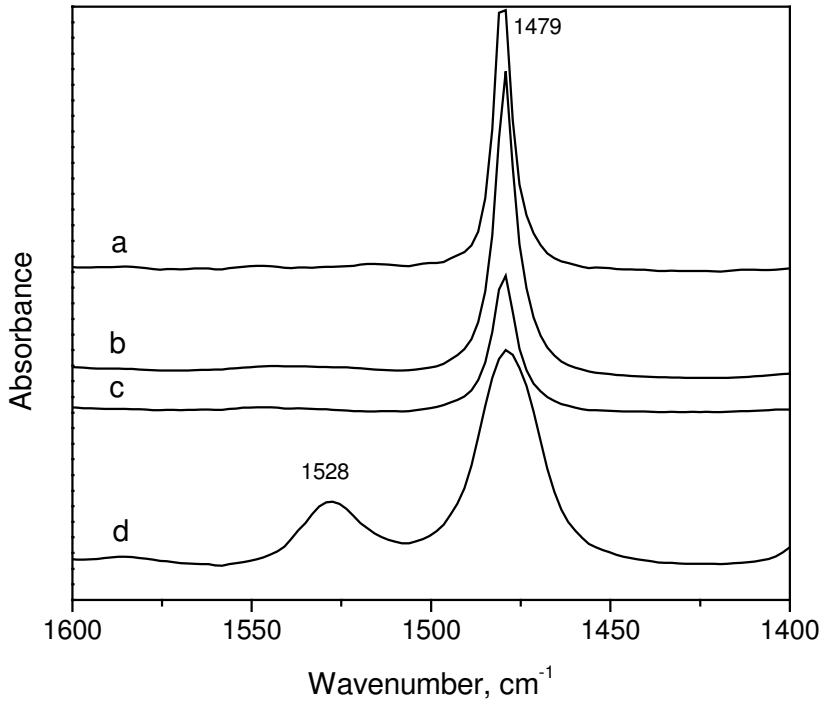


**Figure 4.17**. In-plane C-C stretching ($\nu_{19}$) vibrations of benzene (0.3 mmol $g^{-1}$) adsorption on different samples curve (a) Al-ZSM-5, (b) Al-Beta and (c) Al-MCM-41. Curve (d) refers to the spectrum of liquid phase benzene.

**Table 4.2**

Comparative width of in-plane C-C stretch vibrational band ($\nu_{19}$) at 1479 $cm^{-1}$ and C-C stretching vibrations ($\nu_{19} + \nu_8$) at 3037 $cm^{-1}$ of benzene on adsorption in different samples and the intensity ratios of selected in-plane vibrational bands

| Sample Name | [a]Band width of vibrations at | | [b]Peak ratio |
|---|---|---|---|
| | 1479 $cm^{-1}$ | 3037 $cm^{-1}$ | 3037/1479 |
| Al-ZSM-5 | 11.9 | 6.5 | 0.34 |
| Al-Beta | 14.1 | 7.6 | 0.45 |
| Al-MCM-41 | 17.3 | 9.7 | 0.48 |
| Silicalite-1 | 14.0 | 9.7 | 1.14 |
| Si-Beta | 17.3 | 10.5 | 1.93 |
| Si-MCM-41 | 18.4 | 10.8 | 2.2 |
| Liquid Benzene | 30.3 | 21.0 | 4.0 |
| Vapor Benzene | 45.8 | 33.7 | – |

[a]FWHM = Full width at half maximum

[b]Estimated from the absorbance value of respective IR bands for 0.3 mmol $g^{-1}$ benzene loading.

### *4.5.1.2. Adsorption of Deuterated Benzene ($C_6D_6$) in Al-ZSM-5 and Al-MCM-41*

The IR bands formed on adsorption of deuterated benzene exhibited almost similar splitting pattern as described above for $C_6H_6$. The bands arising due to fundamental vibrations and due to combinations of vibrations, which are in the plane of benzene ring remained unchanged in frequency. On the other hand, the bands due to combinations of out-of-plane vibrations undergo splitting and frequency shift, depending again on the presence of Al in a sample and the pore characteristics as seen in case zeolite Beta. Curves a, b and c in Fig. 4.18 show the comparative out-of-plane region bands on adsorption of $C_6D_6$ over Al-ZSM-5, Al-Beta and Al-MCM-41 samples, respectively. Curve (d) refers to the IR spectrum of $C_6D_6$ in liquid form. In case of Al-ZSM-5, 1453 $cm^{-1}$ band due to combination $\nu_{10} + \nu_{17}$ out-of-plane stretching vibrations of $C_6D_6$ undergo splitting four different bands with the peak maxima at 1450, 1460, 1468 and 1422 $cm^{-1}$ (curve a). In Al-Beta sample, (section 4.4.1.3.), the 1453 $cm^{-1}$ band undergo splitting into two bands at 1450 and 1460 $cm^{-1}$ (cf. Fig. 4.10). On the other hand, IR spectrum for Al-MCM-41 sample showed a single band at 1461 $cm^{-1}$ without any splitting in out-of-plane bending vibrations of deuterated benzene. A shift of ~8 $cm^{-1}$ with respect to vibrational spectrum of liquid $C_6D_6$ is noticeable in curve (c) of Fig. 4.18.

No splitting was observed in the $\nu_{19}$ stretching band (1330 $cm^{-1}$) or in the C-D stretch band at 2281 $cm^{-1}$ in all the three samples. The $\nu_{20}$ C-D stretch vibrational band at 2281 $cm^{-1}$ for $C_6D_6$ adsorbed (0.3 mmol $g^{-1}$) in Al-ZSM-5, Al-Beta and Al-MCM-41 samples are compared along with liquid of deuterated benzene in curves a, b, c and d, respectively in Figs. 4.18 and 4.19. The bands of each of these match well with that of the liquid $C_6D_6$ (curve d) with no measurable shift.

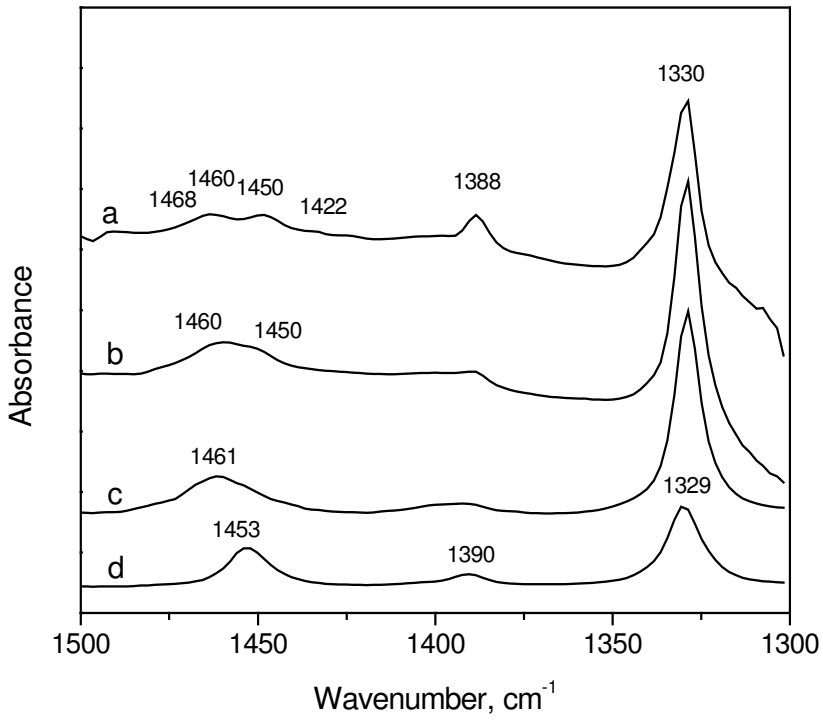


**Figure 4.18.** Comparative plot of C-H out-of-plane region IR bands for adsorption of 0.3 mmol of $C_6D_6$ per gm on Al-ZSM-5 (curve a), Al-Beta (curve b) and Al-MCM-41 (curve c). Curve (d) presents IR spectrum of liquid $C_6D_6$.

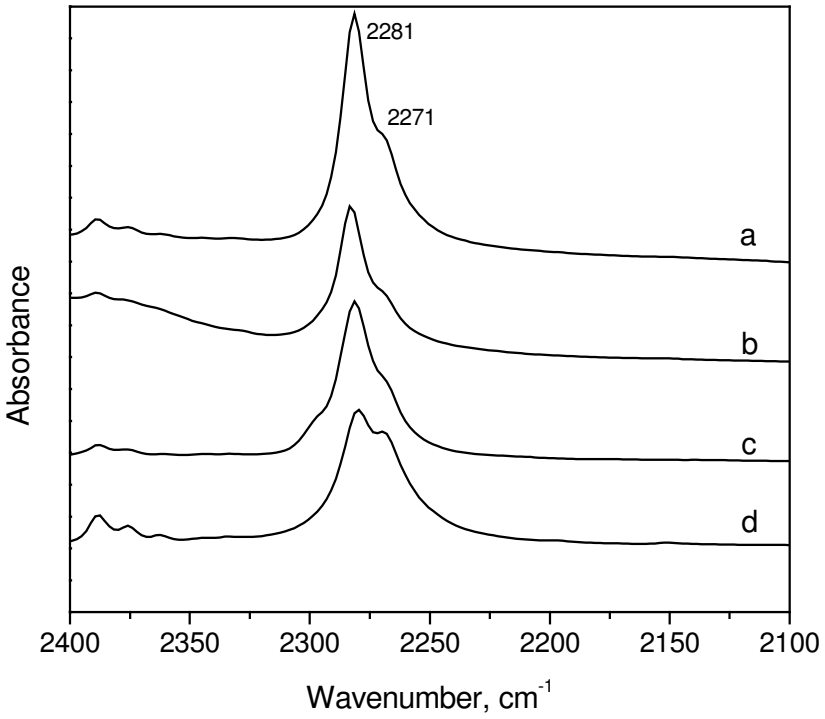


**Figure 4.19.** Comparison of C-C/C-H in-plane vibration bands of $C_6D_6$ for 0.3 mmol $g^{-1}$ loading on Al-ZSM-5 (curve a), Al-Beta (curve b) and Al-MCM-41 (curve c). Curve (d) presents IR spectrum of liquid $C_6D_6$.

### *4.5.1.3. OH/OD Stretching Bands*

Effect of adsorption of benzene on hydroxy region IR bands of Al-ZSM-5 shows the similar trend as observed in case of zeolite Beta.[51] However, the adsorption of deuterated benzene on Al-ZSM-5 shows different behavior as compared to Al-Beta (Section 4.4.1.4, Fig. 4.14) and is presented in Fig. 4.20. Curve (a) represents OH region IR spectrum of Al-ZSM-5, activated *in-situ* at 573 K without any exposure to $C_6D_6$. It

shows the presence of three overlapping ν(OH) bands at 3744, 3680 and 3612 $cm^{-1}$. Curve (b) represents the negative hydroxy bands after exposure of 0.6 mmol $g^{-1}C_6D_6$. Curves c-f refer to the OH region bands when an Al-ZSM-5 sample was subjected to post-thermal treatment at 353, 423, 473 and 523 K. Appearance of two additional bands at 2747 and 2681 $cm^{-1}$ is an important feature of this figure. The intensity of band 2681 $cm^{-1}$ (corresponding to ν(OH) band at 3608 $cm^{-1}$) and 2747 $cm^{-1}$(corresponding to ν(OH) band at 3735 $cm^{-1}$) increase linearly with rise in temperature.

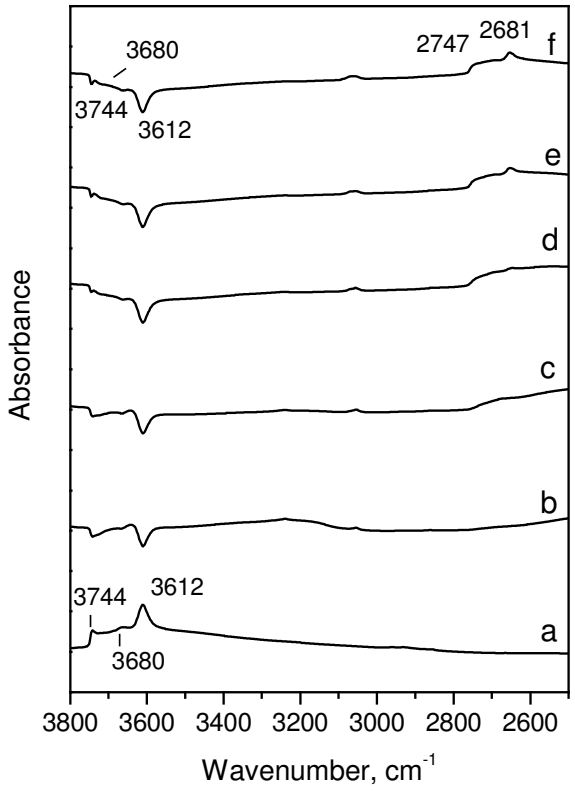


**Figure 4.20.** Effect of annealing on the ν(OH) and ν(OD) region IR bands on Al-ZSM-5 sample Curve (a) represents pre activated Al-ZSM-5, Curve (b) refers to the 0.6 mmol $g^{-1}$ $C_6D_6$ on Al-ZSM-5.Curves c-f present spectral feature of annealing on Al-ZSM-5 (after 0.6 mmol $g^{-1}$ $C_6D_6$ loading) at 353, 423, 473 and 523 K, respectively.

The adsorption of deuterated benzene on Al-MCM-41 shows different behavior in OH/OD region as drawn in Fig. 4.21. In this figure, curve (a), depicts the IR spectrum of pretreated Al-MCM-41 before exposure to the $C_6D_6$. Curve (b) refers to the spectral features observed after exposure of 0.6 mmol $g^{-1}C_6D_6$. Curve c-f corresponds to the OH region bands when an activated Al-MCM-41 sample was exposed to $C_6D_6$ at temperatures 353, 423, 473 and 523 K. It is paramount to mention that no H-D isotopic exchange was observed in Al-MCM-41 even at a higher temperature of 523 K as seen in Fig. 4.21, curve (f).

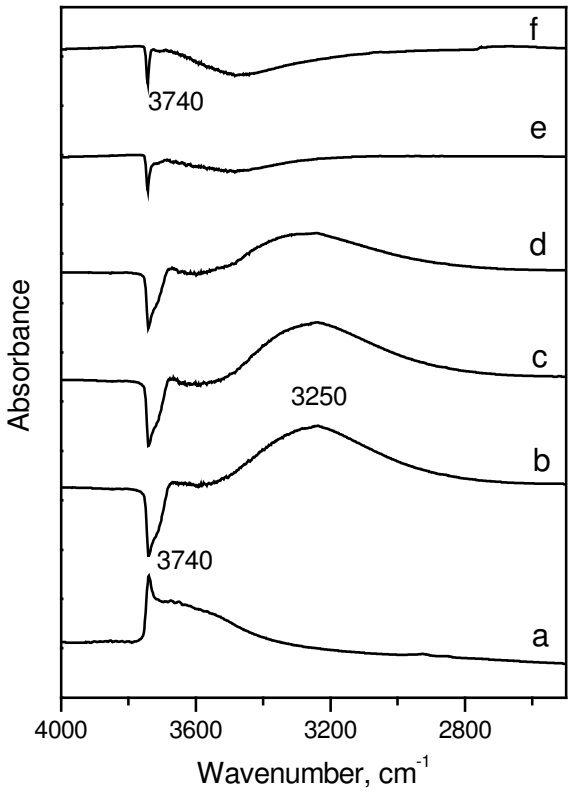


**Figure 4.21.** Effect of $C_6D_6$ adsorption on the $\nu$(OH) and $\nu$(OD) region IR bands on Al-MCM-41 sample curve (a) represents activated Al-MCM-41, Curve (b) refers to the 0.6 mmol $g^{-1}$ $C_6D_6$ on Al-MCM-41. Curves c-f presents spectral feature of Al-MCM-41 exposed to 0.6 mmol $g^{-1}$ $C_6D_6$ at 353, 423, 473 and 523 K, respectively.

### *4.5.1.4. Adsorption of Benzene ($C_6H_6$) and Deuterated Benzene ($C_6D_6$) in Silicalite-1, Si-Beta and Si-MCM-41*

Adsorption of benzene has been studied over Silicalite-1, Si-Beta and Si-MCM-41 in order to investigate the effect of presence of framework $Al^{3+}$ and variation in the pore characteristics under identical conditions as studied in case of Al-containing counterparts. The salient features of occlusion of adsorbates, $C_6H_6$ and $C_6D_6$, in Silicalite-1, Si-Beta and Si-MCM-41 are listed below.

The frequencies of all in-plane vibrations of adsorbed benzene and deuterated benzene over Silicalite-1 and Si-MCM-41 show similar behavior as that of Si-Beta described in detail in section 4.4.1.2. The intensity of ν(OH) bands is comparable in Si-MCM-41 and Silicalite-1 as that of Al-MCM-41 and Al-ZSM-5. As expected, intensity of these bands was very low in Si-Beta due to its synthesis in fluoride medium.

During adsorption studies of different guest molecules inside the cages of zeolites and other porous materials out-of-plane vibrations are prone undergo splitting depending upon the polarity of guest molecules, pore characteristics of the host matrices and presence of cation. Taking in account these facts, the adsorption of benzene and deuterated benzene are discussed in detail over Silicalte-1, Si-Beta and Si-MCM-41 in Figs. 4.22 and 4.23, respectively.

Curves a, b and c in Fig. 4.22 depict the effect of 0.3 mmol $g^{-1}$ benzene loading on Silicalite-1, Si-Beta and Si-MCM-41, respectively. Curves (d) and (e) refer to the spectral features of liquid and vapor phase benzene. As it seen from Fig. 4.22, no splitting was observed in case all the three siliceous samples, as seen in case of Al-containing samples, Al-Beta (Section 4.4.1.1.1), Al-ZSM-5 (Section 4.5.1.1.1). This outlines the role of

presence of $Al^{3+}$ sites in the host matrices. However, all the three samples shows change in wavenumber of out-of-plane bands. The band at 1815 $cm^{-1}$ ($\nu_{10} + \nu_{17}$) in liquid benzene changes to 1807, 1811 $cm^{-1}$ in Silicalite-1 and Si-Beta samples. In case of mesoporous material Si-MCM-41, the shift of ~8 $cm^{-1}$ was observed (Fig. 4.22, curve c). This can be explained only the basis of pore characteristics of the samples. Similarly, the band at 1960 $cm^{-1}$ ($\nu_5 + \nu_{17}$ vibrations) for liquid benzene shows the absorbance at 1953, 1956 and 1968 $cm^{-1}$ in case of Silicalite-1, Si-Beta and Si-MCM-41 samples, respectively. This may be due to lower pore opening of Silicalite-1 compared to large pore zeolite Beta where elliptical opening of 7.6 × 6.4 Å is only site available for adsorption. Si-MCM-41 is hexagonal mesoporous material with pore opening of 20-100 Å and due to this the transport of small hydrocarbons such as benzene is an easy affair inside the network of MCM-41.

Adsorption of deuterated benzene ($C_6D_6$) in out-of-plane bending vibrations over Silicalite-1, Si-Beta and Si-MCM-41 shows similar behavior as that of benzene. Fig. 4.23 gives an account of comparative out-of-plane region bands on adsorption of $C_6D_6$ over the samples Silicalite-1, Si-Beta and Si-MCM-41, respectively. Curve (d) refers to the IR spectrum of $C_6D_6$ in liquid form. As discussed in case of benzene adsorption above out-of-plane band at 1453 $cm^{-1}$ in liquid sample due to combination $\nu_{10} + \nu_{17}$ out-of-plane stretching vibrations of $C_6D_6$ show different shift in the frequency maxima for different samples. In Silicalite-1, 1453 $cm^{-1}$ the band appears at 1447 $cm^{-1}$ where as in case of Si-Beta the frequency maxima was found to be 1450 $cm^{-1}$. In all siliceous mesoporous material used in the present study, Si-MCM-41, the same band was observed at 1460 $cm^{-}$

[1]. These observations are in line with the adsorption of benzene molecule on these materials as discussed earlier.

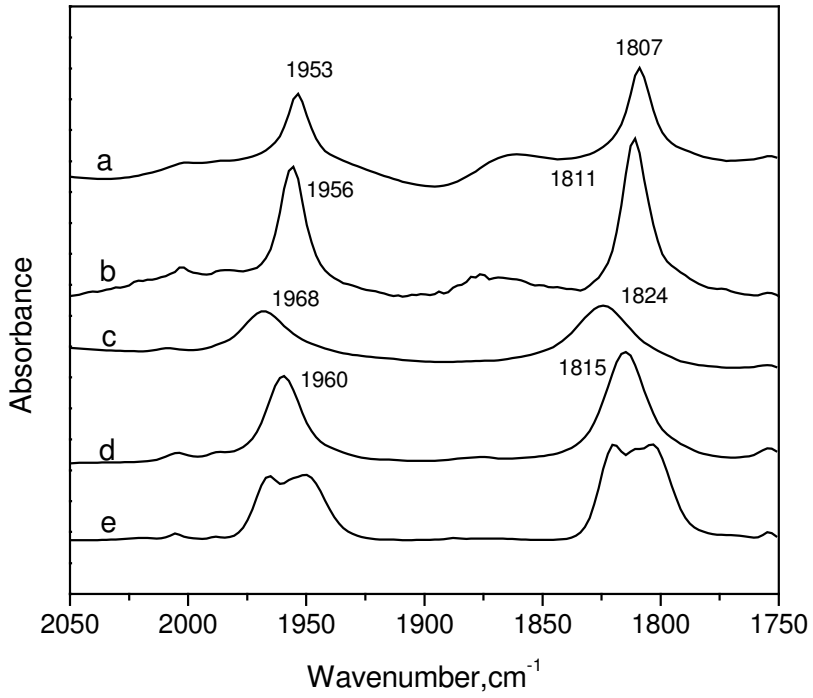


**Figure 4.22.** Comparative plot of C-H out-of-plane region IR bands for adsorption of 0.3 mmol $g^{-1}$ benzene on Silicalite-1 (curve a), Si-Beta (curve b) and Si-MCM-41 (curve c). Curves (d) and (e) present IR spectrum of liquid and vapor phase benzene.

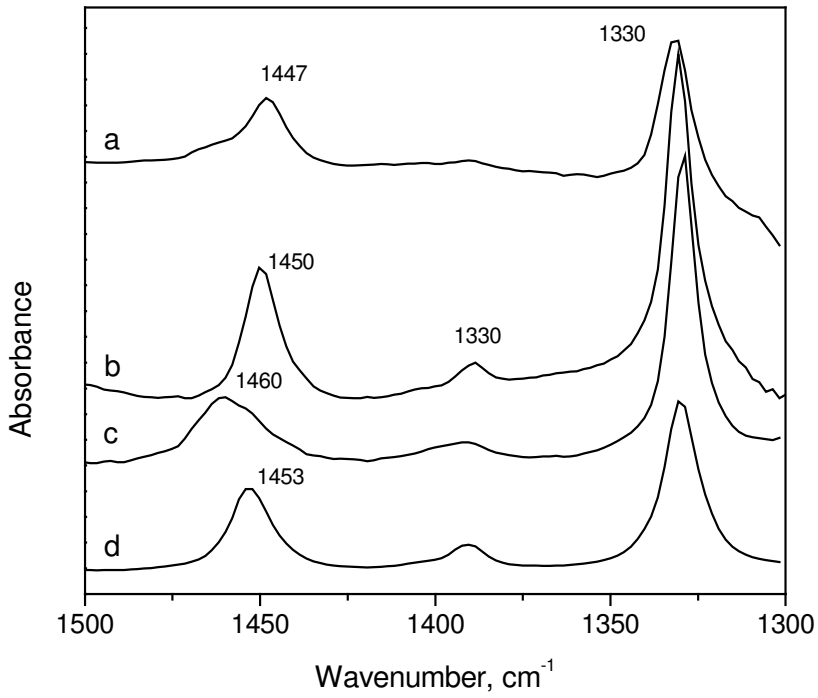


**Figure 4.23.** Comparison of C-H out-of-plane bending vibrations for adsorption of 0.3 mmol $g^{-1}$ $C_6D_6$ on different siliceous samples; Silicalite-1 (curve a), Si-Beta (curve b) and Si-MCM-41 (curve c). Curve (d) presents IR spectrum of liquid $C_6D_6$.

### 4.5.2. Discussion

The IR spectroscopy results presented above clearly reveal that in-plane C-H/C-C, out-of-plane C-H, and fundamental $\nu_{19}$ C-C stretch vibrations undergo remarkable changes (e.g. frequency shift, band splitting and change in the line-width) when benzene molecules are entrapped in the narrow cavities of zeolitic materials. Furthermore, the extent of these changes depends upon the chemical and structural characteristics of the host matrix. Accordingly, the vibrational bands of $C_6H_6$ and $C_6D_6$

molecules adsorbed in microporous zeolites ZSM-5, Beta and mesoporous MCM-41 (Figs. 4.15-4.19) are found to exhibit similarities in some respect while dissimilarities in other.

Following are the main observations

(i) The main similarity in these bands is complete absence of PQR branches in the $\nu_{19}$ vibrational bands (Figs. 4.17 and 4.18) irrespective of the host material indicating that benzene exist in a condensed phase in zeolite cavities, the density of which was grater than that of liquid benzene.

(ii) The relative intensity of various in-plane and out-of-plane vibrations does not match with the intensity ratios observed normally for liquid or vapor phase of benzene. For instance, 3037/1479 $cm^{-1}$ bands ratio in Table 4.2. As discussed in several publications by Gupta and co-workers,[24-28] the increase in the intensity of the fundamental vibration ($\nu_{19}$) at 1479 $cm^{-1}$ and other in-plane vibrations is a feature associated with the transformation of benzene to more condensed state.

(iii) The full width at half maximum (FWHM) of different vibrational bands is found to show a strong relationship with the pore structure of the host zeolite. For instance, the value of FWHM for 1479 $cm^{-1}$ is observed to be 6.5, 7.6 and 9.7 $cm^{-1}$ for adsorption of benzene in Al-ZSM-5, Al-Beta and Al-MCM-41. This follows a systematic variation as per the pore size of these materials. These observations are in agreement with the earlier findings that the density of the adsorbate in zeolitic pores may depend upon the pore size; smaller the pore higher is the density. It is also important to note that the half width value in case of Silicalite-1, Si-Beta and Si-MCM-41 was found to be higher. This can be

attributed to the weaker intermolecular bonding due to absence of $Al^{3+}$ sites and therefore lesser clustering.

(iv) Another striking difference is seen in the splitting pattern of out-of-plane vibrations of benzene in Figs. 4.15 and 4.18. Thus, each of the C-H out-of-plane vibrational bands of benzene adsorbed in Al-ZSM-5 undergo splitting into four bands 2006, 1986, 1971 and 1956 $cm^{-1}$ in place of liquid benzene band at 1960 $cm^{-1}$ and another set of bands at 1873, 1852, 1830 and 1810 $cm^{-1}$ in place of a single band appearing at 1815 $cm^{-1}$ (Fig. 4.15, curve a). In case of zeolite Beta, we observe a pair of two bands with frequencies at 1971, 1956 $cm^{-1}$ instead of 1960 $cm^{-1}$ and 1830 and 1812 $cm^{-1}$ in place of liquid benzene band 1815 $cm^{-1}$ (Fig. 4.15, curve b). On the contrary, no splitting is observed in these bands for adsorption of benzene in MCM-41 (Fig. 4.15, curve c), besides a broadening and shift to higher frequencies by ~12 to 15 $cm^{-1}$. The splitting of the out-of-plane C-H bending bands of benzene on entrapment in the microporous aluminosilicates has been discussed by Sahasrabudhe *et al.* in detail[25,26] and this phenomenon has been attributed to the formation of benzene clusters in the confinement of zeolitic cavities. It has been demonstrated that the clustering of benzene molecules may produce changes in IR spectra similar to those observed on compression or during liquid to solid phase transformations. Furthermore, the clustering of benzene molecules in zeolitic pores is envisaged to occur if they are placed one by the side of another and with their planes parallel to the wall of the zeolite channels. In this mode of the packing, benzene molecules will experience immense $\pi$-$\pi$ band interaction resulting on splitting of out-of-

plane C-H vibrations. Such a stacking of benzene molecules will also lead to compression of C-H bands, to an increase in the effective force constants and hence to an upward shift in frequency of split out-of-plane C-H vibrational bands,[24] as is actually seen in Fig. 4.15. Furthermore, the compression of the benzene molecules would also depend upon the pore characteristics, smaller the pore size higher will be the compression thus resulting in the band splitting. This is in agreement with the observations in Fig. 4.15 and 4.18. Thus, in case of MCM-41 with pore size 2.8 nm, the extent of this intermolecular interaction is likely to small and this is clearly reflected in no splitting of benzene bands in curve (c) of Fig. 4.15, besides a positive frequency shift. Zeolite Beta consists of large pore 12-membered ring with cross sectional pore diameter 7.3 × 7.1 Å along a and b (straight channels) and 5.5 × 5.5 Å along *c* direction. A considerable clustering of benzene and resultant band splitting may therefore occur for the molecules trapped in the micropores of channels in c-direction. On the other hand, 10-membered Al-ZSM-5 zeolite consists of a elliptical straight channels (5.1 × 5.6 Å) and near circular interconnectivity zigzag channels (5.4 × 5.6 Å) with an intersection dimension of ~8 Å. It can be envisaged that the cluster of benzene molecules may form in both the straight and interconnecting channels of ZSM-5, thus giving rise to independent pair of bands, as seen in curve (a) of Fig. 4.18. The results of our study are thus in complete harmony with the findings reported earlier.[24-28]

(v) A comparison of the benzene out-of-plane vibrational bands shown in Fig. 4.15 and 4.22 demonstrate that these process of benzene clustering is promoted

significantly by the framework $Al^{3+}$ cations of the porous silicates as suggested earlier,[51] the electrostatic charge associated with $Al^{3+}$ may facilitate the intermolecular binding and hence and the clustering of the benzene molecules.

(vi) IR results in Figs. 4.20 and 4.21 suggest that the benzene clusters may influence the hydroxy bands in zeolite cavities, depending upon the pore characteristics. The displacement of -OH groups by occluded zeolite clusters and resultant D-isotopic exchange with $C_6D_6$ molecules have been described earlier (Section 4.4.1.4). Present results reveal that such isotopic exchange may occur only with highly condensed cluster in microporous such as, in ZSM-5 (Fig. 4.20) and not in mesoporous materials (Fig. 4.21).

### 4.5.3. Conclusions

A comparative study on the in-plane and C-H/C-C, out-of-plane C-H and the fundamental $\nu_{19}$ C-C stretch vibrations of benzene molecules adsorbed in zeolites ZSM-5, Beta and mesoporous material MCM-41 reveals that the benzene molecules adsorbed in these porous silicates exist in a highly clustered state and the density of this compressed state depends upon the structure and the size of zeolite pores. The Extent of benzene clustering is found to follow an order ZSM-5 > Beta > MCM-41. The electrostatic charge as associated with $Al^{3+}$cations in aluminosilicates is found to play an important role in enhancing this benzene-benzene intermolecular interaction, giving rise eventually to this clustered state of benzene. The loading dependent increase in the intensity of different vibrational bands mentioned above indicates that as compared to ZSM-5, a smaller fraction of benzene gets trapped inside the MCM-41. This can be

attributed to the greater transnational mobility of the benzene molecular clusters in the two dimensional array of non-connecting cylindrical mesoporous of MCM-41 compared to benzene occluded in the microporous interconnected channels of ZSM-5 or zeolite Beta.

## 4.7. REFERENCES


1. *Introduction to zeolite science and practice*; Bekkum, H. V.; Flanigen, E. M.; Jacobs, P. A. Eds.; Elsevier: Amsterdam, 2001.
2. Corma, A.; Garcia, H. *Chem. Rev.* **2003**, *103*, 4307.
3. Clerici, M. G. *Top. Catal.* **2000**, *13*, 373.
4. Lechert, H., Wittern, K. P. *Ber. Bunsenges. Phys. Chem*. **1978**, *82*, 1054.
5. Jobic, H.; Renouprez, A. J.; Fitch, A. N.; Lauter, H. J. *J. Chem. Soc. Faraday Trans*. **1987**, *83*, 3199.
6. Barthomeuf, D.; De Mallmann, A. *Stud. Surf. Sci. Catal*. **1988**, *37*, 365.
7. Uytterhoeven, L.; Morteir, W. J. *J. Chem. Soc. Faraday Trans*. **1992**, *88*, 2753.
8. Silbernagel, B. G.; Garcia, A. R.; Newsam, J. M. *Colloid. Surf. Sci.* **1993**, *A 72*, 71.
9. Liu, S. B.; Ma, L. J.; Lin, M. W.; Wu, J. F.; Chen, T. L. *J. Phys. Chem*. **1992**, *96*, 8120.
10. Fitch, A. N.; Jobic, H.; Renouprez, A. *J. Chem. Soc. Chem. Commun*.**1985**, 284.
11. Barthomeuf, D. *Catal. Rev. Sci. Eng*. **1996**, *38*, 521.
12. Shen, J. -P.; Ma, J.; Sun, T.; Jiang, D. -Z.; Min, E. -Z. *J. Chem. Soc. Faraday Trans.* **1994**, *90*, 1351.
13. Coughlan, B.; Carroll, W.; Malley, P. O.; Nunam, J. *J. Chem. Soc. Faraday Trans. I* **1981**, *77*, 3037.
14. Ward, J. W. *J. Catal*. **1968**, *10*, 34.
15. Su, B. L.; Manoli, J. M.; Potvin, C.; Barthomeuf, D. *J. Chem. Soc. Faraday Trans.* **1993**, *89*, 857.
16. Primet, M.; Garbowski, E.; Mathieu, M. V.; Imelik, B. *J. Chem. Soc. Faraday Trans*. *I* **1980**, *76*, 1942.
17. Angell, C. L.; Howell, M. V. *J. Colloid Interface Sci*. **1968**, *28*, 279.
18. Dzwigaj, S.; De Mallman, A.; Barthomeuf, D. *J. Chem. Soc. Faraday Trans.* **1990**, *86*, 431.
19. Su, B. L.; Manoli, J. M.; Potvin, C.; Barthomeuf, D. *J. Chem. Soc. Faraday Trans*. **1993**, *89*, 857.

20. Huang, Y.; Havenga, E. A. *J. Phys. Chem. B* **2000**, *104*, 5084.
21. Goyal, R.; Fitch, A. N.; Jobic, H. *J. Phys. Chem. B* **2000**, *104*, 2878.
22. Choudhary, V. R.; Srinivasan, K. R. *J. Catal.* **1986**, *102*, 316.
23. Portsmouth, R. L.; Duer, M. J.; Gladden, L. F. *J. Chem. Soc Faraday Trans.* **1995**, *91*, 559.
24. Tripathi, A. K.; Sahasrabudhe, A.; Mitra, S.; Mukhopadhyay, R.; Gupta, N. M.; Kartha, V. B. *Phys. Chem. Chem. Phys.* **2001**, *3*, 4449.
25. Sahasrabudhe, A.; Kamble, V. S.; Tripathi, A. K.; Gupta, N. M. *J. Phys. Chem. B* **2001**, *105*, 4374.
26. Sahasrabudhe, A.; Mitra, S.; Tripathi, A. K.; Mukhopadhyay, R.; Gupta, N. M. *J. Phys. Chem. B* **2002**, *106*, 10923.
27. Sahasrabudhe, A.; Mitra, S.; Tripathi, A. K.; Mukhopadhyay, R.; Gupta, N. M. *Phys. Chem. Chem. Phys.* **2003**, *5*, 3066.
28. Gupta, N. M.; Kumar, D.; Kamble, V. S.; Mitra, S.; Mukhopadhyay, R.; Kartha, V. B. *J. Phys. Chem. B* **2006**, *110*, 4815.
29. Newsam, J. M.; Treacy, M. M. J.; Koetsier, W. T.; De Gruyter, C. B. *Proc. R. Soc. Lond.* **1988**, *A420*, 375.
30. Alberti, A.; Cruciani, G.; Galli, E.; Merlino, S.; Millini, R.; Quartieri, S.; Vezzalini, G.; Zanardi, S. *J. Phys. Chem. B* **2002**, *106*, 10227.
31. Higgins, J. B.; LaPierre, R. B.; Schlenker, J. L.; Rohrman, A. C.; Wood, J. D.; Kerr, G. T.; Rohrbaugh, W. J. *Zeolites* **1988**, *8*, 446.
32. Treacy, M. M. J.; Newsam, J. M. *Nature* **1988**, *332*, 249.
33. Corma, A.; Navarro, M. T.; Rey, F.; Rius, J.; Valencia, S. *Angew. Chem. Int. Ed. Engl.* **2001**, *40*, 2277.
34. Gupta, N. M.; Kamble, V. S.; Iyer, R. M.; Thampi, K. R.; Gratzel, M. *J. Catal.* **1992**, *137*, 473.
35. Kamble, V. S.; Gupta, N. M.; Kartha, V. B.; Iyer, R. M. *J. Chem. Soc. Faraday Trans. I* **1993**, *89*, 1143.
36. Mair, R. D.; Horning, D. F. *J. Chem. Phys.* **1949**, *17*, 1236.
37. Millar, F. A. *J. Chem. Phys.* **1956**, *24*, 996.
38. Abramov, V. N.; Kiselev, A. V.; Lygin, V. I. *Russ. J. Phys. Chem.* **1963**, *37*,

613.

39. Coughlan, B.; Keane, M. A. *J. Chem. Soc. Faraday Trans.* **1990**, *86,* 3961.
40. Dzwigaj, S.; De Mallmann, A.; Barthomeuf, D. *J. Chem. Soc. Faraday Trans.* **1990**, *86*, 431.
41. Hollenberg, J. L.; Dows, J. A. *J. Chem. Phys.* **1962**, *37*, 1300.
42. Nair, R. D.; Hornig, D. F. *J. Chem. Phys.* **1949**, *17,* 1236.
43. Wendelbo, R.; Malhebe, R. R. *Microporous Mater.* **1997**, *10*, 231.
44. Guisnet, M.; Ayrault, P.; Coutanceau, C.; Alvarez, M. F.; Datka, J. *J. Chem. Soc. Faraday Trans.* **1997**, *93*, 1661.
45. Bortnovsky, O.; Sobalik, Z.; Wichterlova, B.; Bastl, Z. *J. Catal.* **2002,** *210,* 171.
46. Lohse, U.; Altrichter, B.; Donath, R.; Fricke, R.; Jancke, K.; Parlitz, B.; Schreier, E. *J. Chem. Soc. Faraday Trans.* **1996**, *92*, 159.
47. Fernandez, A. -B.; Marinas, A.; Blasco, T.; Fornes, V.; Corma, A. *J. Catal.* **2006**, *243*, 270.
48. Sobalik, Z.; Belhekar, A. A.; Tvaruzkova, Z.; Wichterlova, B. *Appl. Catal. A Gen.* **1999**, *188*, 175.
49. *Atlas of zeolite structure types*, *4th revised edition*; Meir, W. M.; Oslon, D. H.; Baerlocher, C. Eds. Elsevier: 1996.
50. Corma, A. *Chem. Rev.* **1997**, *97*, 2373.
51. Kadgaonkar, M. D.; Kasture, M. W.; Kumar, R.; Kartha, V. B.; Gupta, N. M. *J. Phys. Chem. C* **2007**, *111*, 9927.

## 5.1. INTRODUCTION

Generally, metals other than silicon are substituted in the silica framework of microporous and mesoporous materials in order to impart the catalytic properties of different silicate catalysts. For instance, it has been possible to generate significant catalytic activity in different zeolites by incorporating divalent (Co, Zn), trivalent (Al, B, Fe, Cr), or tetravalent (Ti, V, Sn, Zr, Mn) metal ions in the structural network.[1,2] Among these, substitution of trivalent (Al, Ga, Fe etc.) and tetravalent metal (Ti, V, Ce etc.) ion in the zeolitic structure is routinely practiced to induce acidic and/or redox properties in the zeolites.[3,4] In the present study, an attempt has been made to incorporate Al and Ti in polymorph B enriched structure, NCL-7 denoted as Al-NCL-7 and Ti-NCL-7. The detailed synthesis procedure and characterization of these samples are described in chapter 2 and 3, respectively. In the present chapter, catalytic activity of these newly synthesized polymorph B-enriched metallo-silicates of NCL-7 (polymorph B : polymorph A = 65 : 35) is compared with normal zeolite Beta (polymorph B : polymorph A = 55 : 45).

Section 5.2 of present chapter deals with the acid catalyzed isopropylation of benzene over Al-NCL-7. In section 5.3 the epoxidation of norbornene has been used as a test reaction to study catalytic activity of Ti-NCL-7.

## 5.2. ISOPROPYLATION OF BENZENE

Isopropyl benzene or cumene is an important industrial intermediate for the production of phenol. The use of Friedel-Crafts catalysts[5] or solid phosphoric acid catalysts to obtain cumene, suffer substantially from the drawbacks of corrosion and

environmental hazards.[6] To minimize these drawbacks, a variety of solid catalysts, especially zeolites, have been studied for this reaction.[7-10] Zeolite Beta has been proven to be a potential catalyst on account of its high activity, selectivity, and stability, under both liquid and vapor phase conditions.[11-14] The parameters such as Si/Al ratio, isomorphous substitution, alkylating agent, temperature, space velocity, and reactant mole ratios are reported for alterations in the product selectivity.[15-16]

### 5.2.1. Experimental

The vapor phase catalytic isopropylation of benzene (S. d. fine, India, + 99 %) with 2-propanol (S. d. fine, India, + 99 %) was carried out at moderate temperature (483 K) and atmospheric pressure using a fixed bed vertical down-flow glass reactor of 15 mm internal diameter. The temperature was maintained at ± 2 K. The catalyst powder was pressed at 1.55 x $10^2$ kPa of pressure, palletized, crushed and sieved to obtain 60-80 mesh (ASTM, USA) size particles. The catalyst (2.0 g) was loaded at the center of the reactor in such a way that catalyst bed was sandwiched between inert porcelain beads. It was equipped with a thermocouple in a thermo well for sensing the reaction temperature. The catalyst was activated at 673 K for 8 h in a flow of dry air, flushed with nitrogen and cooled to reaction temperature before conducting the reactions. The reactants (Benzene:IPA = 6.5:1 mole/mole) were injected using a syringe pump (Sage instruments, Model 352, USA) into the reactor. The reproducibility of feeding by a syringe was checked more than 3 times and it was observed to be same. At the same time mass balance for various experiments was found to be within the range of 96 ± 2 %.

Nitrogen was used as a carrier gas with a flow of 35 mL/min. The products were chilled (ice cold), collected and analyzed by gas chromatograph (Agilent 6890 series, GC system) using flame ionization detector and HP high-resolution (20 % permethylated β-cyclodextrin) capillary column (30 m × 0.320 mm × 0.25 μm). The products were identified using gas chromatography-mass spectrometry (Shimadzu, GCMS-QP 2000A). The reaction conditions were maintained as reported in the literature.[17]

### 5.2.2. Results and Discussion

The isopropylation of benzene was carried out as a test reaction to compare the catalytic activity and selectivity of Al-NCL-7 and Al-Beta samples under identical reaction conditions in order to investigate the effect of enrichment of polymorph B to 65 % in Al-NCL-7 (compared to Al-Beta containing the 55 % of polymorph B).

Figure 5.1 depicts the comparative study on isopropylation of benzene under identical condition over Al-Beta (Si/Al = 100) and Al-NCL-7 sample (Si/Al = 100) synthesized in fluoride medium. Figure 5.1 A and C presents the conversion of benzene as a function of reaction time over these catalysts. Al-Beta sample shows comparatively higher conversion (38 mole %) than Al-NCL-7 (32 mole %). It can be attributed to the increase of pore constraint along with concentration of polymorph B in c-direction of BEA type topology as postulated earlier.[18] As discussed in detailed in chapter 3, the polymorphic concentration of polymorph B is higher in Al-NCL-7 (polymorph B : polymorph A = 65 : 35) as compared to normal Al-Beta (polymorph B : polymorph A = 55 : 45). The similar constraint was observed in adsorption of benzene and deuterated benzene over all siliceous analogs of NCL-7 compared to Beta (Chapter 4). It is well

known that the catalytic properties of the zeolites and metallosilicates originate from their capacity to adsorb different molecules and their acidity (both density and strength). Lower adsorption capacity arising due to constraint in pore characteristics of polymorph B enriched structure, NCL-7, seems to be responsible factor for lower catalytic activity. Furthermore, curves a and b in Fig. 5 B and D shows the almost equal selectivity for cumene and diisopropylbenzene in case of Al-Beta and Al-NCL-7, respectively. The analogous selectivity of the products is in line with the presumption that the inherent faulting of the zeolite Beta structure does not affect the accessible pore volume significantly, it increases the tortuous nature of the pore system considerably.

Table 5.1 depicts the performance of different polymorph B enriched Al-NCL-7 as a function of aluminum content at 483 K for time on stream of 4 h. When the Al-content in Al-NCL-7 lowered from Si/Al ratio 100 to 150, conversion of benzene decreases from 32 mole % to 18 mole % (Table 5.1, Entry 2-4).

The isopropylation of benzene was also carried over standard Al-Beta sample (Si/Al = 15) synthesized in hydroxide medium for comparison purpose. As seen from the entry 5 in the Table 5.1, selectivity of cumene decreased to 89 % and comparatively high amount of other products such as diisopropyl benzene (8 %), toluene and $C_8$ aromatics (3 %) were formed. The alkylation of benzene with isopropanol is known to proceed through the dehydration of an alcohol to alkene formation and the alkene reacts via a carbonium ion mechanism with gas-phase benzene or cumene to produce cumene and/or diisopropylbenzene (DIPB), respectively.[14] In addition to the isopropylation, other undesired reactions such as isomerization, cracking, and disproportionation of alkyl aromatics also occur, resulting in the formation of compounds such as toluene and $C_8$

aromatics.[15,16] Due to presence of such products formed by secondary reaction in the locus of the reaction pathway, the yield of cumene drops considerably,

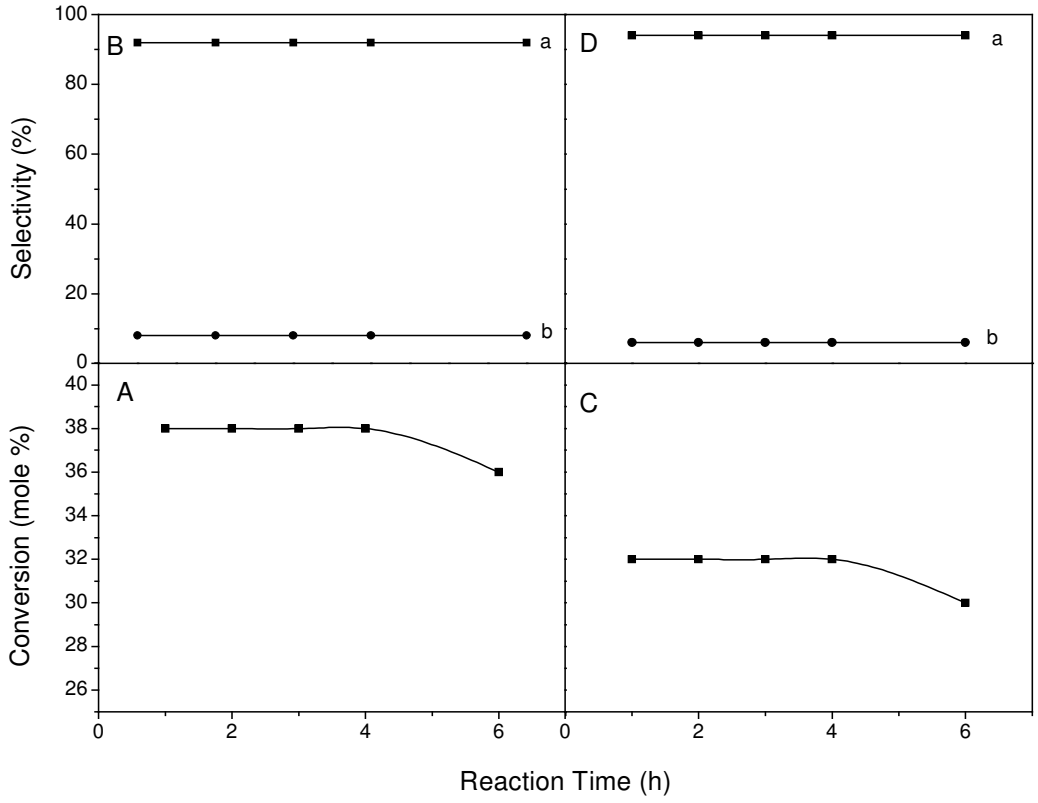


**Figure 5.1.** Comparative study of isopropylation of benzene in terms of conversion and selectivity for Al-Beta (A and B) and Al-NCL-7 (C and D). Curves a and b in B and D represents selectivity for cumene and diisopropylbenzene, respectively.

**Table 5.1**

Comparison of Different Catalysts for Isopropylation of Benzene

| Entry No. | Sample | Si/Al[a] | Benzene Conv. (mole %) | TOF[b] ($h^{-1}$) | Selectivity (%) | | |
|---|---|---|---|---|---|---|---|
| | | | | | cumene | $D_{iso}$[c] | Others[d] |
| 1 | Al-Beta | 100 (116) | 38 | 43 | 92 | 08 | _ |
| 2 | Al-NCL-7 | 100 (113) | 32 | 36 | 94 | 06 | _ |
| 3 | Al-NCL-7 | 125 (137) | 24 | 32 | 94 | 06 | _ |
| 4 | Al-NCL-7 | 150 (156) | 18 | 28 | 94 | 06 | _ |
| 5 | [e]Al-Beta | 15 (16) | 74 | 12 | 89 | 08 | 03 |

Reaction conditions: Temperature = 483 K, Substrate (benzene):alkylating agent (2-propanol) = 6.5:1 mole/mole, LHSV = 2.5 mL/h, Time on stream = 4 h.

[a] Values in the parenthesis indicates Si/Al ratio in the solid sample calculated using AAS

[b]TOF = (Numbers of moles of product formed/number of moles of Al atoms)/Time required in h

[c] Diisopropyl benzene

[d] toluene and $C_8$ aromatics

[e] synthesized in hydroxide medium

## 5.3. EPOXIDATION OF NORBORNENE

Ti-containing silicates of different topology have been used in a wide range of oxidation reactions involving $H_2O_2$ as an oxidant.[19] There are copious amount of reports available on the epoxidation of alkenes over Ti-Beta using $H_2O_2$ as an oxidant.[20-22] However, very few reports are available on the epoxidation of bulkier molecules, particularly, norbornene, using heterogeneous catalysts.[23,24] Epoxidation of norbornene in homogenous system suffers from drawbacks of separation and selectivity.[25-26] Norbornene and its derivatives such as epoxy norbornene, diol etc. have wide applications in polymer synthesis, pharmaceutical intermediates and routine organic synthesis. As reported earlier, epoxidation of norbornene over Ti-containing silicate is a sensitive reaction towards the pore characteristics of the catalysts used.[22]

Taking in account above observations, epoxidation of norbornene has been employed as a test reaction to investigate the effect of subtle changes in the pore characteristics of Ti-NCL-7 and Ti-Beta due to change in the polymorphic proportion of polymorphs B and A in BEA type topology in the present chapter. The catalytic runs were also performed on TS-1 and Ti-MCM-41 for comparative purpose.

### 5.3.1. Experimental

The liquid-phase oxidation of norbornene was carried out in a two-necked 50 mL round bottom flask immersed in a thermostated oil bath maintained at 343 K temperature. In a typical procedure, 20 mmol of substrate, norbornene, was added to the 10 mmol of oxidant, $H_2O_2$ (30 wt % aqueous solution), in presence of 100 mg of catalyst and 24 g of

acetonitrile. The reaction products were analyzed using Agilent 6890 series GC system (HP chiral, 20 % permethylated β-cyclodextrin, 30m × 0.32mm × 0.25 μm film thickness), GCIR (Perkin Elmer, GC-IR 2000) and GCMS (Shimadzu, GCMS-QP 2000A).

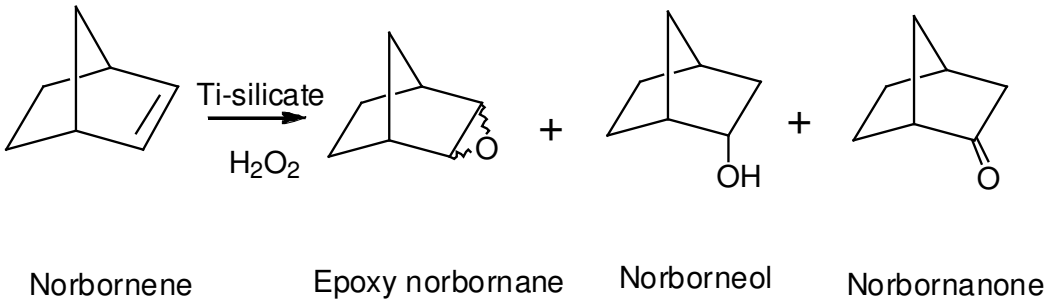


**Scheme 5.1.** Schematic representation of epoxidation of norbornene over Ti-silicates

### 5.3.2. Results and Discussion

Figure 5.2 A and C presents the conversion of norbornene over Ti-Beta and Ti-NCL-7 samples, respectively using $H_2O_2$ as oxidant at 343 K. As seen from the figure, the catalytic activity Ti-Beta and Ti-NCL-7 is comparable under identical conditions. The conversion of norbornene increases with time up to 4 h and remains constant thereafter. Furthermore, the selectivity of epoxynorbornane, norborneol and norbornanone remains same. The analogous selectivity of the products is in line with the presumption that the inherent faulting of the zeolite Beta structure does not affect the accessible pore volume significantly, it increases the tortuous nature of the pore system considerably as discussed in detail above.

Table 5.2 depicts the effect of Ti-content on the epoxidation of norbornene (Table 5.2, entries 2-4). As expected, decrease in the catalytic activity was observed when the Ti-content in the sample decreases from Si/Ti = 100 to Si/Ti = 150 in Ti-NCL-7. To investigate the effect of different pore characteristic, Ti-MCM-41 and TS-1 were used as reference samples.

When the catalytic activity of epoxidation of norbornene was compared over Ti-MCM-41 (Si/Ti = 25), the obtained conversion was 15 %. At the same time, the selectivity of epoxynorbornane decreases to 70 % at the cost of norborneol and norbornone. The low selectivity for epoxynorbornane can be attributed to the large pore size of Ti-MCM-41 (~3 nm). Although, Ti-MCM-41 is an active catalyst for the epoxidation reaction, the lower catalytic activity and selectivity can be accredited to the relatively high hydrophilic interior of M41S material[27] or inaccessibility of Ti-sites due to its incorporation inside the silica walls as reported earlier.[28]

Furthermore, TS-1 was found to be inactive for epoxidation reaction (Table 5.2, Entry 6). It can be ascribed to the smaller pore size of TS-1 i.e. norbornene is too large to enter the channels of Ti-silicates of MFI topology, TS-1 as described earlier.[22] The Ti/NCL-7 catalyst prepared by impregnation route was also found to be inactive (Table 5.2, Entry 7). It underlines the crucial role of framework titanium in the reaction.

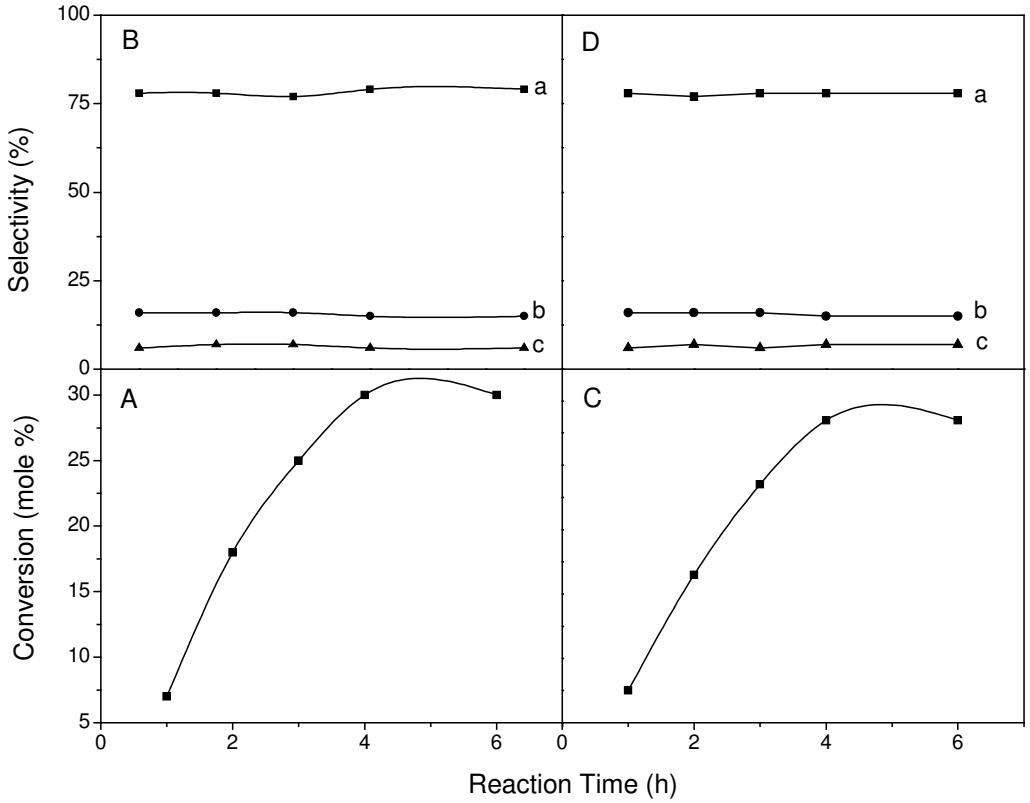


**Figure 5.2.** Comparative study of epoxidation of norbornene in terms of conversion and selectivity for Ti-Beta (A and C) and Ti-NCL-7 (C and D). Curves a, b and c in B and D represents selectivity for epoxynorbornane, norborneol and norbornanone, respectively.

**Table 5.2**

Epoxidation of Norbornene over Different Titanium Silicates

| Entry No. | Sample | Si/Ti[a] | Norbornene Conv. (mole %) | TOF[b] | Selectivity (%) | | |
|---|---|---|---|---|---|---|---|
| | | | | | Epoxynor-bornane | Norbo-rneol | Norborna-none |
| 1 | Ti-Beta | 100 (118) | 30 | 107 | 79 | 15 | 06 |
| 2 | Ti-NCL-7 | 100 (122) | 26 | 96 | 78 | 15 | 07 |
| 3 | Ti-NCL-7 | 125 (138) | 18 | 75 | 80 | 15 | 05 |
| 4 | Ti-NCL-7 | 150 (168) | 12 | 72 | 80 | 15 | 05 |
| 5 | Ti-MCM-41 | 25 (29) | 15 | 13 | 70 | 20 | 10 |
| 6 | TS-1 | 30 (33) | _ | _ | _ | _ | _ |
| 7 | [c]Ti/NCL-7 | 100 | _ | _ | _ | _ | _ |

Reaction conditions: Substrate: 20 mmol norbornene, Oxidant: 10 mmol of aqueous hydrogen peroxide (30 wt %), Catalyst amount: 100 mg, Solvent: 24 g of acetonitrile and Reaction temperature: 343 K

[a] Values in the parenthesis indicates Si/Ti ratio in the solid sample calculated using AAS

[b] (Numbers of moles of product formed/number of moles of Ti atoms)/Time required in h

[c] Ti impregnated NCL-7 sample (Si/Ti = 100) prepared using post synthesis method (Chapter 2, Section 2.5.1.2)

## 5.4. CONCLUSIONS

Isopropylation of benzene and epoxidation of norbornene, were used as test reaction to compare the catalytic activity of newly synthesized polymorph B enriched analog of zeolite beta, Al-NCL-7 and Ti-NCL-7, respectively. Al-NCL-7 and Ti-NCL-7 showed comparable selectivity in the isopropylation of benzene and epoxidation of norbornene. However, slightly low conversion was obtained due to pore constraint along c-direction with increase in concentration of polymorph B along c-direction in BEA type topology. In the epoxidation of norbornene, Ti-MCM-41 (Si/Ti = 25) showed lower conversion because relatively high hydrophilic interior of M41S material whereas TS-1 was found to be completely inactive.

## 5.5. REFERENCES


1. Corma, A. *Chem. Rev.* **1997**, *97*, 2373.
2. Zhao, X. S.; Lu, G. Q.; Miller, G. *Ind. Eng. Chem. Res.* **1996**, *35*, 2090.
3. Biz, S.; Occelli, M. L. *Cat. Rev. Sci. Eng.* **1998**, *41*, 329.
4. Trong, D.; Desplanier-Giscard, D.; Danumah, C.; Kaliaguine, S. *Appl. Catal. A* **2003**, *253*, 545.
5. Miki, H. *US Pat.* 4,347,393, **1982**.
6. Jones, E. K.; Dettner, D. D.*US Pat.* 2,860,173, **1958**.
7. Kaeding, W. W.; Holland, R. F. *J. Catal.* **1988**, *109*, 212.
8. Mortikov, E. S.; Mirzabekova, S. R.; Pogovelov, A. G.; Konov, N. F.; Zerhanova, R. F.; Dorogochinskii, A. Z.; Minachev, K. M. *Naftekhimiya* **1988**, *16*, 701.
9. Pradhan, A. R.; Rao, B. S.; Shiralkar, V. P. in: *ZEOCAT 90 Conference* **1990**.
10. Bellussi, G.; Pazzuconi, G.; Perego, C.; Girotti, G.; Terzoni, G. *J. Catal.* **1995**, *157*, 227.
11. Yeh, C. Y.; Barner, H. E.; Suci, G. D. in: Garmisch-Partenkirchen (Ed.), *Zeolites and Related Microporous Materials: State of the Art,* Elsevier, Amsterdam, **1994**, *84 A*, 2311.
12. Smirnov, A. V.; Renzo, F. D.; Lebedeva, O. E.; Brunel, D.; Chiche, B.; Tavalro, A.; Ramanovsky, B. V. In Cou, H. et al. (Eds.); *Progress in Zeolite and Microporous Materials*; Elsevier: Amsterdam, **1997**, *105B*, 1325.
13. Halgeri, A. B.; Das, J. *Appl. Catal. A* **1999**, *181*, 347.
14. Sridevi, U.; Satyanarayan, C. V. V.; Rao, B. S.; Pradhan, N. C.; Rao, B. K. B.; Bokade, V. V. *J. Mol. Catal. A Chem.* **2002**, *181*, 257.
15. Reddy, K. S. N.; Rao, B. S.; Shiralkar, V. P. *Appl. Catal. A* **1993**, *95*, 53.
16. Pradhan, A. R.; Kotasthane, A. N.; Rao, B. S. *Appl. Catal.* **1991**, *72*, 311.
17. Kasture, M. W.; Niphadkar, P. S.; Sharanappa, N.; Mirajkar, S. P.; Bokade, V. V.; Joshi, P. N. *J. Catal.* **2004,** *227,* 375.
18. Newsam, J. M.; Treacy, M. M. J.; Koetsier, W. T.; De Gruyter, C. B. *Proc. R. Soc. Lond.* **1988,** *A420,* 375.

19. Bellussi, G.; Rigutto, M. S. *Stud. Surf. Sci. Catal.* **1994**, *85*, 177.

20. (A) Corma, A.; Esteve, P.; Martinez, A. *J. Catal.* **1996**, *161*, 11. (B) Blasco, T.; Camblor, M. A.; Corma, A.; Esteve, P.; Guil, J. M.; Martinez A.; Perdigon-Melon, J. A.; Valencia S. *J. Phys. Chem. B* **1998**, *102*, 75.

21. Laha, S. C.; Kumar, R. *J. Catal.* **2002**, *208*, 339.

22. Van der Wall, J. C.; Rigutto, M. S.; Van Bekkum, H. *Appl. Catal. A* **1998**, *167*, 331.

23. Kala Raj, N. K.; Ramaswamy, A. V.; Manikandan, P. *J. Mol. Catal. A Chem.* **2005**, *227*, 37.

24. Patel, S. A.; Sinha, S.; Mishra; A. N.; Kamath, B. V.; Ram, R. N. *J. Mol. Catal. A Chem.* **2003**, *192*, 53.

25. Budnik, R. A.; Kochi, J. K. *J. Org. Chem.* **1976**, *41*, 1384.

26. Bai, Y.; Chiniwalla, P.; Elce, E.; Shick, R. A.; Sperk J.; Ann, S.; Allen, B.; Kohl, P. A. *J. Appl. Poly. Sci.* **2004**, *91*, 3023.

27. Jentys, A.; Pham, N. H.; Vinek, J. *J. Chem. Soc. Faraday Trans.* **1996**, *92*, 3287.

28. Oldroyd, R.D.; Thomas, J. M.; Maschmeyer, T.; Macfaul, P. A.; Snelgrove, D. W.; Ingold, K. U.; Wayner, D. D. M.; *Angew Chem. Int. Ed.* **1996**, *35*, 2787.

## 6.1. SUMMARY

The present thesis gives an account of synthesis and characterization of novel polymorph B enriched intergrowths of zeolite Beta entitled as NCL-5, NCL-6 and NCL-7 with polymorphic composition of polymorph B : polymorph A as 90 : 10, 75 : 25 and 65 : 35, respectively. It also gives an insight of catalytic comparison of Al-NCL-7 and Ti-NCL-7 with Al-Beta and Ti-Beta. The present thesis is divided into six chapters including the present one as follows.

**Chapter 1** gives general introduction of microporous materials with particular emphasis on zeolites. The different properties of zeolitic materials and the techniques used to characterize these materials are discussed in brief. The different synthesis approaches and parameters affecting the synthesis of zeolite are discussed in detail. Faulting in the structure of zeolite Beta is also outlined. This chapter also describes the sorption, binding and transport properties of guest molecules in the confined geometry of zeolitic pore system, an important aspect for the fundamental understanding of the behavior of these molecules in inter-crystalline spaces governing the molecular shape selectivity in zeolite catalyzed reactions is discussed. Based on these informations, the scope and objective of the present work have been outlined.

**Chapter 2** presents experimental results on synthesis of polymorph B-enriched intergrowth of zeolite Beta, NCL-5, NCL-6 and NCL-7, having the polymorph B and A in the proportions of 90 : 10, 75 : 25 and 65 : 35, respectively. The effect of different synthesis parameters such as water concentration, concentration of structure directing agent (SDA), use of different promoters and its concentration and crystallization

temperature is outlined. The incorporation of hetero metals such as Al- and Ti- in NCL-7 samples with the variation in Al and Ti content has been described. The synthesis procedure for the reference materials used for comparison purpose such as Al-ZSM-5, Silicalite-1, Si-Beta, Al-Beta, Al-MCM-41 and Si-MCM-41 is also discussed.

**Chapter 3** deals with the characterization of novel BEA type intergrowths, NCL-5, NCL-6 and NCL-7, in comparison with Si-Beta. The phase purity of the samples was established using XRD. DIFFaX code used for deriving the composition and enrichment of polymorph B is discussed with intrinsic details. Preference for DIFFaX code over Reitveld is also explained. The results obtained after characterizing NCL-5, NCL-6 and NCL-7 samples with different tools such as $N_2$ adsorption, FTIR and $^{29}$Si MAS NMR spectroscopy are discussed.

This chapter also summarizes techniques used to characterize Al-NCL-7 and Ti-NCL-7. The results obtained from XRD patterns, DIFFaX code, diffuse reflectance UV-visible spectroscopy and $^{27}$Al MAS NMR to ascertain phase purity, polymorphic composition, environment of Ti in Ti-NCL-7 and coordination of Al in Al-NCL-7 have been discussed. The physico-chemical properties of reference materials of M41S and MFI topology used in the present thesis for comparative purpose is described in brief.

**Chapter 4** focuses on the binding state of $C_6H_6$ and $C_6D_6$ molecules in the zeolites of BEA family, differing from each other in Si/Al ratio and consisting of the intergrowth of polymorphs B and A in different proportions. The use of *in situ* FTIR spectroscopy employed to investigate the influence of subtle chemical and structural

changes in BEA family, caused by a change in Si/Al ratio or proportions of polymorphs A and B, on the binding and the transport properties of an adsorbate is discussed. Al-Beta, Si-Beta, NCL-5, NCL-6 and NCL-7 were used as host matrices and benzene, a non-polar molecule of dimensions matching that of the channels and pore openings of zeolite samples under study, has been chosen as a probe molecule for this purpose. In order to further discern the nature of the guest-host interaction, hexadeuterated benzene ($C_6D_6$) was also employed as adsorbate. The results obtained with different topologies such as MFI (Silicalite-1 and Al-ZSM-5), M41S (Si-MCM-41 and Al-MCM-41) are compared.

**Chapter 5** outlines the comparison of Ti- and Al-containing NCL-7 (polymorph B : polymorph A 65 : 35) samples with different Si/M ratio (where M= Ti or Al) with normal Beta in isopropylation of benzene and epoxidation of norbornene, respectively. The catalytic activity is further compared using M/Beta and M/NCL-7 synthesized using post synthesis modification methods.

**Chapter 6** summarizes the results obtained and the basic findings of the present work.

## 6.2. CONCLUSIONS

The new structures of BEA type topology denoted as NCL-5, NCL-6 and NCL-7 with enrichment of polymorph B *ca.* 90, 75 and 65 % vis-à-vis polymorph A are successfully synthesized for the first time. The synthesis parameters such as $TEAOH/SiO_2$, $H_2O/SiO_2$, effect of promoter and temperature are optimized. Synthesis of NCL-7 can be achieved in the temperature range 373-413 K, $TEAOH/SiO_2$ molar ratio

0.68-0.88, $HClO_4/SiO_2$ molar ratio 0.08 to 1.2 and $H_2O/SiO_2$ molar ratio 9.5. NCL-5 phase, with the enrichment of polymorph B *ca.* 95 %, can be synthesized in $TEAOH/SiO_2$ molar ratio 0.68-0.88, $H_2O/SiO_2$ molar ratio 6.0-7.5 using $HClO_4$ as promoter. The key factors, which enabled to get preferentially higher concentration of polymorph B of zeolite Beta family, are the use of perchlorate as promoter oxyanion in fluoride medium and the $H_2O/SiO_2$ molar ratio. Furthermore, Al and Ti are incorporated in the structure of NCL-7 having the enrichment of polymorph B to 65 %.

The polymorphic composition of NCL-5, NCL-6 and NCL-7 is elucidated using Reitveld refinement and DIFFaX code. DIFFaX is preferred over Reitveld refinement due to inherent stacking present in BEA structure. The structure elucidation and polymorphic composition, deduced using DIFFaX code, unambiguously reveals that there is *ca.* 95, 75 and 65 % enrichment of polymorph B in NCL-5, NCL-6 and NCL-7 zeolites, respectively.

Polymorph B enriched structures, NCL-5, NCL-6 and NCL-7, were thoroughly characterized using different essential characterization tools such as $N_2$ adsorption, $^{29}$Si-MAS NMR and Framework FTIR spectroscopy. $^{29}$Si MAS NMR showed absence of $Q^3$ species for the samples. The framework FTIR spectral analysis of NCL-5, NCL-6, NCL-7 and Si-Beta samples supported the postulate that there is more tortuousity of channel structure of zeolite Beta increases with increase in proportion of polymorph B. Comparison of framework IR spectrum of NCL-5 and Si-Beta indicates that relative intensity of 1097 $cm^{-1}$ band increases significantly vis-à-vis 1018 $cm^{-1}$ band, which is almost absent by the relative intensities of 1097 and 1018 $cm^{-1}$ vibrations in NCL-5 sample (polymorph B : polymorph A = 90 : 10) in comparison with Si-Beta (polymorph

B : polymorph A = 55 : 45) in which the band at 1018 $cm^{-1}$ and 1097 $cm^{-1}$ possesses almost equal intensity. This was also corroborated by the similar trend in low frequency bands at 460 and 423 $cm^{-1}$.

The enrichment of polymorph B in Al- and Ti-NCL-7, calculated using DIFFaX technique, is estimated to be *ca.* 65 % vis-à-vis polymorph A. $^{27}$Al MAS NMR study reveals that maximum amount of aluminum in Al-NCL-7 is present in tetrahedral coordination. Similar observations were obtained in case of Ti-NCL-7 samples using diffuse reflectance UV-Vis spectroscopy where all the Ti-NCL-7 samples shows a strong charge to metal transfer band around 220 nm due to tetrahedral coordination of titanium.

The adsorption and binding state of benzene and hexadeuterated benzene was employed as preferential tool in order to investigate the adsorption of benzene in BEA type zeolite as a function of the subtle changes in pore dimensions resulting due to change in polymorphic composition of zeolite Beta (polymorphs A and B) and presence of framework Al. The results reveal that an important role is played by the electrostatic field associated with the framework cations and also the channel structure in deciding the intermolecular bonding and hence the clustering of smaller molecules when confined in the microporous aluminosilicates. The loading-dependent changes observed in the width and the relative intensity of different CH vibrational bands have revealed that while the presence of $Al^{3+}$ cations promoted this clustering process, the increase in the polymorph B content in a sample resulted in the constrained transport and adsorption of benzene molecules in the channels. The benzene clusters trapped in zeolite Beta channels lead to the physical displacement and reorientation of surface hydroxy groups, thus facilitating weak hydrogen bonding between them. Such displacement of the hydroxy groups would

be facilitated by the packing of the benzene molecules side-by-side with their planes parallel to the zeolitic channels, the inter-molecular interaction occurring through the π-cloud. The occluded benzene molecules undergo a process of partial H/D isotopic exchange with the surface hydroxyl groups, and the extent of this exchange increased with the rise in temperature. Comparison study with MFI and M41S samples further reveals the important role played by the channel structure of the host materials.

The catalytic activity of Al-NCL-7 was compared with Al-Beta for isopropylation of benzene as a test reaction. The selectivity of cumene remains almost same in case both the catalyst under identical conditions. However, the activity of Al-NCL-7 is observed to be lower, compared to Al-Beta. The lower activity of Al-NCL-7 can be attributed to the increase in tortuous nature of channel system in BEA structure with increase in polymorph B. The results obtained in this study are in well agreement with the FTIR study where relative intensities of 1097 and 1018 $cm^{-1}$ assigned to the polymorph A and polymorph B, respectively increases with polymorph B. Also, the adsorption capacity of Si-NCL-7 (polymorph B : polymorph A = 65 : 35) was found to be smaller in comparison with Si-Beta (polymorph B : polymorph A = 55 : 45) (Chapter 4). Comparison of catalytic activity between Ti-Beta and Ti-NCL-7 in epoxidation of norbornene also shows similar trend.

# Appendix A

**Table A.1**

**Specification of the chemicals used for various syntheses**

| No. | Chemicals/reagents (Source) | Chemical formula or composition | Purity (%) |
|---|---|---|---|
| 1. | Fumed silica (Sigma, USA) | $SiO_2$ | 99 |
| 2. | Tetraethyl orthosilicate, TEOS (Aldrich, USA) | Si $(OC_2H_5)_4$ | 98 |
| 3. | Hydrofluoric acid (Loba Chemie, India) | HF 40 % aqueous solution | 98 |
| 4. | Tetraethylammonium hydroxide (Aldrich, USA) | $(C_2H_5)_4$ N (OH), 35 % aqueous solution | 99 |
| 5. | Perchloric acid (Loba Chemie, India) | $HClO_4$, 70 % aqueous solution | 99 |
| 6. | Aluminum isopropoxide (Aldrich, USA) | Al $[OCH (CH_3)_2]_3$ | 99.9 |
| 7. | Isopropanol, IPA (Merck, Germany) | $(CH_3)_2CHOH$ | 99 |
| 8. | Titanium (IV) isopropoxide | Ti $[OCH (CH_3)_2]_4$ | 99.9 |
| 9. | Sodium aluminate (Loba Chemie, India) | $NaAlO_2$, 43.65% $Al_2O_3$, 39.0% $Na_2O$ and 17.35% $H_2O$ | 98 |
| 10. | Sodium silicate (UCIL, India) | $Na_2SiO_3$, 28.48 % $SiO_2$, 9.03 % $Na_2O$ and 62.5% $H_2O$ | 98 |
| 11. | Silica sol (V. P. Chemicals, India) | 40 % aqueous solution of $SiO_2$ | 98 |
| 12. | Sodium hydroxide (Loba Chemie, India) | NaOH | 99 |
| 13. | Ammonium nitrate (Loba Chemie, India) | $NH_4NO_3$ | 99.5 |
| 14. | Tetrapropylammonium hydroxide, TPAOH (V. P. Chemicals, India) | $(CH_3CH_2CH_2)_4N$ (OH), 20 % aqueous solution | 99 |
| 15. | Aluminum sulfate | $Al_2(SO_4)_3.18H_2O$ | 98 |

| | | |
|---|---|---|
| 16. Triethylbutylammonium bromide, TEBABr (V. P. Chemicals, India) | $[(C_2H_5)_3\ N(C_4H_9)]\ Br$ | 99 |
| 17. Sulphuric acid (Loba Chemie, India) | $H_2SO_4$ | 98 |
| 18. Tetramethylammonium hydroxide, TMAOH (Loba Chemie, India) | $(CH_3)_4NOH$, 25 wt % aqueous solution | 98 |
| 19. Cetyltrimethylammonium bromide, CTABr (Loba Chemie, India) | $CH_3(CH_2)_{15}N(CH_3)_3Br$ | 99 |
| 20. Phosphoric acid (s. d. Fine Chem., India) | $H_3PO_4$, 85 wt % aqueous solution | 98 |
| 21. Ammonium acetate (s. d. Fine Chem., India) | $NH_4OOCCH_3$ | 99 |

# LIST OF PUBLICATIONS

1. Synthesis and characterization of NCL-5, NCL-6 and NCL-7: New zeolites enriched with polymorph B of the BEA family

**Kadgaonkar, M. D.**; Kasture M. W.; Bhange, D. S.; Joshi, P. N.; Ramaswamy, V.; Gupta N. M.; Kumar, R. *Microporous Mesoporous Mater.* **2007**, *105*, 82.

2. Influence of Pore Structure and Framework Al Sites on the State of Benzene ($C_6H_6$ and $C_6D_6$) Molecules Entrapped in the Zeolites of BEA Type: In Situ IR Spectroscopy Study

**Kadgaonkar**, **M. D.**; Kasture, M. W.; Kartha, V. B.; Kumar, R.; Gupta, N. M. *J. Phys. Chem. C* **2007**, *111,* 9927.

3. NCL-7, A Novel All Silica Analog of Polymorph B-rich Member of BEA Family: Synthesis and Characterization

**Kadgaonkar, M. D.**; Kasture, M. W.; Bhange, D. S.; Joshi, P. N.; Ramaswamy, V.; Kumar, R. *Microporous Mesoporous Mater.* **2007**, *101,* 108.

4. Cerium containing MCM-41: Synthesis, characterization and its use in various acid catalyzed reactions

**Kadgaonkar**, **M. D.**; Laha, S. C.; Pandey, R. K.; Kumar, P.; Kumar R. *Catalysis Today* **2004,** *97*, 225.

5. Studies of Promoter (Phosphate) Enhanced Crystallization of Siliceous MCM-41

Laha, S. C.; **Kadgaonkar**, **M. D.**; Anuji, A.; Ganapathy, S.; Amoureux, J. P.; Kumar, R. *J. Phys. Chem. B* **2003,** *107*, 14171.

6. Highly Chemo-Selective acylation of Amines, Alcohols, Thiols and Bifunctional compounds catalyzed by cerium containing MCM-41, (Ce-MCM-41)

Laha, S. C.; Pandey, R. K.; **Kadgaonkar**, **M. D.**; Kumar, P.; Kumar, R. *Bull. Catal. Soc. India* ***2002***, *1,* 38.

7. Synthesis, Characterization and Catalytic Application of Ti-containing Polymorph B-enriched NCL-7

**Kadgaonkar**, **M. D.**; Kasture, M. W.; Bhange, D. S.; Joshi, P. N.; Ramaswamy, V.; Gupta, N. M.; Kumar, R. (**Manuscript under preparation**).

8. Al-containing Polymorph B-enriched NCL-7 Analog: Synthesis, Characterization and Catalytic Evaluation

**Kadgaonkar**, **M. D.**; Kasture, M. W.; Bhange, D. S.; Joshi, P. N.; Ramaswamy, V.; Gupta, N. M.; Kumar, R. (**Manuscript under preparation**).

## SELECTED PRESENTATIONS IN SYMPOSIA/CONFERENCES

1. **M. D. Kadgaonkar**, R. Kumar and N. M. Gupta "Influence of pore structure and framework Al-sites on the state of benzene molecules adsorbed in BEA, MFI and M41S type materials: In-situ FTIR study" 8th National symposium and INDO-US seminar on Catalysis, *April 16-18, 2007* Dehradun, India.

2. **M. D. Kadgaonkar,** N. M. Gupta and R. Kumar Influence of pore structure and framework Al-sites on the state of benzene molecules adsorbed in zeolites Beta and ZSM-5: in situ FTIR study 15th International Zeolite Conference, *August 12 – 17, 2007* Beijing, China.

3. **M. D. Kadgaonkar,** M. W. Kasture, M. A. Bhagwat, P. N. Joshi, V. Ramaswamy, R. Kumar "NCL-7, A Novel All Silica Analog of Polymorph B-rich Member of BEA Family: Synthesis and Characterization" International Symposium on Zeolites and Microporous Crystals (ZMPC 2006), *July 30 - Aug 2, 2006* Tonago, Tottori Prefecture, Japan.

4. **M. D. Kadgaonkar**, S. C. Laha, R. K. Pandey, P. Kumar, R. Kumar "Cerium-containing MCM-41 materials as selective acylation and alkylation catalysts" Indo-Pacific Catalysis Association (IPCAT-3) Conference, *November 16-18, 2003* in Taipei, Taiwan.